Richard Meister, BSc

Auxiliary Master Equation Approach to the Effect of Electron-Phonon Interaction on the Anderson Impurity Model

MASTER'S THESIS

to achieve the university degree of

Diplom-Ingenieur

Master's degree programme: Technical Physics

submitted to

Graz University of Technology

Supervisor

Univ.-Prof. Dr.rer.nat. Enrico Arrigoni

Institute of Theoretical and Computational Physics

Faculty of Mathematics, Physics, and Geodesy

Graz, October 2017

AFFIDAVIT

I declare that I have authored this thesis independently, that I have not used other than the declared sources/resources, and that I have explicitly indicated all material which has been quoted either literally or by content from the sources used. The text document uploaded to TUGRAZonline is identical to the present master‘s thesis.

Date

Signature

Abstract

The trend of ever shrinking microelectronics makes it interesting to investigate the behavior – most importantly the current-voltage characteristics – of single molecules connecting two metallic contacts. Of interest for this thesis are in particular the effects of vibrations within such a molecule on the electronic transport. This is investigated in the work at hand by analyzing properties of the Anderson-Holstein model, which is a simplified system containing an electronic level coupled to a single harmonic oscillator. The model is solved with the auxiliary master equation approach, whereby the contacts are approximated by an open quantum system, consisting of a small number of bath sites coupled to a Markovian environment, whose dynamics are governed by the Lindblad master equation. Because this approach is non-perturbative, it allows for calculations in any parameter regime. The goal of this thesis is to implement numerical procedures to efficiently solve the master equation and investigate its outcome. The results for the spinless version of the model for weak to strong electron-phonon coupling at different phonon energies are compared with the outcome of other methods. The prominent effect of the Franck-Condon blockade is reproduced in the full interacting system at finite temperature, and calculations investigating the influence of on-site Coulomb repulsion at the impurity on the current are also presented.

Kurzfassung

Der Trend zu immer kleineren Strukturen in der Mikroelektronik macht es interessant das Verhalten – speziell die Strom-Spannungs-Charakteristik – von einzelnen Molekülen zwischen zwei metallischen Kontakten zu untersuchen. In dieser Arbeit interessieren wir uns vor allem für die Effekte, die interne Schwingungsfreiheitsgrade solcher Moleküle auf den elektronischen Transport haben. Diese werden in unserem Fall durch die Analyse des Anderson-Holstein Modells untersucht, das ein vereinfachtes System darstellt, bestehend aus einem einzelnen elektronischen Niveau, gekoppelt an einen harmonischen Oszillator. Dieses Modell wird mit dem Auxiliary Master Equation Approach gelöst, bei dem die Kontakte durch ein offenes Quantensystem dargestellt werden, welches aus einer endlichen Zahl an Badplätzen besteht, die an eine Markovsche Umgebung gekoppelt sind. Die Dynamik wird in diesem Fall von der Lindblad Mastergleichung beschrieben. Weil dieses Vorgehen nicht störungstheoretisch ist, kann es für Berechnungen in jedem Parameterbereich angewandt werden. Das Ziel der Arbeit ist es, die numerischen Methoden zur Behandlung des Modells effizient zu implementieren und die Lösungen zu untersuchen. Die Ergebnisse der spinlosen Version des Modells für schwache bis starke Elektron-Phonon-Kopplungen bei unterschiedlichen Phononenenergien werden mit den Ergebnissen anderer Methoden verglichen. Der markante Effekt der Franck-Condon-Blockade wird im vollständig wechselwirkenden System beobachtet und Berechnungen, die den Einfluss lokaler Coulomb-Abstoßung untersuchen, werden ebenfalls präsentiert.

> The code that is the hardest to debug is the code you know cannot possibly be wrong.

Acknowledgements

Naturally, writing a thesis always comes with ups and downs. I was lucky enough to have people around me who pushed me on the ups and made the downs more endurable. Here I want to mention some of these people.

First and foremost I would like to thank my supervisor Prof. Enrico Arrigoni for giving me the opportunity to investigate this interesting topic. It was great to work and discuss issues that arose during my thesis with him. Interesting and helpful conversations were also held with Prof. Wolfgang von der Linden, who had clever ideas for some of my problems.

The people who probably contributed the most to my thesis are my colleagues Delia Fugger, who helped me out a great deal especially in the beginning, and Toni Dorda as well as Max Sorantin, who gave me more useful input than anyone else.

Special thanks go to my good friend Christian Kokail, who always had an out-of-the-box view and therefore provided much useful advice and new ideas whenever I was stuck.

I would of course also like to thank my family, especially my mother Melitta, for supporting me all along and making all of this possible in the first place. A big thanks also goes to my sister Astrid, with Mario, Jana, and Lena, for lightening up my breaks and providing some much-needed distraction from time to time.

This work was supported by the Austrian Science Fund (FWF). Computational results have been achieved in part by using the Vienna Scientific Cluster (VSC), and the dCluster at the TU Graz.

Contents

List of Figures

Chapter 1

Introduction

Since the introduction of electronic circuits, their size gradually decreased. Especially with the rise of microchips, starting in the early 1970s with the Intel 4004 being the first microprocessor [1], electronic components shrunk dramatically. The minimum feature size – which is the length of an element on a processor that can be accurately generated – decreased from 10 µm for the Intel 4004 [2, 3] to only 14 nm for chips produced in 2017 [4].

At the length scales involved in commercially available microelectronics today, their behavior – except for some nifty techniques like flash memory – can be treated mostly in a classical picture. But, upon further miniaturization, quantum effects will start playing an increasingly important role for the description of such devices, until for single-molecular and single-atomic structures they completely dominate their properties. Such a device, consisting of only one organic molecule, was first proposed by Aviram and Ratner [5] in 1947.

To manufacture devices at molecular and atomic levels, their properties must first be studied extensively. One important field of interest is the voltage-current characteristic of junctions at the nano scale. Such a junction consists of two leads at different chemical potentials (a bias voltage) that are connected by a microscopic structure. Numerous experiments have been conducted in recent years investigating such properties of junctions consisting of, for example, quantum dots [6–9] and single molecules [10–17].

Interesting effects can arise from the fact that charged and uncharged states of such a molecular junction may have different equilibrium geometries. Thus, when electrons are transferred onto and off of the junctions, they induce vibrations that will affect the overall transport properties. This has in part already been studied experimentally [18–22] as well as theoretically under various assumptions [23–27]. We will apply an approach suggested by Arrigoni et al. [28] to this specific problem and implement a method that – in principle – works in any parameter regime.

The structure of the thesis is as follows. First, in chapter 2, we elaborate on the existing theoretical frameworks made use of. Chapter 3 focuses on the details of our implementation and the numerical methods used – namely the Arnoldi scheme [29] and the two-sided Lanczos [30] – as well as computational considerations like convergence criteria. Lastly, in chapter 4, we present our results, compare them to other methods treating the same model, and conclude the thesis with final remarks in chapter 5, where also the strengths and weaknesses of the approach and the algorithms are elaborated.

The original work done within the present thesis are the analytical section 2.4.3, the numerics in sections 3.1 and 3.2, as well as investigating the suitability of the presented algorithms for the solution of the problem. Furthermore, because of the bosonic degrees of freedom, the code for the numerical solution had to be written and tested from scratch.

Chapter 2

Model and Method

In this chapter we introduce the model, method, notation, and formalism used, as well as give the analytical basics needed to treat the problem at hand. Section 2.1 gives a mathematical and physical description of the system we investigate, namely the Anderson-Holstein model [31–33]. Our goal is to treat it with a scheme named auxiliary master equation approach [28, 34]. Tools needed for this method are the density operator formalism, and consequently open quantum systems, described in sec. 2.2 and 2.3, loosely following references [35] and [36]. To numerically treat such systems, the so-called superfermion formalism, introduced by Dzhioev and Kosov [37], is explained and extended by us to the case of bosons in sec. 2.4. Moreover, nonequilibrium Green functions are covered in sec. 2.5, making extensive use of reference [38]. These concepts are then combined in section 2.6 to motivate the use of the auxiliary master equation approach. Lastly, we apply a useful transformation suggested by Lang and Firsov [39] to the auxiliary open quantum system.

2.1 Anderson-Holstein model

To study transport phenomena out of equilibrium with electron-phonon coupling, we will investigate a simplified model which is a combination of a single impurity, first suggested by Anderson [31] and originally used to study magnetic impurities in metals, coupled to a small polaron, as described by Holstein [32, 33]. It is therefore often referred to as the Anderson-Holstein model.

The system at hand constists of two leads – one left and one right, with different chemical potentials μ_{L} and μ_{R} – in which the electrons do not interact with each other. These leads are coupled to a central region – the junction, which we will call impurity from here on – by electronic hopping terms. The impurity itself is described by a spin-degenerate electronic single-particle state which has an onsite energy and a Coulomb repulsion term. Vibrations are described by a harmonic

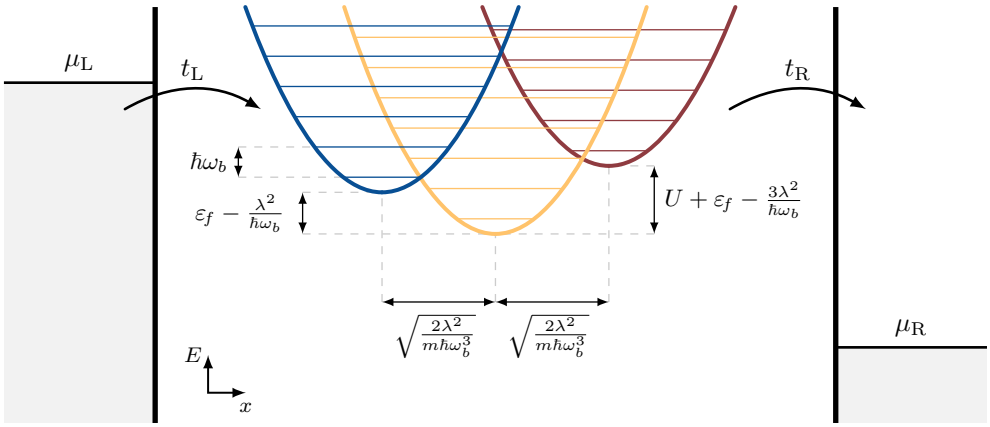

Figure 2.1: Energy sketch of the system. The filled states in the leads are marked in light gray. The parabolas are the potentials of the uncharged (—), singly charged (—), and doubly charged (—) electronic states with their allowed energy levels (if the impurity was isolated).

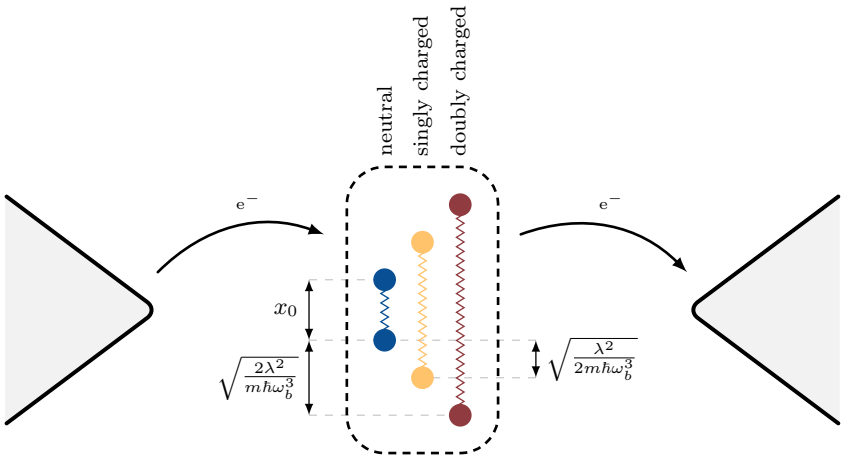

Figure 2.2: Spatial sketch of the model. The triangles left and right represent the leads, the dashed frame in the center is the impurity, where the colors stand for the mutually exclusive differently charged states. The filled circles connected by springs mark the atoms of the impurity in their neutral ●, singly charged ●, and doubly charged ● equilibrium positions. The x-axis is vertical in this illustration. The horizontal offset of the atoms is for better visibility only.

oscillator with its energy levels. The electronic and vibrational degrees of freedom are coupled by an electron-phonon coupling term. So the total Hamiltonian of the system in second quantization reads as

$$\hat{H} = \sum_{\sigma} \varepsilon_f c_{f\sigma}^\dagger c_{f\sigma} + U c_{f\uparrow}^\dagger c_{f\uparrow} c_{f\downarrow}^\dagger c_{f\downarrow} + \sum_{k,\alpha,\sigma} \varepsilon_{k\alpha} c_{k\alpha\sigma}^\dagger c_{k\alpha\sigma} + \sum_{k,\alpha,\sigma} t_\alpha \left(c_{f\sigma} c_{k\alpha\sigma}^\dagger + c_{f\sigma}^\dagger c_{k\alpha\sigma} \right) + \sum_{\sigma} \lambda (b^\dagger + b) c_{f\sigma}^\dagger c_{f\sigma} + \hbar\omega_b b^\dagger b \quad (2.1)$$

where $\sigma \in \{\uparrow, \downarrow\}$ is the spin, $\alpha \in \{\mathrm{L}, \mathrm{R}\}$ denotes the left and right lead, k numbers the electronic states in the leads, f means the electronic state localized at the impurity, variants of $c^\dagger$ and c create and annihilate electrons in the states characterized by their indices, respectively, and $b^\dagger$ and b are the ladder operators of the harmonic oscillator. Hats on creation and annihilation operators are omitted for readability throughout the thesis. The first four terms describe the purely electronic system, the last term is the unperturbed harmonic oscillator, and the term in between characterizes the electron-phonon coupling. This coupling term, which is proportional to the position operator of the harmonic oscillator, $(b^\dagger + b) \sim \hat{x}$, models the aforementioned fact that if electrons are present, the equilibrium distances within the impurity change.

The parameters of the model are U, which is the Coulomb repulsion at the impurity, all ε, which are onsite energies for every single-electron state, the energy level spacing of the harmonic oscillator $\hbar\omega_b$, the hopping strength from lead α to the impurity t_α, and λ, which is the electron-phonon coupling strength.

It is often convenient to not consider spin and investigate phononic effects of a spinless system, which is equivalent to the limit $U \to \infty$. In this case, all σ in eq. 2.1 as operator and summation indices are dropped, and the U-term vanishes. Therefore, the Hamiltonian becomes

$$\hat{H} = \varepsilon_f c_f^\dagger c_f + \sum_{k,\alpha} \varepsilon_{k\alpha} c_{k\alpha\sigma}^\dagger c_{k\alpha} + \sum_{k,\alpha} t_\alpha \left(c_f c_{k\alpha}^\dagger + c_f^\dagger c_{k\alpha} \right) + \lambda (b^\dagger + b) c_f^\dagger c_f + \hbar\omega_b b^\dagger b. \quad (2.2)$$

Figure 2.1 shows a simple representation of the energy levels in the system. Electrons are transferred from and to the leads with amplitudes t_L and t_R. Depending on the onsite energy ε_f and the Coulomb repulsion U, the charged and uncharged impurities have shifted energies. Most importantly, with n being the number of electrons at the impurity, the electron-phonon coupling term shifts the charged potential additionally by $\Delta E = -n^2\lambda^2/\hbar\omega_b$ in energy, and also by $\Delta x = n(2\lambda^2/m\hbar\omega_b^3)^{1/2}$ in position (see sec. A.1). However, for such a one-dimensional sketch it is hard to find a meaningful physical interpretation.

To visualize what the model actually represents, figure 2.2 is much more useful. There, the vertical axis is x, and y is plotted horizontally. In contrast to fig. 2.1,

the leads are now off in the y- instead of the x- direction. But since they couple exclusively with the constant hopping amplitudes t_L and t_R, the precise direction is not relevant. The dashed frame in the central region shows the impurity in its neutral, its singly charged, and its doubly charged state. So, depending on the charge, it will be in one of the three shown configurations.

The important thing to note is that the $\hat{x}$-operator in the harmonic oscillator no longer means a displacement of the impurity itself, but rather the magnitude of a distortion within the impurity. Now it is easy to see how the electron-phonon coupling models the shift of atomic equilibrium positions in a molecule. For the sketch we chose the simplest form of such an impurity, namely a diatomic one. In the neutral state, the atoms have some equilibrium distance x_0. Upon adding a negative charge to the molecule, their equilibrium separation increases, as can be seen in the sketch. One might argue that the model also holds approximately for more complicated molecules, if the frequency separation of the lowest eigenmode from the rest is large.

For all considerations in this thesis we always assume that a unique steady state exists, i. e. the driven system has one and only one stable state that does not change over time.

Unless otherwise noted, we will from here on set $e \equiv \hbar \equiv m_\mathrm{e} \equiv k_\mathrm{B} \equiv 1$. For the energy we will use different units depending on whatever is most convenient for a specific setup, which will be discussed later.

2.2 Statistical ensembles of quantum states

One distinct realization of a quantum mechanical system can always be described by some state vector $|\psi\rangle$. If, however, the state of the system is not definitely known, but rather only the probability of the system being in each of its possible states, like is the case in an ensemble of particles, state vectors are no longer sufficient to describe the physical situation. Roughly following the basics in [35] and [36], such cases must be described by an operator which projects onto the individual states with their respective probabilities, which is called the density operator.

$$\hat{\rho} = \sum_i p_i \, |\psi_i\rangle\langle\psi_i| \tag{2.3}$$

The possible states the system can be in are numbered by i. If all $|\psi_i\rangle$ are orthonormal, p_i is the probability of the system being in that particular state. Since $\hat{\rho}$ is Hermitian, one can always choose the vectors $|\psi_i\rangle$ to be orthonormal. For the following arguments we will therefore assume such an orthonormal set of vectors. Clearly, the probabilities must sum up to 1, so

$$\sum_i p_i = 1.$$

The trace of an operator is independent of the basis, and from the equation above one can see that in the $|\psi_i\rangle$ basis, $\mathrm{tr}(\hat{\rho}) = 1$, which is therefore an intrinsic property of $\hat{\rho}$. Additionally, because $p_i \geq 0$, $\hat{\rho}$ is also positive semidefinite.

To calculate expecation values, one must now average over the individual expecation values of the states the system can be in, weighted with their respective probabilities. With a complete orthonormal basis $|\varphi_i\rangle$ this reduces to

$$\begin{aligned}\langle \hat{O} \rangle &= \sum_i p_i \langle \psi_i | \hat{O} | \psi_i \rangle = \sum_{i,j} p_i \langle \psi_i | \hat{O} | \varphi_j \rangle \langle \varphi_j | \psi_i \rangle \\ &= \sum_{i,j} \langle \varphi_j | \psi_i \rangle p_i \langle \psi_i | \hat{O} | \varphi_j \rangle = \sum_j \langle \varphi_j | \left(\sum_i p_i |\psi_i\rangle\langle\psi_i| \hat{O} \right) |\varphi_j\rangle \\ &= \sum_j \langle \varphi_j | \hat{\rho} \hat{O} | \varphi_j \rangle = \mathrm{tr}(\hat{\rho} \hat{O}).\end{aligned}$$

Density operators are particularly useful when dealing with large systems, where one is actually only interested in a small subsystem. For consistent terminology we will in such cases refer to the total system as *universe*, the subsystem will be called just *system*, and the universe without the subsystem is the *environment*. A *pure state* of the universe, that is one which is described by a sinlge state vector $|\Psi\rangle$, can in general not be mapped to a single state in the system, as there might be entanglement between the it and the environment.

This pure state of the universe can of course also be written as a density operator

$$\hat{\rho} = |\Psi\rangle\langle\Psi| ,$$

which has the the property of $\hat{\rho}^2 = \hat{\rho}$, which is unique to pure states.

If the universe is comprised of a system s and an environment e, $|\Psi\rangle$ can be written as a linear combination of orthonormal basis states $|s_i\rangle \otimes |e_j\rangle$, where i and j take the quantum numbers of the system and the environment, respectively. One can define the so-called *partial trace* as

$$\mathrm{tr}_e(\hat{\rho}) \coloneqq \sum_{i,j,k} |s_i\rangle \left(\langle s_i| \otimes \langle e_k| \hat{\rho} |s_j\rangle \otimes |e_k\rangle \right) \langle s_j| .$$

All expectation values of operators acting solely on the system remain invariant under this operation, as is shown in sec. A.2.

$$\mathrm{tr}\left(\hat{\rho} \left(\hat{O}_s \otimes \mathbb{1} \right) \right) = \mathrm{tr}_s \left(\hat{\rho}_s \hat{O}_s \right)$$

tr_s, analogous to tr_e, is the trace only over the degrees of freedom of s. If the system is entangled with the environment, the *reduced density matrix* $\hat{\rho}_s = \mathrm{tr}_e(\hat{\rho})$ will no longer be pure, even if $\hat{\rho}$ is (see sec. A.3). This is why, even if one is not dealing with an ensemble of particles, it is necessary to treat systems interacting with environments in this denisty matrix formalism, rather than with state vectors.

2.2.1 Time evolution of a density matrix

The time evolution of a vector in an isolated system is given by the Schrödinger equation.

$$i\frac{\partial}{\partial t}\left|\psi\right\rangle = \hat{H}\left|\psi\right\rangle$$

If $\hat{H}$ is not explicitly time dependent, the solution is

$$\left|\psi(t)\right\rangle = e^{-i\hat{H}(t-t_0)}\left|\psi(t_0)\right\rangle.$$

For explicitly time dependent Hamiltonians (containing e. g. varying external fields), the order in time must be considered, because $\hat{H}(t)$ might not commute with itself at different times t. Therefore a time-ordering operator $\hat{\mathcal{T}}$ is introduced, that sorts operators in such a way that earlier times always appear to the right of later times. This way, the most general solution for $t > t_0$ is

$$\left|\psi(t)\right\rangle = \hat{\mathcal{T}}e^{-i\int_{t_0}^{t}\hat{H}(t')dt'}\left|\psi(t_0)\right\rangle.$$

The time-ordered exponential can be combined into the unitary time-evolution operator $\hat{U}$, in which case the equation above becomes

$$\left|\psi(t)\right\rangle = \hat{U}(t,t_0)\left|\psi(t_0)\right\rangle,$$

where

$$\hat{U}(t,t_0) \coloneqq \hat{\mathcal{T}}e^{-i\int_{t_0}^{t}\hat{H}(\tau)d\tau}.$$

Note that the Hermitian adjoint of $\hat{U}$ contains the anti-time-ordering operator $\hat{\tilde{\mathcal{T}}}$, which sorts in exact reverse order from $\hat{\mathcal{T}}$.

With the definiton of $\hat{\rho}$ for a closed system introduced in the last section it is straightforward that the time evolution is given by

$$\hat{\rho}(t) = \hat{U}(t,t_0)\hat{\rho}(t_0)\hat{U}^\dagger(t,t_0),$$

from which follows that

$$\begin{aligned}\frac{\partial}{\partial t}\hat{\rho}(t) &= \left(\frac{\partial}{\partial t}\hat{U}(t,t_0)\right)\hat{\rho}(t_0)\hat{U}^\dagger(t,t_0) + \hat{U}(t,t_0)\hat{\rho}(t_0)\left(\frac{\partial}{\partial t}\hat{U}^\dagger(t,t_0)\right)\\ &= -i\hat{H}(t)\hat{U}(t,t_0)\hat{\rho}(t_0)\hat{U}^\dagger(t,t_0) + \hat{U}(t,t_0)\hat{\rho}(t_0)\hat{U}^\dagger(t,t_0)i\hat{H}(t)\\ &= -i(\hat{H}(t)\hat{\rho}(t) - \hat{\rho}(t)\hat{H}(t)) = -i[\hat{H}(t),\hat{\rho}(t)],\end{aligned} \tag{2.4}$$

where the fact that the inner derivative is once on the left and once on the right of $\hat{U}$ is a consequence of the different time-ordering operators.

2.3 Open quantum systems

Combining the time evolution with the previously introduced partial trace, the reduced density matrix at time t is given by

$$\hat{\rho}_s(t) = \mathrm{tr}_e(\hat{U}(t,t_0)\hat{\rho}(t_0)\hat{U}^\dagger(t,t_0)). \tag{2.5}$$

This will necessitate the knowledge of the full system, which is often infeasable. One therefore seeks to describe the time evolution of the system by a quantum Markov process [35], which is an extension of a classical Markov process to a quantum mechanical system. This is equivalent to dropping all memory effects in the environment, as the basic property of a Markov process is exactly that the history need not be known for the next time step [40].

Analogous to a classical Markov process, the time evolution of a quantum Markov process is described by a semigroup, called a quantum dynamical semigroup [41]. Its most important property is

$$\hat{U}_s(t_3,t_2)\hat{U}_s(t_2,t_1) = \hat{U}_s(t_3,t_1),$$

where $\hat{U}_s$ is now the (non-unitary) time evolution operator of the system and the propagation occurs only forward in time with $t_3 > t_2 > t_1 \geq 0$. If the system is not externally driven with a time-dependent influence – that is it is homogenious in time – only differences in time must be considered and with $\hat{U}_s(t_2 - t_1) \coloneqq \hat{U}_s(t_1,t_2)$ the equation above reduces to

$$\hat{U}_s(t_1)\hat{U}_s(t_2) = \hat{U}_s(t_1+t_2),$$

with $t_1, t_2 \geq 0$.

It can be shown [42, 43] that the most general time evolution described by a quantum dynamical semigroup (as defined in [40]) that is homogenious in time is given by

$$\frac{\partial}{\partial t}\hat{\rho}_s(t) = -i[\hat{H}_s, \hat{\rho}_s(t)] + \sum_{k,l}\Gamma_{lk}\left(2\hat{L}_k\hat{\rho}_s(t)\hat{L}_l^\dagger - \{\hat{\rho}_s(t), \hat{L}_l^\dagger\hat{L}_k\}\right) =: \hat{\hat{\mathcal{L}}}\hat{\rho}_s(t) \tag{2.6}$$

with the Hermitian, positive semidefinite matrix $\underline{\Gamma}$ and a Hermitian operator $\hat{H}_s$, acting as a Hamiltonian of the system. Eq. 2.6 is called the Lindblad equation, where the $\hat{L}_k$ – often named Lindblad operators – form a complete basis of orthonormal operators in the subspace s, which is defined as

$$\mathrm{tr}_s(\hat{L}_i^\dagger\hat{L}_j) = \delta_{i,j}.$$

The superoperator $\hat{\hat{\mathcal{L}}}$ is often referred to as Liouvillian. In this form, the system is an *open quantum system*, as the environment is no longer part of its state, but the system is still "open" for interactions with it.

The commutator in eq. 2.6 bears some resemblence to eq. 2.4 for a closed system and describes the Hermitian part of the time evolution, while the other terms generate a dissipative contribution. Note that $\hat{H}_s$ is often simply the Hamiltonian of the isolated system – as is in our model – but this is not necessarily the case. There might be Hermitian influences of the environment on the system, which are then part of $\hat{H}_s$.

The Lindblad equation can also be derived from the microscopic dynamics of the universe, using certain approximations [35]. This involves starting from eq. 2.5 and assuming the environment part of the density operator $\mathrm{tr}_s(\hat{\rho})$ is time independent, which implies that the environment is only negligibly influenced by the system (called Born approximation). Then the Markov property is imposed, which, as mentioned before, postulates that the time evolution of the system density operator at time t only depends on the state of the system at t, and not its history. These assumptions, combined as Born-Markov approximation, are justified whenever the correlations in the environment decay much faster than the time scale over which the state of the system changes. Lastly, a so-called secular approximation is performed, which averages over fast oscillating terms in the environment and leads to eq. 2.6.

From here on we will omit the index s for $\hat{\rho}_s$ and rename $\hat{\rho}$ to $\hat{\rho}_u$.

2.4 Superfermion formalism

Because the time evolution of an open quantum system (eq. 2.6) contains $\hat{\hat{\mathcal{L}}}$, a superoperator, it is not convenient to work with the density operator directly, since its application to $\hat{\rho}$ can not be described by a matrix-vector multiplication. Instead, we employ a scheme suggested by Dzhioev and Kosov [37] for purely fermionic systems and extend it to bosons, which allows us to re-write eq. 2.6 into a matrix-vector form.

2.4.1 Basics

For this section, first a fermionic system of N single-particle states $|k\rangle$, characterized by the quantum number $k \in \{1, 2, \ldots, N\}$ will be considered. It is convenient to work in second quantization and choose the basis vectors as $|\boldsymbol{n}\rangle$, where $\boldsymbol{n}$ is a sequence of numbers $\boldsymbol{n} \coloneqq (n_1, n_2, n_3, \ldots, n_N)$, and n_k is the occupation number of the single-particle state $|k\rangle$. In this basis, the density operator can be written as

$$\hat{\rho} = \sum_i p_i \, |\psi_i\rangle\langle\psi_i| = \sum_{\boldsymbol{m},\boldsymbol{n}} \sum_i p_i \, \langle \boldsymbol{m}|\psi_i\rangle \, \langle\psi_i|\boldsymbol{n}\rangle \, |\boldsymbol{m}\rangle\langle\boldsymbol{n}| = \sum_{\boldsymbol{m},\boldsymbol{n}} \rho_{\boldsymbol{m},\boldsymbol{n}} \, |\boldsymbol{m}\rangle\langle\boldsymbol{n}|$$

where the sum over $\boldsymbol{m}$ and $\boldsymbol{n}$ means all possible configurations $(m_1, m_2, \cdots, m_N)$ and $(n_1, n_2, \cdots, n_N)$.

To write this density matrix $\rho_{\boldsymbol{m},\boldsymbol{n}}$ as a vector, a new Fock space is introduced, which contains the original single-particle states, and also a duplicate of each of those states. These – now twice as many – states are used to construct a new Fock space, the so-called superfermion – or augmented – space. To distinguish them from the original states, all duplicates are denoted with a tilde over their quantum numbers. They will also be referred to as *tilde states*, as opposed to the *original*, or *non-tilde states*. The basis vectors in this superfermion space are $|\boldsymbol{n}, \widetilde{\boldsymbol{m}}\rangle$, where both $\boldsymbol{n}$ and $\boldsymbol{m}$ contain occupation numbers $(n_1, n_2, \cdots, n_N)$ and $(m_1, m_2, \cdots, m_N)$ as above, $\boldsymbol{n}$ is the occupation in the original, and $\boldsymbol{m}$ is the occupation in tilde space.[1]

Because of the additional single-particle states, there are now more creation and annihilation operators, which by construction of the Fock space have the usual anticommutation properties.

$$\{c_m, c_n\} = \{\tilde{c}_m, \tilde{c}_n\} = \{c_m, \tilde{c}_n\} = 0$$

$$\{c_m^\dagger, c_n^\dagger\} = \{\tilde{c}_m^\dagger, \tilde{c}_n^\dagger\} = \{c_m^\dagger, \tilde{c}_n^\dagger\} = 0$$

$$\{c_m, c_n^\dagger\} = \{\tilde{c}_m, \tilde{c}_n^\dagger\} = \{c_m, \tilde{c}_n^\dagger\} = \delta_{m,n}$$

Here, $c_m^\dagger$ (c_m) creates (annihilates) a particle in the single-particle state $|m\rangle$ in original space, and $\tilde{c}_m^\dagger$ ($\tilde{c}_m$) creates (annihilates) a particle in the single-particle state $|\widetilde{m}\rangle$ in tilde space.

Any operator $\hat{O}$ in second quantization in the original space can be written as a sum of products of creation and annihilation operators. To transfer them to the superfermion space, their operators in the non-augmented space are replaced by the corresponding counterparts in the augmented space.

Because of the linearity of the following argument, it is sufficient to consider only products of creators and annihilators. The matrix elements of operators acting only in the original space defined in this way are

$$\langle \boldsymbol{m}, \widetilde{\boldsymbol{p}}|\hat{O}|\boldsymbol{n}, \widetilde{\boldsymbol{q}}\rangle = (-1)^{N^{\text{basis}}_{\boldsymbol{m},\boldsymbol{p}}} (-1)^{N_{\boldsymbol{p}} N_O} (-1)^{N^{\text{basis}}_{\boldsymbol{n},\boldsymbol{q}}} \langle \boldsymbol{m}|\hat{O}|\boldsymbol{n}\rangle \, \delta_{\boldsymbol{p},\boldsymbol{q}}$$

where $N^{\text{basis}}_{\boldsymbol{m},\boldsymbol{p}}$ is the number of transpositions needed to sort all tilde creators to the left of all non-tilde creators in a state $|\boldsymbol{m}, \widetilde{\boldsymbol{p}}\rangle$, which of course depends on the order of operators chosen for $|\boldsymbol{m}, \widetilde{\boldsymbol{p}}\rangle$. The choice made in this thesis will be discussed in the next subsection. Furthermore, $N_{\boldsymbol{p}} = \sum_k p_k$ is the number of fermions represented by the quantum number $\boldsymbol{p}$, in this case the number of electrons in tilde single-particle-states, and N_O is the number of fermionic operators in $\hat{O}$. This sign comes about from the fact that all tilde annihilators in the state $\langle \boldsymbol{m}, \widetilde{\boldsymbol{p}}|$ must first be interchanged with all creators and annihilators in $\hat{O}$, before meeting their

[1] Note that the tilde only indicates that the quantum number signifies the occupations in tilde space, not that $\widetilde{\boldsymbol{n}}$ is a different number from $\boldsymbol{n}$. So a state $|\boldsymbol{n}, \widetilde{\boldsymbol{n}}\rangle$ has the exact same occupations in original and tilde space.

counterpart in $|\boldsymbol{n}, \widetilde{\boldsymbol{q}}\rangle$, giving a factor of -1 at every transposition. The Kronecker delta $\delta_{\boldsymbol{p},\boldsymbol{q}}$ arises from the fact that $\hat{O}$ only contains non-tilde operators.

The first operator to investigate is the denisty operator, which in the chosen basis for the superfermion space takes the form

$$\begin{aligned}\hat{\rho} &= \sum_{\substack{\boldsymbol{m},\boldsymbol{n}\\ \boldsymbol{q},\boldsymbol{r}}} |\boldsymbol{m}, \widetilde{\boldsymbol{q}}\rangle\langle \boldsymbol{m}, \widetilde{\boldsymbol{q}}|\, \hat{\rho}\, |\boldsymbol{n}, \widetilde{\boldsymbol{r}}\rangle\langle \boldsymbol{n}, \widetilde{\boldsymbol{r}}| = \sum_{\substack{\boldsymbol{m},\boldsymbol{n}\\ \boldsymbol{q},\boldsymbol{r}}} \underbrace{\langle \boldsymbol{m}, \widetilde{\boldsymbol{q}}|\hat{\rho}|\boldsymbol{n}, \widetilde{\boldsymbol{r}}\rangle}_{\sim \rho_{\boldsymbol{m},\boldsymbol{n}}\delta_{\boldsymbol{q},\boldsymbol{r}}} |\boldsymbol{m}, \widetilde{\boldsymbol{q}}\rangle\langle \boldsymbol{n}, \widetilde{\boldsymbol{r}}| \\ &= \sum_{\boldsymbol{m},\boldsymbol{n},\boldsymbol{r}} (-1)^{N^{\text{basis}}_{\boldsymbol{m},\boldsymbol{r}}} (-1)^{N^{\text{basis}}_{\boldsymbol{n},\boldsymbol{r}}} \rho_{\boldsymbol{m},\boldsymbol{n}} |\boldsymbol{m}, \widetilde{\boldsymbol{r}}\rangle\langle \boldsymbol{n}, \widetilde{\boldsymbol{r}}|\end{aligned}$$

where fermi signs occur only from re-sorting the basis, not from transpositions with $\hat{\rho}$, because in the density operator creators and annihilators always appear in pairs.

Now, with the definition of the vector

$$|I\rangle \coloneqq \sum_{\boldsymbol{m}} e^{i\varphi_{\boldsymbol{m}}} |\boldsymbol{m}, \widetilde{\boldsymbol{m}}\rangle$$

with arbitrary phases $\varphi_{\boldsymbol{m}}$ and, subsequently

$$\begin{aligned}|\rho\rangle \coloneqq \hat{\rho}\,|I\rangle &= \sum_{\boldsymbol{k},\boldsymbol{m},\boldsymbol{n},\boldsymbol{r}} e^{i\varphi_{\boldsymbol{k}}} (-1)^{N^{\text{basis}}_{\boldsymbol{m},\boldsymbol{r}}} (-1)^{N^{\text{basis}}_{\boldsymbol{n},\boldsymbol{r}}} \rho_{\boldsymbol{m},\boldsymbol{n}} |\boldsymbol{m}, \widetilde{\boldsymbol{r}}\rangle \underbrace{\langle \boldsymbol{n}, \widetilde{\boldsymbol{r}}|\boldsymbol{k}, \widetilde{\boldsymbol{k}}\rangle}_{\delta_{\boldsymbol{n},\boldsymbol{k}}\delta_{\boldsymbol{r},\boldsymbol{k}}} \\ &= \sum_{\boldsymbol{m},\boldsymbol{n}} e^{i\varphi_{\boldsymbol{n}}} (-1)^{N^{\text{basis}}_{\boldsymbol{m},\boldsymbol{n}}} (-1)^{N^{\text{basis}}_{\boldsymbol{n},\boldsymbol{n}}} \rho_{\boldsymbol{m},\boldsymbol{n}} |\boldsymbol{m}, \widetilde{\boldsymbol{n}}\rangle\end{aligned}$$

the density matrix can effectively be turned into a density vector.

The quantities of interest are actually expectation values of operators in the original non-augmented space. Conveniently, sandwiching a non-tilde operator $\hat{O}$ with an even number of creators and annihilators between $\langle I|$ and $|I\rangle$ in the superfermionic space is equivalent to taking its trace in the original Fock space.

$$\begin{aligned}\langle I|\hat{O}|I\rangle &= \sum_{\boldsymbol{m},\boldsymbol{n}} \left(e^{-i\varphi_{\boldsymbol{m}}} \langle \boldsymbol{m}, \widetilde{\boldsymbol{m}}|\right) \hat{O} \left(e^{i\varphi_{\boldsymbol{n}}} |\boldsymbol{n}, \widetilde{\boldsymbol{n}}\rangle\right) \\ &= \sum_{\boldsymbol{m},\boldsymbol{n}} e^{i(\varphi_{\boldsymbol{n}} - \varphi_{\boldsymbol{m}})} \underbrace{\langle \boldsymbol{m}, \widetilde{\boldsymbol{m}}|\hat{O}|\boldsymbol{n}, \widetilde{\boldsymbol{n}}\rangle}_{\langle \boldsymbol{m}|\hat{O}|\boldsymbol{n}\rangle \delta_{\boldsymbol{m},\boldsymbol{n}}} = \sum_{\boldsymbol{n}} \langle \boldsymbol{n}|\hat{O}|\boldsymbol{n}\rangle = \operatorname{tr}(\hat{O})\end{aligned}$$

Here, no fermi sign appears, because the number of creation and annihilation operators in $\hat{O}$ is even, and the basis resorting sign is cancelled by $\delta_{\boldsymbol{m},\boldsymbol{n}}$. With this result, one can immediately see that

$$\langle I|\rho\rangle = \langle I|\hat{\rho}|I\rangle = \operatorname{tr}(\hat{\rho}) = 1$$

and calculating expectation values in the original Fock space reduces to

$$\langle I|\hat{O}|\rho\rangle = \langle I|\hat{O}\hat{\rho}|I\rangle = \operatorname{tr}(\hat{O}\hat{\rho}) = \langle \hat{O}\rangle$$

if the number of creators and annihilators in $\hat{O}$ is even.

2.4.2 Operator properties

Because fermions anticommute, one must decide on the order of operators for the basis states. It is convenient to choose

$$|\boldsymbol{m}, \widetilde{\boldsymbol{n}}\rangle \coloneqq \prod_k \left[(c_k^\dagger)^{n_k} (\tilde{c}_k^\dagger)^{m_k} \right] |0\rangle$$

with an arbitrary but fixed sequence of k, and the vacuum state in superfermion space $|0\rangle$. For this case, $N^{\text{basis}}_{\boldsymbol{m},\boldsymbol{n}}$ is given in section A.6. The phases in the vector $|I\rangle$ are chosen to be

$$\varphi_{\boldsymbol{m}} \coloneqq \frac{3\pi}{2} \sum_k m_k$$

which means that

$$e^{i\varphi_{\boldsymbol{m}}} = e^{\frac{3\pi i}{2} \sum_k m_k} = (-i)^{\sum_k m_k} = (-i)^{N_{\boldsymbol{m}}}.$$

With these choices, some helpful relations arise. The application of non-tilde creation and annihilation operators to the vector $|I\rangle$ (see section A.5) yields the important results

$$c_k |I\rangle = -i\tilde{c}_k^\dagger |I\rangle \qquad \text{and} \qquad c_k^\dagger |I\rangle = -i\tilde{c}_k |I\rangle . \tag{2.7}$$

Because operators in original and tilde space anticommute with each other in any case, for bilinear operators this extends to

$$\begin{aligned} f_k f_l |I\rangle = f_k(-i\tilde{f}_l^\dagger) |I\rangle &= i\tilde{f}_l^\dagger f_k |I\rangle \\ &= i\tilde{f}_l^\dagger(-i\tilde{f}_k^\dagger) |I\rangle = \tilde{f}_l^\dagger \tilde{f}_k^\dagger |I\rangle \end{aligned}$$

where f is either c or $c^\dagger$. More general, this holds for all even-numbered products of operators.

$$\begin{aligned} f_k f_l \dots f_m f_n |I\rangle &= f_k f_l \dots \tilde{f}_n^\dagger \tilde{f}_m^\dagger |I\rangle \\ &= \tilde{f}_n^\dagger \tilde{f}_m^\dagger \dots f_k f_l |I\rangle = \tilde{f}_n^\dagger \tilde{f}_m^\dagger \dots \tilde{f}_l^\dagger \tilde{f}_k^\dagger |I\rangle \end{aligned} \tag{2.8}$$

Notice that in addition to taking the Hermitian conjugate of every operator, the order of the tilde operators is reversed when comparing it to the original space operators. These relations will later be helpful in re-writing the Liouville operator into matrix form.

2.4.3 Extension to bosons

To be able to treat molecular vibrations in this formalism, we need to extend it to also include phonons, i. e. bosonic particles. To the best of our knowledge, this has not been done before. For the model at hand it is sufficient to introduce a single boson level.

In the non-augmented space, the bosonic part of the system in second quantization is given by the basis states $|p\rangle$, with $p \in \mathbb{N}_0$ being the occupation number of the level. The total state of the system is then the tensor product of the electronic and the phononic part $|\boldsymbol{m}\rangle_\mathrm{f} \otimes |p\rangle_\mathrm{b}$.

To construct an augmented space for this system, the electronic part is treated as before, and analogously the bosonic level is duplicated and incorporated into a new bosonic Fock space. The copy is again denoted with a tilde to distinguish it from the original level. This bosonic augmented space now has operators with the commutation rules

$$\begin{aligned}[b, \tilde{b}\,] &= [b^\dagger, \tilde{b}^\dagger] = 0 \\ [b^\dagger, \tilde{b}\,] &= [b, \tilde{b}^\dagger] = 0 \\ [b, b^\dagger] &= [\tilde{b}, \tilde{b}^\dagger] = 1\end{aligned}$$

where $b^\dagger$ and b are the known bosonic creation and annihilation operators

$$b^\dagger |p, \widetilde{q}\rangle = \sqrt{p+1}\, |p+1, \widetilde{q}\rangle \qquad \text{and} \qquad b\, |p, \widetilde{q}\rangle = \sqrt{p}\, |p-1, \widetilde{q}\rangle\,,$$

and tilde variants are the analogous operators for the tilde level.

The total augmented space is given by the tensor product of the fermionic and bosonic Fock spaces, with the basis states $|\boldsymbol{m}, \widetilde{\boldsymbol{n}}\rangle_\mathrm{f} \otimes |p, \widetilde{q}\rangle_\mathrm{b}$ which will be denoted as $|\boldsymbol{m}, \widetilde{\boldsymbol{n}}, p, \widetilde{q}\rangle$.

For the electronic part, the order of operators in the basis states is taken over from above. Since the tilde and non-tilde bosonic creators commute with each other and also all electronic operators, the order in which they are specified is not relevant. Thus, the basis states are

$$\begin{aligned}|\boldsymbol{m}, \widetilde{\boldsymbol{n}}, p, \widetilde{q}\rangle &\coloneqq \frac{(b^\dagger)^p}{\sqrt{p!}} \frac{(\tilde{b}^\dagger)^q}{\sqrt{q!}} \prod_k \left[(c_k^\dagger)^{n_k} (\tilde{c}_k^\dagger)^{m_k} \right] |0\rangle_\mathrm{f} \otimes |0\rangle_\mathrm{b} \\ &= \prod_k \left[(c_k^\dagger)^{n_k} (\tilde{c}_k^\dagger)^{m_k} \right] |0\rangle_\mathrm{f} \otimes |p, \widetilde{q}\rangle_\mathrm{b}\end{aligned}$$

where variants of $|0\rangle$ denote the vacuum states in the augmented fermionic and bosonic space.

With phonons, the vector $|I\rangle$ is redefined to be

$$|I\rangle \coloneqq \sum_{\boldsymbol{m}, q} (-i)^{N_{\boldsymbol{m}}}\, |\boldsymbol{m}, \widetilde{\boldsymbol{m}}, q, \widetilde{q}\rangle\,.$$

With this, sandwiching a non-tilde operator with an even number of fermionic operators between $\langle I|$ and $|I\rangle$ is still equivalent to taking its trace in non-augmented space, as can be seen from

$$\begin{aligned}\langle I|\hat{O}|I\rangle &= \sum_{\boldsymbol{m},\boldsymbol{n},p,q} \left(i^{N_{\boldsymbol{m}}} \langle \boldsymbol{m}, \widetilde{\boldsymbol{m}}, p, \widetilde{p}|\right) \left(\hat{O}_\mathrm{f} \otimes \hat{O}_\mathrm{b}\right) \left((-i)^{N_{\boldsymbol{n}}} |\boldsymbol{n}, \widetilde{\boldsymbol{n}}, q, \widetilde{q}\rangle\right) \\ &= \sum_{\boldsymbol{m},\boldsymbol{n},p,q} i^{N_{\boldsymbol{m}}-N_{\boldsymbol{n}}} \underbrace{\langle \boldsymbol{m}, \widetilde{\boldsymbol{m}}|\hat{O}_\mathrm{f}|\boldsymbol{n}, \widetilde{\boldsymbol{n}}\rangle}_{\langle \boldsymbol{m}|\hat{O}_\mathrm{f}|\boldsymbol{n}\rangle \delta_{\boldsymbol{m},\boldsymbol{n}}} \underbrace{\langle p, \widetilde{p}|\hat{O}_\mathrm{b}|q, \widetilde{q}\rangle}_{\langle p|\hat{O}_\mathrm{b}|q\rangle \delta_{p,q}} \\ &= \sum_{\boldsymbol{m},p} \langle \boldsymbol{m}|\hat{O}_\mathrm{f}|\boldsymbol{m}\rangle \, \langle p|\hat{O}_\mathrm{b}|p\rangle = \mathrm{tr}(\hat{O})\end{aligned}$$

where $\hat{O} = \hat{O}_\mathrm{f} \otimes \hat{O}_\mathrm{b}$ with $\hat{O}_\mathrm{f}$ being the part of the operator acting in the electronic space, and $\hat{O}_\mathrm{b}$ acting only on the phonons.

Because the bosons do not interfere with the electronic creation and annihilation operators, eqs. 2.7 still apply. Additionally, we also get such rules for the bosonic operators (see Section A.5), which are

$$b\,|I\rangle = \tilde{b}^\dagger\,|I\rangle \qquad \text{and} \qquad b^\dagger\,|I\rangle = \tilde{b}\,|I\rangle\,. \tag{2.9}$$

2.5 Nonequilibrium Green functions

To calculate properties of the impurity, we will use the framework of nonequilibrium Green functions (Negf). This formalism provides powerful tools to calculate local, experimentally accessible quantities like e. g. density of states, electron density, and electrical current, without diagonalizing the full manybody Hamiltonian, which in practice is very often impossible.

The central objects are two-time correlation functions of field operators, the Green functions. For the purposes of our model – as we are interested in the electronic transport properties of the impurity – the operators are electron creators and annihilators of the level at the impurity $c^{(\dagger)}_{f\sigma}$. The Green functions are in general matrices with the degrees of freedom of their creation and annihilation operators. To keep the notation simple, we will suppress these indices of the operators in this section and not explicitly mark the Green functions as matrices. Also, scalar quantities implicitly become diagonal matrices, wherever appropriate.

Covering the full spectrum of properties and derivations for equilibrium- and nonequilibrium Green functions is beyond the capacity of this thesis, so we will only give a brief sketch of the differences of equilibrium- and nonequilibrium formulations, and state the most important results needed for the implemented method. Details on the fundamentals of the formalism and full derivations can be found in numerous introductory books [38, 44–46].

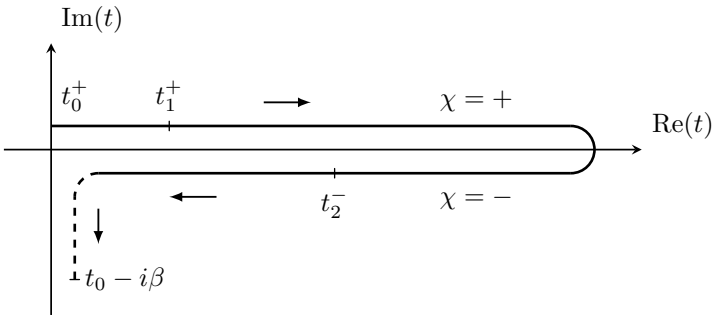

Figure 2.3: Sketch of the Keldysh contour $\mathcal{C}$. Lines are offset from the axes for better visibility only. The dashed part is not relevant for the steady state. The marked times are arbitrary examples to illustrate the contour ordering. In the contour-ordered sense, $t_0^+ >^{\mathcal{C}} t_1^+ >^{\mathcal{C}} t_2^-$.

Keldysh contour In equilibrium, the starting point is usually the time-ordered Green function, because of its perturbation expansion. To calculate it, one makes use of the Gell-Mann and Low theorem [47], and the fact that the wave functions at $t \to -\infty$ and $t \to +\infty$ differ only by a phase factor. In nonequilibrium, however, this will in general not be the case, as there is no physical reason for a driven system to ever return to its ground state, if the driving force is not turned off.

From here on it is best to switch to the Heisenberg picture, where – in contrast to the Schrödinger picture – instead of the states, the operators evolve with time. Both pictures are set to coincide at a reference time $t = t_0$, where the driving force is not yet present. From the basic definition of a two-time correlation function

$$\langle c(t_1)c^\dagger(t_2)\rangle = \mathrm{tr}\left(\hat{\rho}_{t_0}\hat{U}^\dagger(t_1,t_0)\, c\, \hat{U}(t_1,t_0)\hat{U}^\dagger(t_2,t_0)\, c^\dagger\, \hat{U}(t_2,t_0)\right)$$

one can see that the system time-evolves from t_0 to t_1, where c is applied, then to t_2 (the parts back to and from t_0 cancel), where $c^\dagger$ is applied, and then back to t_0.[2] This can be summed up as a "round-trip", starting from some initial time, time-evolving in the positive direction and then back to the initial time, applying the operators in appropriate places along the way. Such a path is called a *Keldysh contour* $\mathcal{C}$.

Often times, one wants to start from a density operator in thermal equilibrium at t_0. This can be achieved by also evolving the system along the imaginary time axis from$t = t_0$ to $t = t_0 - iT^{-1}$ which then adds a third branch to the Keldysh contour. We are, however, only interested in steady state properties, i. e. times $t \to \infty$, or, equivalently, $t_0 \to -\infty$. In this case, initial correlations are usually lost and this so-called Matsubara branch can be ignored.

[2]Note that $\hat{U}$ contains the full Hamiltonian, so in most cases direct evaluation of the expression above is not possible.

Contour ordering The concept of the Keldysh contour leads to the introduction of the contour-ordered Green function

$$G(t_1^{\chi_1}, t_2^{\chi_2}) = -i \langle \hat{\mathcal{T}}_{\mathcal{C}}[c(t_2^{\chi_2})c^\dagger(t_1^{\chi_1})]\rangle = -i \operatorname{tr}\left(\hat{\rho}_{t_0}\, \hat{\mathcal{T}}_{\mathcal{C}}[c(t_2^{\chi_2})c^\dagger(t_1^{\chi_1})]\right).$$

The additional index $\chi \in \{+,-\}$ defines whether the time resides on the contour part of increasing $(+)$ or decreasing $(-)$ time. The contour-ordering operator $\hat{\mathcal{T}}_{\mathcal{C}}$ sorts its arguments in the sequence they appear on the Keldysh contour, so all "+" times before all "−" times, two "+" times chronologically, and two "−" times antichronologically. It can be shown [38, p. 68] that $G(t_1^{\chi_1}, t_2^{\chi_2})$ has a perturbation expansion analogous to the time-ordered Green functions in equilibrium. Therefore, the Dyson equation [48]

$$G(t_1^{\chi_1}, t_2^{\chi_2}) = G_0(t_1^{\chi_1}, t_2^{\chi_2}) + \int_{\mathcal{C}} G_0(t_1^{\chi_1}, t')\Sigma(t', t'')G(t'', t_2^{\chi_2})dt'dt''$$

where G_0 is the (so-called bare) Green function of the noninteracting system and Σ is the self-energy,[3] also holds for the contour-ordered Green functions in nonequilibrium [49].

There are four different combinations for χ_1 and χ_2, and depending on those, one can define different Green functions, which are all contained in G.

$$\begin{aligned}
G_c(t_1, t_2) &= -i \langle \hat{\mathcal{T}}[c(t_2)c^\dagger(t_1)]\rangle && \chi_1 = + \quad \chi_2 = + \\
G^>(t_1, t_2) &= -i \langle c(t_2)c^\dagger(t_1)\rangle && \chi_1 = + \quad \chi_2 = - \\
G^<(t_1, t_2) &= +i \langle c^\dagger(t_1)c(t_2)\rangle && \chi_1 = - \quad \chi_2 = + \\
G_{\bar{c}}(t_1, t_2) &= -i \langle \hat{\bar{\mathcal{T}}}[c(t_2)c^\dagger(t_1)]\rangle && \chi_1 = - \quad \chi_2 = -
\end{aligned}$$

The time-ordering ($\hat{\mathcal{T}}$) and anti-time-ordering operator ($\hat{\bar{\mathcal{T}}}$) are the same as introduced in section 2.2.1, and sort earliest times to the right and left, respectively, accounting for any possible fermi signs. $G^>$ and $G^<$ are called the *greater* and *lesser*, and G_c and $G_{\bar{c}}$ are the *time-ordered (causal)* and *anti-time-ordeded (anti-causal)* Green functions, respectively. The two latter can be constructed from the two former by introducing appropriate Heaviside step functions Θ. Furthermore, $G^> + G^< = G_c + G_{\bar{c}}$, so one of the functions can be replaced by a linear combination of the others. It is convenient to choose

$$\begin{aligned}
G^{\mathrm{R}}(t_1, t_2) &= \Theta(t_2 - t_1)(G^>(t_1, t_2) - G^<(t_1, t_2)) \\
G^{\mathrm{A}}(t_1, t_2) &= \Theta(t_1 - t_2)(G^<(t_1, t_2) - G^>(t_1, t_2)) \\
G^{\mathrm{K}}(t_1, t_2) &= G^>(t_1, t_2) + G^<(t_1, t_2)
\end{aligned}$$

as linearly independent functions, where G^{R} is the *retarded*, G^{A} is the *advanced*, and G^{K} is the *Keldysh* Green function.

[3] Like G, Σ is a matrix in the degrees of freedom of the creators and annihilators, and their products are matrix products in the usual sense.

Langreth theorem For the steady state, the contour integrals of the products appearing in the Dyson equation $C(t_1,t_2) = \int_\mathcal{C} A(t_1,t')B(t',t_2)dt'$ can – by analytic continuation of the integrand on the complex plane – be expressed by integrals on the real time axis, using the definitions of greater and lesser Green functions [50]. These relations, known as Langreth theorem, are

$$\begin{aligned} C^{\gtrless}(t_1,t_2) &= \int_{-\infty}^{\infty} A^{\mathrm{R}}(t_1,t')B^{\gtrless}(t',t_2) + A^{\gtrless}(t_1,t')B^{\mathrm{A}}(t',t_1)dt' \\ C^{\mathrm{K}}(t_1,t_2) &= \int_{-\infty}^{\infty} A^{\mathrm{R}}(t_1,t')B^{\mathrm{K}}(t',t_2) + A^{\mathrm{K}}(t_1,t')B^{\mathrm{A}}(t',t_1)dt' \\ C^{\mathrm{A,R}}(t_1,t_2) &= \int_{-\infty}^{\infty} A^{\mathrm{A,R}}(t_1,t')B^{\mathrm{A,R}}(t',t_2) \end{aligned}$$

which immediately generalize to multiple products by repeated application.

Matrix form The Langreth theorem can be very elegantly implemented by casting the advanced, retarded, and Keldysh Green function into a matrix of the form

$$\underline{\underline{G}}(t_1,t_2) \coloneqq \begin{pmatrix} G^{\mathrm{R}}(t_1,t_2) & G^{\mathrm{K}}(t_1,t_2) \\ 0 & G^{\mathrm{A}}(t_1,t_2) \end{pmatrix}$$

where the usual matrix product rules apply, and products of the elements of such a matrix $A(t_1,t_2)$ and $B(t_1,t_2)$ implicitly mean an integration of the form $C(t_1,t_2) = \int A(t_1,t')B(t',t_2)dt'$.

Frequency domain In the steady state, by definition, the system is not changing with time. Therefore, the Green functions can only depend on the time difference $t = t_2 - t_1$. With the definition

$$\underline{\underline{G}}(t) = \underline{\underline{G}}(t_2 - t_1) \coloneqq \underline{\underline{G}}(0, t_2 - t_1)$$

they become one-variable functions. Of course, the expectation values are now to be evaluated with the steady-state density operator $\hat{\rho}_{\mathrm{ss}}$. Furthermore, they can be transformed into frequency domain by a Fourier transformation. In this context, the prefactor of $(2\pi)^{-1}$ is usually attributed to the inverse transformation, i. e. no prefactor appears from time- to frequeny domain.

$$\underline{\underline{G}}(\omega) = \mathcal{F}[\underline{\underline{G}}(t)] = \int_{-\infty}^{\infty} \underline{\underline{G}}(t)e^{i\omega t}dt$$

Very conveniently, the convolution-type products defined above become regular multiplications in frequency space.

$$C(\omega) = \mathcal{F}[C(t)] = \int_{-\infty}^{\infty} A(t') \underbrace{\int_{-\infty}^{\infty} B(t-t') e^{i\omega t} dt}_{e^{i\omega t'}\mathcal{F}[B(t)]} dt'$$

$$= \underbrace{\int_{-\infty}^{\infty} A(t') e^{i\omega t'} dt'}_{\mathcal{F}[A(t')]} B(\omega) = A(\omega)B(\omega)$$

Consequently, the products in the Dyson equation

$$\underline{\underline{G}}(\omega) = \underline{\underline{G}}_0(\omega) + \underline{\underline{G}}_0(\omega)\underline{\underline{\Sigma}}(\omega)\underline{\underline{G}}(\omega) \tag{2.10}$$

become regular matrix products of objects with the structure

$$\underline{\underline{G}}(\omega) = \begin{pmatrix} G^{\mathrm{R}}(\omega) & G^{\mathrm{K}}(\omega) \\ 0 & G^{\mathrm{A}}(\omega) \end{pmatrix}. \tag{2.11}$$

The explicit forms of these Green functions in the frequency domain in terms of the Hamilton eigenstates and energies are given in sec. A.4. From these it can be seen that $G^{\mathrm{A}}(\omega) = G^{\mathrm{R}\dagger}(\omega)$, such that it is sufficient to know one of the two.

Fluctuation-dissipation theorem In equilibrium, these Green functions are all linked together by the fluctuation-dissipation theorem [38, p. 45]. They can be expressed in terms of the so-called *spectral function*

$$A(\omega) = \frac{i}{2\pi}[G^{\mathrm{R}}(\omega) - G^{\mathrm{A}}(\omega)] = \frac{i}{2\pi}[G^{>}(\omega) - G^{<}(\omega)] = -\frac{1}{\pi}\operatorname{Im}(G^{\mathrm{R}}(\omega)) \tag{2.12}$$

whose diagonal elements represent the local density of states. For systems in thermal equilibrium, the relations

$$G^{<}(\omega) = 2\pi i f(\omega; T, \mu) A(\omega)$$
$$G^{>}(\omega) = -2\pi i [1 - f(\omega; T, \mu)] A(\omega)$$

hold, where

$$f(\omega; T, \mu) \coloneqq \left(e^{\frac{\omega-\mu}{T}} - 1\right)^{-1}$$

is the Fermi function at temperature T with the chemical potential μ. Since all other Green functions can be expressed by means of $G^{\gtrless}(\omega)$, there is only one independent function in equilibrium. These expressions also show the interesting propterty that $G^{<}(\omega)$ contains the occupied states, while $G^{>}(\omega)$ represents the empty states.

In nonequilibrium, however, the distribution of electrons is not simply given by the Fermi function, but instead is not derivable from first principle. Therefore, to describe the physics of the model, two functions are required, of which $G^{\gtrless}(\omega)$ in our case is the most convenient choice.

Hybridization function The electronic Green function of the noninteracting impurity, i. e. the system with the Hamiltonian

$$\hat{H} = \sum_{\sigma} \varepsilon_f c^\dagger_{f\sigma} c_{f\sigma} + \sum_{k,\alpha,\sigma} \varepsilon_{k\alpha} c^\dagger_{k\alpha\sigma} c_{k\alpha\sigma} + \sum_{k,\alpha,\sigma} t_\alpha \left(c_{f\sigma} c^\dagger_{k\alpha\sigma} + c^\dagger_{f\sigma} c_{k\alpha\sigma} \right)$$

with the parameters mentioned in the introduction, is given by [38, p. 191]

$$\underline{\underline{G}}_0^{-1}(\omega) = \underline{\underline{g}}_0^{-1}(\omega) - \underline{\underline{\Delta}}(\omega) \tag{2.13}$$

where $\underline{\underline{g}}_0(\omega)$ is the Green function of the decoupled noninteracting impurity, and the so-called hybridization function is given by

$$\underline{\underline{\Delta}}(\omega) = \sum_{\alpha} t_\alpha^2 \underline{\underline{g}}_\alpha(\omega)$$

with $\underline{\underline{g}}_\alpha(\omega)$ being the Green function of the noninteracting lead α. Because the disconnected leads are in thermal equilibrium, their Green functions are completely determined by their density of states, temperature, and chemical potential.

In the spin basis, g_0^{R} and g_0^{K} are diagonal. The retarded Green function is given by $g_0^{\mathrm{R}} = (\omega - \varepsilon_f + i0^+)^{-1}$ (cf. eq. A.1). The Keldysh part (eq. A.3) for a single spin reduces to

$$g_0^{\mathrm{K}} = 2\pi i \delta(\omega - \varepsilon_f) \left(p_k |\langle \psi_k | 1 \rangle|^2 - p_k |\langle \psi_k | 0 \rangle|^2 \right)$$

where $|0\rangle$ and $|1\rangle$ are the empty and filled states of the impurity, respectively, and p_k and $|\psi_k\rangle$ are the weights and states in the density operator. Obviously, this expression depends on the initial configuration of the impurity. In most cases, however, this is not relevant for the coupled Green function in the steady state, with the argument from above that initial correlations will be lost in the limit $t \to \infty$.

This can also be seen by inverting eq. 2.13. In general, components of the inverse of a Keldysh structure as defined in eq. 2.11 are given by

$$\left(G^{-1}\right)^{\mathrm{R,A}} = \left(G^{\mathrm{R,A}}\right)^{-1} \qquad \text{and} \qquad \left(G^{-1}\right)^{\mathrm{K}} = -\left(G^{\mathrm{R}}\right)^{-1} G^{\mathrm{K}} \left(G^{\mathrm{A}}\right)^{-1}$$

as can easily be checked by simple multiplication. Substituting eq. 2.13 in for $(G^{-1})^{\mathrm{K}}$ and multiplying from the left and right by G_0^{R} and G_0^{A} yields

$$G_0^{\mathrm{K}} = -G_0^{\mathrm{R}} \left(\left(g_0^{-1}\right)^{\mathrm{K}} - \Delta^{\mathrm{K}} \right) G_0^{\mathrm{A}} = G_0^{\mathrm{R}} \left(g_0^{\mathrm{R}}\right)^{-1} g_0^{\mathrm{K}} \left(g_0^{\mathrm{A}}\right)^{-1} G_0^{\mathrm{A}} + G_0^{\mathrm{R}} \Delta^{\mathrm{K}} G_0^{\mathrm{A}}.$$

Using $G^{\mathrm{A}} = G^{\mathrm{R}\dagger}$, the first summand is

$$|g_0^{\mathrm{R}} - \Delta^{\mathrm{R}}|^{-2} \cdot 2\pi i \underbrace{\frac{1}{\pi} \frac{0^+}{(\omega - \varepsilon_f)^2 + (0^+)^2}}_{\delta(\omega - \varepsilon_f)} [(\omega - \varepsilon_f)^2 + (0^+)^2]$$

which can be neglected if $\mathrm{Im}[\Delta^{\mathrm{R}}(\omega)] \neq 0$ at all zeros of $(\omega - \varepsilon_f - \mathrm{Re}[\Delta^{\mathrm{R}}(\omega)])$, because then $|g_0^{\mathrm{R}} - \Delta^{\mathrm{R}}|^{-2} = [(\omega - \varepsilon_f - \mathrm{Re}[\Delta^{\mathrm{R}}(\omega)])^2 + (0^+ - \mathrm{Im}[\Delta^{\mathrm{R}}(\omega)])^2]^{-1}$ is finite and the whole term is proportional to 0^+.

Current The current across the impurity can be expressed in terms of local Green functions by the Meir-Wingreen formula [51], of which we use a symmetrized version suggested by Haug and Jauho [38, p. 190].

$$J = \frac{i}{4\pi}\int \mathrm{tr}\left([\gamma_{\mathrm{L}}(\omega)-\gamma_{\mathrm{R}}(\omega)]G^{<}(\omega) + [f(\omega;T,\mu_{\mathrm{L}})\gamma_{\mathrm{L}}(\omega) - f(\omega;T,\mu_{\mathrm{R}})\gamma_{\mathrm{R}}(\omega)][G^{\mathrm{R}}(\omega)-G^{\mathrm{A}}(\omega)]\right) d\omega \quad (2.14)$$

In this expression, $\gamma_{\mathrm{L,R}} = -2t_{\mathrm{L,R}}^2\,\mathrm{Im}(g_{\mathrm{L,R}}^{\mathrm{R}})$ is proportional to the imaginary part of the retarded hybridization function of lead L or R, f is the Fermi function as defined above, and $\mu_{\mathrm{L,R}}$ is the chemical potential of each lead.

2.6 Auxiliary master equation approach

In determining the full interacting (so-called dressed) Green function at the impurity, the most difficult part is usually finding the self-energy. The auxiliary master equation approach (Amea) [28, 34] provides an approximate, non-perturbative method do accomplish this.

By combining eq. 2.13 and the Dyson equation 2.10, the Green function at the impurity is given by

$$\underline{\underline{G}}^{-1}(\omega) = \underline{\underline{g}}_0^{-1} - \underline{\underline{\Delta}} - \underline{\underline{\Sigma}}.$$

The vital point to recognize is that the effect of the environment on the impurity's Green function is completely determined by the hybridization function. This gives rise to the idea of replacing the inifinite physical leads with a numerically treatable, finite open quantum system, whose hybridization function approximates that of the physical system reasonably well.

Such a finite open – so-called auxiliary – system is realized by considering only the isolated impurity and connecting it to N_{B} artificial electronic bath sites and a continuous environment as introduced in sec. 2.3. The Lindblad equation describing this system is defined in a slightly different form from above.

$$\hat{\tilde{\mathcal{L}}}\hat{\rho} = -i[\hat{H}_{\mathrm{aux}},\hat{\rho}] + \sum_{k,l=0}^{N_{\mathrm{B}}}\sum_{\sigma}\left[\Gamma_{lk}^{(1)}\left(2\,c_{k\sigma}\,\hat{\rho}\,c_{l\sigma}^{\dagger} - \{\hat{\rho}, c_{l\sigma}^{\dagger}c_{k\sigma}\}\right) + \Gamma_{lk}^{(2)}\left(2\,c_{l\sigma}^{\dagger}\,\hat{\rho}\,c_{k\sigma} - \{\hat{\rho}, c_{k\sigma}c_{l\sigma}^{\dagger}\}\right)\right] \quad (2.15)$$

All indices except f now number the states localized at the bath sites, while f still stands for the single-electron state located at the impurity. The auxiliary Hamiltonian is given by the sum of that of the isolated impurity and the hoppings in the bath sites.

$$\hat{H}_{\mathrm{aux}} = \sum_{k,l}\sum_{\sigma} E_{kl}\,c_{k\sigma}^{\dagger}c_{l\sigma} + \sum_{\sigma}\lambda(b^{\dagger}+b)\,c_{f\sigma}^{\dagger}c_{f\sigma} + U c_{f\uparrow}^{\dagger}c_{f\uparrow}c_{f\downarrow}^{\dagger}c_{f\downarrow} + \omega_b\,b^{\dagger}b \quad (2.16)$$

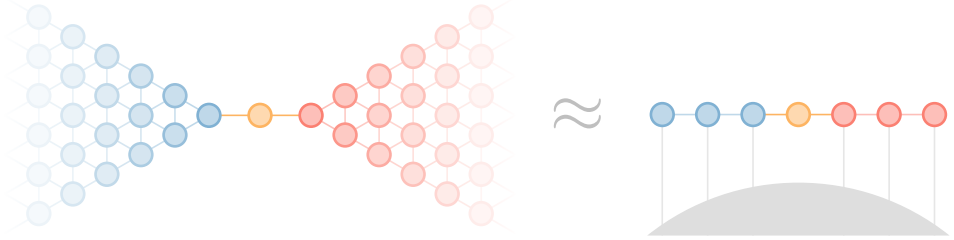

Figure 2.4: Sketch of the mapping from the infinite physical system with an arbitrary density of states (left) to the auxiliary system with $N_\mathrm{B} = 6$ (right).[4] The grey circle segment represents the continuous environment.

The parameters of the auxiliary system are the three matrices $\underline{E}$, $\underline{\Gamma}^{(1)}$, and $\underline{\Gamma}^{(2)}$, where the latter two contain complex numbers, and the former is chosen to be real and tridiagonal without loss of generality [52]. The hybridization can be calculated by considering just the noninteracting part of the Hamiltonian, i. e. only the term containing $\underline{E}$. The bare Green functions are given by [34]

$$\underline{G}_0^\mathrm{R}(\omega) = (\omega - \underline{E} + i\underline{\Lambda}) \qquad \text{and} \qquad \underline{G}_0^\mathrm{K} = 2i\,\underline{G}_0^\mathrm{R}\,\underline{\Omega}\,\underline{G}_0^\mathrm{A}$$

where $\underline{\Lambda} = \underline{\Gamma}^{(2)} + \underline{\Gamma}^{(1)}$ and $\underline{\Omega} = \underline{\Gamma}^{(2)} - \underline{\Gamma}^{(1)}$. The local noninteracting auxiliary Green functions at the impurity are then the components with indices (f, f) of $\underline{G}_0^\mathrm{R}$ and $\underline{G}_0^\mathrm{K}$. With these, the hybridization can be calculated using eq. 2.13.

The parameter matrices can now be chosen such that the hybridization of the auxiliary system approximates the hybridization of the physical system as closely as possible.

$$\underline{\underline{\Delta}}_\mathrm{aux}(\omega) \approx \underline{\underline{\Delta}}_\mathrm{phys}(\omega)$$

For a reasonably small number of N_B, the interacting auxiliary system can be solved numerically, which means that the full Green function at the impurity is computable. Therefore, from the Dyson equation of the auxiliary system

$$\underline{\underline{G}}_\mathrm{aux}^{-1} = \underline{\underline{g}}_{0,\mathrm{aux}}^{-1} - \underline{\underline{\Delta}}_\mathrm{aux} - \underline{\underline{\Sigma}}_\mathrm{aux}$$

the auxiliary self energy can be determined. This serves as an estimation for the physical self energy

$$\underline{\underline{\Sigma}}_\mathrm{phys} \approx \underline{\underline{\Sigma}}_\mathrm{aux}$$

which can be used to approximate the dressed physical Green function using the Dyson equation. The quality of the result depends of course on how closely the auxiliary hybridization reproduces the physical one. Naturally, the approximation becomes better for bigger N_B, and is exact for $N_\mathrm{B} \to \infty$ [52]. To characterize an auxiliary setup, we will use the total number of sites, which is $N = N_\mathrm{B} + 1$.

[4] The drawing on the right is incomplete insofar as there are also dissipative terms in the Liouville operator that take electrons from one site and put it on another (like a bath-assisted hopping).

2.6.1 Superfermionic representation

With the superfermion formalism established in section 2.4, the Liouville superoperator of the auxiliary system can be re-written into a regular operator.

By multiplying it from the right with $|I\rangle$, eq. 2.15 becomes

$$\dot{\hat{\rho}}\,|I\rangle = |\dot{\rho}\rangle = \hat{\tilde{\mathcal{L}}}\hat{\rho}\,|I\rangle = \hat{\tilde{\mathcal{L}}}_{\mathrm{H}}\hat{\rho}\,|I\rangle + \hat{\tilde{\mathcal{L}}}_{\mathrm{D}}\hat{\rho}\,|I\rangle\,. \tag{2.17}$$

Considering the summands seperately, one finds (cf. sec. A.7)

$$\hat{\tilde{\mathcal{L}}}_{\mathrm{H}}\hat{\rho}\,|I\rangle = -i[\hat{H}_{\mathrm{aux}},\hat{\rho}]\,|I\rangle = -i(\hat{H}_{\mathrm{aux}} - \hat{\tilde{H}}_{\mathrm{aux}})\,|\rho\rangle$$

for the Hermitian part, with $\hat{H}_{\mathrm{aux}}$ as in eq. 2.16 and

$$\hat{\tilde{H}}_{\mathrm{aux}} = \sum_{k,l}\sum_{\sigma} E_{kl}\,\tilde{c}^{\dagger}_{l\sigma}\tilde{c}_{k\sigma} + \sum_{\sigma}\lambda(\tilde{b}+\tilde{b}^{\dagger})\,\tilde{c}^{\dagger}_{f\sigma}\tilde{c}_{f\sigma} + U\tilde{c}^{\dagger}_{f\downarrow}\tilde{c}_{f\downarrow}\tilde{c}^{\dagger}_{f\uparrow}\tilde{c}_{f\uparrow} + \omega_b\,\tilde{b}^{\dagger}\tilde{b}.$$

Similarly, the dissipative part becomes (cf. sec. A.7)

$$\begin{aligned}\hat{\mathcal{L}}_{\mathrm{D}}\,|\rho\rangle = \sum_{k,l}\sum_{\sigma}\Big[&\Gamma^{(1)}_{lk}\left(-2i\,c_{k\sigma}\tilde{c}_{l\sigma} - \tilde{c}^{\dagger}_{k\sigma}\tilde{c}_{l\sigma} - c^{\dagger}_{l\sigma}c_{k\sigma}\right) + \\ &+ \Gamma^{(2)}_{lk}\left(-2i\,c^{\dagger}_{l\sigma}\tilde{c}^{\dagger}_{k\sigma} - c_{k\sigma}c^{\dagger}_{l\sigma} - \tilde{c}_{l\sigma}\tilde{c}^{\dagger}_{k\sigma}\right)\Big]\,|\rho\rangle\,.\end{aligned} \tag{2.18}$$

Because in our case the Liouvielle operator is time-independent, the time evolution of $|\rho\rangle$ is now given by

$$|\rho(t)\rangle = e^{\hat{\mathcal{L}}t}\,|\rho(0)\rangle\,.$$

In this formalism, the problem of determining the steady state has been reduced to finding an eigenvector of $\hat{\mathcal{L}}$, because in the steady state, the density operator – and thus $|\rho\rangle$ – is stationary. From

$$\frac{\partial}{\partial t}|\rho_{\mathrm{ss}}\rangle = \hat{\mathcal{L}}\,|\rho_{\mathrm{ss}}\rangle \stackrel{!}{=} 0$$

follows that the steady state vector $|\rho_{\mathrm{ss}}\rangle$ is the right eigenvector of $\hat{\mathcal{L}}$ with eigenvalue 0. The corresponding left eigenvector (which must exist, see sec. A.10), can be found by taking the time derivative of the density operator's trace. It must vanish, because the trace is statically one.

$$\frac{d}{dt}\,\mathrm{tr}(\hat{\rho}) = \langle I|\dot{\hat{\rho}}|I\rangle = \langle I|\mathcal{L}\hat{\rho}|I\rangle = \langle I|\mathcal{L}|\rho\rangle \stackrel{!}{=} 0$$

This must be true for any density vector, so $\langle I|\,\hat{\mathcal{L}} = 0$.

Another useful property is that the eigenvalues η_k of $\hat{\mathcal{L}}$ must all have $\mathrm{Re}(\eta_k) \leq 0$, because $e^{\hat{\mathcal{L}}t}\,|\rho\rangle$ is a valid density vector for any t, and exponentially growing solutions could not preserve the trace. Furthermore, $\hat{\mathcal{L}}$ commutes with the operator $\hat{\delta}_n \coloneqq c^{\dagger}_f c_f - \tilde{c}^{\dagger}_f\tilde{c}_f$. Since $\hat{\delta}_n\,|I\rangle = 0$, the steady state must also satisfy $\hat{\delta}_n\,|\rho_{\mathrm{ss}}\rangle = 0$.

2.6.2 Green functions

Due to the Markovian nature of the auxiliary system, special care must be taken in order to correctly calculate the Green functions. They can be obtained using the quantum regression theorem [35, 53]. It states that the time evolution of $\hat{A}\hat{\rho}$, with an arbitrary operator $\hat{A}$, is given by the same quantum dynamical semigroup as that of $\hat{\rho}$. The requirement for its validity is that all assumptions made before about the universe density operator $\hat{\rho}_u$ also hold for $\hat{A}\hat{\rho}_u$. One must be extra careful when dealing with fermionic operators, as some terms in the Liouville operator in the non-augmented space get negative signs [54]. In the superfermion formalism, however, these signs cancel and the time evolution becomes

$$\frac{\partial}{\partial t}|\rho_A(t)\rangle = \hat{\mathcal{L}}\,|\rho_A(t)\rangle$$

with $|\rho_A(t_1)\rangle \coloneqq \hat{A}\,|\rho(t_1)\rangle$. This again has the formal solution

$$|\rho_A(t)\rangle = e^{\hat{\mathcal{L}}(t-t_1)}\,|\rho_A(t_1)\rangle$$

with the important restriction that $t > t_1$, because the Liouvillian only propagates forwards in time.

From the original definition of $G^{\gtrless}(t)$ one can see that $G^{\gtrless}(t) = -G^{\gtrless\,\dagger}(-t)$. This can be used to construct the Green function for all times from forward propagation only, because in the steady state $\langle c^\dagger c(-t)\rangle = \langle c^\dagger(t)c\rangle$. For $G^>$ the conditions are obvious, for $G^<$ one must consider that it contains a propagation forwards in time only for negative arguments.

$$\begin{aligned}\underline{G}^>(t) &= \Theta(t)\underline{G}^>(t) - \Theta(-t)\underline{G}^{>\,\dagger}(-t)\\ \underline{G}^<(t) &= \Theta(-t)\underline{G}^<(t) - \Theta(t)\underline{G}^{<\,\dagger}(-t)\end{aligned} \tag{2.19}$$

The transformation to the frequency domain is very similar to that of $\underline{G}^{\mathrm{R}}$ and $\underline{G}^{\mathrm{A}}$ (see sec. A.8), with the only difference worth mentioning being that no $i0^+$ is required, because after applying c or $c^\dagger$ to $|\rho_{\mathrm{ss}}\rangle$, the resulting vector has zero overlap with the steady state and is therefore – as mentioned above – exponentially damped anyway. The explicit results for the impurity are

$$\begin{aligned}G^>_{\sigma\sigma}(\omega) = {}& \langle I|c_{f\sigma}(\omega - i\hat{\mathcal{L}})^{-1}c^\dagger_{f\sigma}|\rho_{\mathrm{ss}}\rangle - \langle I|c_{f\sigma}(\omega - i\hat{\mathcal{L}})^{-1}c^\dagger_{f\sigma}|\rho_{\mathrm{ss}}\rangle^\dagger\\ G^<_{\sigma\sigma}(\omega) = {}& \langle I|c^\dagger_{f\sigma}(\omega + i\hat{\mathcal{L}})^{-1}c_{f\sigma}|\rho_{\mathrm{ss}}\rangle - \langle I|c^\dagger_{f\sigma}(\omega + i\hat{\mathcal{L}})^{-1}c_{f\sigma}|\rho_{\mathrm{ss}}\rangle^\dagger\,.\end{aligned}$$

The retarded and advanced Green functions can be pieced together from the different $\Theta(\pm t)$ parts of $G^{\gtrless}(t)$, and the Keldysh Green function is again the sum of $G^{\gtrless}(t)$.

$$\begin{aligned}G^{\mathrm{A}}_{\sigma\sigma} &= \langle I|c^\dagger_{f\sigma}(\omega + i\hat{\mathcal{L}})^{-1}c_{f\sigma}|\rho_{\mathrm{ss}}\rangle + \langle I|c_{f\sigma}(\omega - i\hat{\mathcal{L}})^{-1}c^\dagger_{f\sigma}|\rho_{\mathrm{ss}}\rangle^\dagger\\ G^{\mathrm{R}}_{\sigma\sigma} &= \langle I|c_{f\sigma}(\omega - i\hat{\mathcal{L}})^{-1}c^\dagger_{f\sigma}|\rho_{\mathrm{ss}}\rangle + \langle I|c^\dagger_{f\sigma}(\omega + i\hat{\mathcal{L}})^{-1}c_{f\sigma}|\rho_{\mathrm{ss}}\rangle^\dagger\\ G^{\mathrm{K}}_{\sigma\sigma} &= \langle I|c_{f\sigma}(\omega - i\hat{\mathcal{L}})^{-1}c^\dagger_{f\sigma}|\rho_{\mathrm{ss}}\rangle - \langle I|c_{f\sigma}(\omega - i\hat{\mathcal{L}})^{-1}c^\dagger_{f\sigma}|\rho_{\mathrm{ss}}\rangle^\dagger\\ &\quad + \langle I|c^\dagger_{f\sigma}(\omega + i\hat{\mathcal{L}})^{-1}c_{f\sigma}|\rho_{\mathrm{ss}}\rangle - \langle I|c^\dagger_{f\sigma}(\omega + i\hat{\mathcal{L}})^{-1}c_{f\sigma}|\rho_{\mathrm{ss}}\rangle^\dagger\end{aligned} \tag{2.20}$$

2.7 Unitary transformations

To a quantum mechanical system one can always apply a unitary transformation that will not change the physics of the problem. Such a transformation consists of a unitary operator $\hat{\mathcal{U}}$, i. e. $\hat{\mathcal{U}}^\dagger = \hat{\mathcal{U}}^{-1}$. Operators then transform like

$$\hat{O} \mapsto \hat{\mathcal{U}}^\dagger \hat{O} \hat{\mathcal{U}} =: \hat{O}'$$

and the transformed vectors are given by

$$|\psi\rangle \mapsto \hat{\mathcal{U}}^\dagger |\psi\rangle =: |\psi'\rangle .$$

This way, whenever products of transformed operators with each other or with state vectors appear, the transformations in between them cancel out, since

$$\hat{O}'\hat{P}' |\psi'\rangle = \hat{\mathcal{U}}^\dagger \hat{O} \hat{\mathcal{U}} \hat{\mathcal{U}}^\dagger \hat{P} \hat{\mathcal{U}} \hat{\mathcal{U}}^\dagger |\psi\rangle = \hat{\mathcal{U}}^\dagger (\hat{O}\hat{P} |\psi\rangle).$$

Furthermore, the transformation matrices will multiply to $\mathbb{1}$ whenever expectation values or traces are calculated, because $\langle\psi'|\phi'\rangle = \langle\psi|\hat{\mathcal{U}}\hat{\mathcal{U}}^\dagger|\phi\rangle = \langle\psi|\phi\rangle$, as well as $\mathrm{tr}(\hat{\rho}'\hat{O}') = \mathrm{tr}\,(\hat{\mathcal{U}}^\dagger \hat{\rho} \hat{\mathcal{U}} \hat{\mathcal{U}}^\dagger \hat{O} \hat{\mathcal{U}}) = \mathrm{tr}\,(\hat{\mathcal{U}}\hat{\mathcal{U}}^\dagger \hat{\rho}\, \hat{O}) = \mathrm{tr}\,(\hat{\rho}\, \hat{O})$, due to the invariance of the trace under cyclic permutation of its argument.

2.8 Lang-Firsov transformation

In the case of eqs. 2.1 and 2.2, a very useful transformation was proposed by Lang and Firsov [39], which takes the form

$$\hat{\mathcal{U}} = e^{\hat{S}} \tag{2.21}$$

with the anti-Hermitian operator

$$\hat{S} = \sum_\sigma \gamma c^\dagger_{f\sigma} c_{f\sigma} (b^\dagger - b) \tag{2.22}$$

where $\gamma = -\frac{\lambda}{\omega_b}$. Applying this transformation to the original Hamiltonian will remove the electron-phonon coupling term, albeit at the expense of other terms entering the equation.

We can use the same transformation in the auxiliary system, also with the intent of removing the electron-phonon coupling. Multiplying eq. 2.6 from the left and right by $e^{-\hat{S}}$ and $e^{\hat{S}}$, respectively, yields

$$\dot{\bar{\hat{\rho}}} := e^{-\hat{S}}\, \dot{\hat{\rho}}\, e^{\hat{S}} = e^{-\hat{S}}\, \bar{\hat{\mathcal{L}}} \hat{\rho}\, e^{\hat{S}} = e^{-\hat{S}}\, \bar{\hat{\mathcal{L}}}_{\mathrm{H}} \hat{\rho}\, e^{\hat{S}} + e^{-\hat{S}}\, \bar{\hat{\mathcal{L}}}_{\mathrm{D}} \hat{\rho}\, e^{\hat{S}}$$

where a bar means the transformed operator as in $\bar{\hat{O}} := e^{-\hat{S}} \hat{O} e^{\hat{S}}$.

The first summand is

$$\begin{aligned} e^{-\hat{S}}\,\hat{\hat{\mathcal{L}}}_{\mathrm{H}}\hat{\rho}\,e^{\hat{S}} &= -ie^{-\hat{S}}[\hat{H}_{\mathrm{aux}},\hat{\rho}]\,e^{\hat{S}} \\ &= -i\left(e^{-\hat{S}}\hat{H}_{\mathrm{aux}}\underbrace{e^{\hat{S}}e^{-\hat{S}}}_{\mathbb{1}}\hat{\rho}e^{\hat{S}} - e^{-\hat{S}}\hat{\rho}\underbrace{e^{\hat{S}}e^{-\hat{S}}}_{\mathbb{1}}\hat{H}_{\mathrm{aux}}e^{\hat{S}}\right) \\ &= -i\left(\hat{\hat{H}}_{\mathrm{aux}}\hat{\hat{\rho}} - \hat{\hat{\rho}}\hat{\hat{H}}_{\mathrm{aux}}\right) = -i[\hat{\hat{H}}_{\mathrm{aux}},\hat{\hat{\rho}}] \end{aligned}$$

which means that the Hamiltonian governing the Hermitian part of the time evolution of the transformed density operator $\hat{\hat{\rho}}$ is given by the transformed auxiliary Hamiltonian $e^{-\hat{S}}\,\hat{H}_{\mathrm{aux}}\,e^{\hat{S}}$.

In the second summand, however, the transformation only affects $\hat{\rho}$. This comes about because $\hat{S}$ commutes with all operators except b, c_f, and Hermitian conjugates thereof. In order for the bath hybridization function to have the correct asymptotic behavior, the coefficients $\Gamma_{ij}^{(1,2)}$ must vanish whenever one of the indices matches the index f of the impurity [52, p. 7]. Therefore, in the term

$$e^{-\hat{S}}\,\hat{\hat{\mathcal{L}}}_{\mathrm{D}}\hat{\rho}\,e^{\hat{S}}$$

the unitary operators can be swapped to positions left and right of the density operator, which gives

$$\begin{aligned} e^{-\hat{S}}\,\hat{\hat{\mathcal{L}}}_{\mathrm{D}}\hat{\rho}\,e^{\hat{S}} = \sum_{k,l}\sum_{\sigma}\Big[&\Gamma_{lk}^{(1)}\left(2\,c_{k\sigma}\,\hat{\hat{\rho}}\,c_{l\sigma}^{\dagger} - \{\hat{\hat{\rho}},c_{l\sigma}^{\dagger}c_{k\sigma}\}\right) \\ &+\Gamma_{lk}^{(2)}\left(2\,c_{l\sigma}^{\dagger}\,\hat{\hat{\rho}}\,c_{k\sigma} - \{\hat{\hat{\rho}},c_{k\sigma}c_{l\sigma}^{\dagger}\}\right)\Big] \end{aligned}$$

for the transformed dissipative part. So in total, the time derivative of the transformed density operator is

$$\begin{aligned} \dot{\hat{\hat{\rho}}} = -i[\hat{\hat{H}}_{\mathrm{aux}},\hat{\hat{\rho}}] + \sum_{k,l}\sum_{\sigma}\Big[&\Gamma_{lk}^{(1)}\left(2\,c_{k\sigma}\,\hat{\hat{\rho}}\,c_{l\sigma}^{\dagger} - \{\hat{\hat{\rho}},c_{l\sigma}^{\dagger}c_{k\sigma}\}\right) \\ &+\Gamma_{lk}^{(2)}\left(2\,c_{l\sigma}^{\dagger}\,\hat{\hat{\rho}}\,c_{k\sigma} - \{\hat{\hat{\rho}},c_{k\sigma}c_{l\sigma}^{\dagger}\}\right)\Big]. \end{aligned} \tag{2.23}$$

The calculation of $\hat{\hat{H}}_{\mathrm{aux}}$ is straightforward, and is given in its entirety in section A.9, with the result being

$$\begin{aligned} \hat{\hat{H}}_{\mathrm{aux}} = \sum_{\substack{k\neq f\\ l\neq f}}\sum_{\sigma}E_{kl}\,c_{k\sigma}^{\dagger}c_{l\sigma} + Uc_{f\uparrow}^{\dagger}c_{f\uparrow}c_{f\downarrow}^{\dagger}c_{f\downarrow} + \omega_b\,b^{\dagger}b - \frac{1}{\omega_b}\Big(\sum_{\sigma}\lambda c_{f\sigma}^{\dagger}c_{f\sigma}\Big)^2 \\ + \sum_{k\sigma}\left(E_{kf}c_{k\sigma}^{\dagger}c_{f\sigma}e^{-\frac{\lambda}{\omega_b}(b^{\dagger}-b)} + E_{fk}c_{f\sigma}^{\dagger}e^{\frac{\lambda}{\omega_b}(b^{\dagger}-b)}c_{k\sigma}\right). \end{aligned} \tag{2.24}$$

The transformation removes the electron-phonon coupling term as intended, but re-introduces such a coupling in the creation and annihilation operators for electrons at the impurity, which are of the form $\bar{c}_f = c_f e^{\gamma(b^\dagger - b)}$. Additionally, a term effectively attracting electrons onto the impurity enters, reducing the onsite energy and the Coulomb repulsion.

The changes have a rather intuitive interpretation. The operator $\hat{S}$ is proportional to the momentum operator $\hat{p}$ of the harmonic oscillator, which is the generator for a spatial shift. Therefore, $\exp(\hat{S})$ performs a shift in x. The parameter γ is chosen such that the magnitude of the shift is exactly that of the charged parabolas drawn in fig. 2.1. Furthermore, the associated energy shift ΔE, also given in sec. A.1, now turns up explicitly in the Hamiltonian.

Consequently, when charge is created or annihilated at the impurity, the x-position of the parabola is adjusted accordingly by $\bar{c} = ce^{\gamma(b^\dagger - b)}$ and its Hermitian conjugate, so that the minimum is always centered around zero. Without transformation, the eigenstates of the shifted oscillators must be produced by linear combinations of the states of the unshifted oscillator. This means that, if the shift is large, high bosonic occupation numbers will be present in the steady state, as they are needed to make up the states shifted off to the side. For the implementation this property will play a crucial role, as lower occupation numbers mean a smaller Fock space.

From here, the same transition to superfermion space as in section 2.6.1 can be made, giving the analogous equation

$$|\dot{\bar{\rho}}\rangle \coloneqq \dot{\hat{\bar{\rho}}}\,|I\rangle = -i(\hat{\bar{H}}_{\text{aux}} - \hat{\bar{\bar{H}}}_{\text{aux}})\,|\bar{\rho}\rangle + \hat{\mathcal{L}}_{\text{D}}\,|\bar{\rho}\rangle$$

with $\hat{\mathcal{L}}_{\text{D}}$ from eq. 2.18, $\hat{\bar{H}}_{\text{aux}}$ from eq. 2.24, and

$$\hat{\bar{\bar{H}}}_{\text{aux}} = \sum_{\substack{k\neq f\\ l\neq f}}\sum_{\sigma} E_{kl}\,\tilde{c}^\dagger_{l\sigma}\tilde{c}_{k\sigma} + U\tilde{c}^\dagger_{f\downarrow}\tilde{c}_{f\downarrow}\tilde{c}^\dagger_{f\uparrow}\tilde{c}_{f\uparrow} + \omega_b\,\tilde{b}^\dagger\tilde{b} - \frac{1}{\omega_b}\Big(\sum_{\sigma}\lambda\tilde{c}^\dagger_{f\sigma}\tilde{c}_{f\sigma}\Big)^2 + \\ + \sum_{k\sigma}\left(E_{kf}\tilde{c}^\dagger_{f\sigma}\tilde{c}_{k\sigma}e^{\frac{\lambda}{\omega_b}(\tilde{b}^\dagger - \tilde{b})} + E_{fk}\tilde{c}^\dagger_{k\sigma}\tilde{c}_{f\sigma}e^{-\frac{\lambda}{\omega_b}(\tilde{b}^\dagger - \tilde{b})}\right).$$

Chapter 3

Implementation

This chapter will focus on the technical aspects of how the model was treated numerically. Some details on how the states and operators were implemented and the algorithms used will be given. The considerations about efficiently storing states and operators in computer memory, which were critical to the development of this work, are original to the best of our knowledge. A very important aspect that caused some problems which we were able to solve is the numerical treatment of unitary transformations highlighted in section 3.2. The presented algorithms discussed in sections 3.3 and 3.4 are of course known and have also been used in combination with AMEA before [34], but their suitability for this specific problem had to be investigated.

3.1 Code basics

The code to treat the model numerically was mostly written in MATLAB, with resource-intense calculations not involving matrix-vector products implemented in C (using the MEX interface). This section gives some short comments on the basic aspects of the implementation.

Binary representation of states A state in the superfermion representation consists of $2N$ binary numbers – N for non-tilde and N for tilde-fermions – and the occupations of the tilde- and non-tilde bosonic levels, which – in principle – could be arbitrarily high. So one must first decide to cap the occupation number for bosons at some value. Then a state consists of $2N$ binary numbers and 2 numbers from 0 to the maximum occupation number.

To keep such a state $|\boldsymbol{m}, \widetilde{\boldsymbol{n}}, p, \widetilde{q}\rangle$ in memory efficiently, we first calculate the number of bits needed to store the maximum occupation number for the bosonic levels

$N_{b,\max}$, which is $N_{b,\text{bits}} = \lceil \log_2(N_{b,\max}+1) \rceil$. Then, a 64 bit unsigned integer (`uint64` in MATLAB, `uint64_t` in C) is split up as follows. The first $N_{b,\text{bits}}$ bits on the least significant bit side are used to store the occupation of the non-tilde boson level, the next $N_{b,\text{bits}}$ bits store the occupation of the tilde bosonic level. Going further from the LSB- to the MSB-side, the occupations of the electronic levels are each stored using a single bit in the order $n_{1\uparrow}$, $\widetilde{m}_{1\uparrow}$, $n_{1\downarrow}$, $\widetilde{m}_{1\downarrow}$, $n_{2\uparrow}$, $\widetilde{m}_{2\uparrow}$, $n_{2\downarrow}$, ...

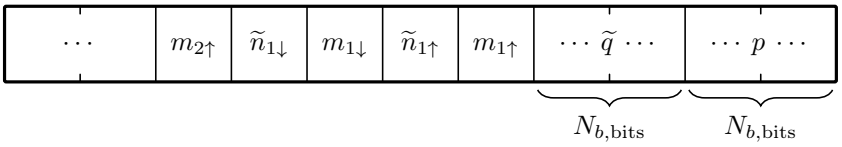

Figure 3.1: Representation of a state in memory. The whole block is 64 bits wide, each section represents one bit.

Fock space Most importantly, one does not need to consider the full Fock space of the problem. As we are interested in the steady state, and it has been shown in sec. 2.6.1 that this vector satisfies $c_f^\dagger c_f - \tilde{c}_f^\dagger \tilde{c}_f \left|\rho_{\text{ss}}\right\rangle = \hat{\delta}_n \left|\rho_{\text{ss}}\right\rangle = 0$, it is sufficient to calculate the matrix representation of $\hat{\mathcal{L}}$ for basis states $\left|\varphi\right\rangle$, where $\hat{\delta}_n \left|\varphi\right\rangle = 0$, in order to find the steady state.

When calculating Green functions, this condition changes to $\hat{\delta}_n \left|\rho\right\rangle = \pm \left|\rho\right\rangle$, depending on whether a creation or annihilation operator was applied to the steady state, because one non-tilde electron was removed or added.

Sparse Liouville operator The matrix representation of the Liouville operator in the superfermion space – even if only the relevant sector mentioned before is considered – is very sparse. Consequently, one must take advantage of this property by using the compressed column storage (the default sparse format in MATLAB). This decreases the speed of matrix-vector multiplications on multicore processors siginficantly, which is why we parallelized this operation using MEX.

Auxiliary parameters To calculate the parameters E_{ij}, $\Gamma_{ij}^{(1)}$, and $\Gamma_{ij}^{(2)}$, we used code developed by Dorda et al. [52]. The algorithm implements parallel tempering [55] to minimize the cost function given by

$$\chi^2 = \sum_{\alpha\in\{\text{R,K}\}} \int_{-\infty}^{\infty} W(\omega) \left| \Delta_{\text{aux}}^{\alpha}\left(\omega; \underline{E}_{ij}, \underline{\Gamma}^{(1)}, \underline{\Gamma}^{(2)}\right) - \Delta_{\text{phys}}^{\alpha}(\omega) \right|^2 d\omega$$

which is a measure of the deviation from the auxiliary hybridization to the physical one. The weighting function $W(\omega)$ can be used to favour smaller deviations in the central region.

3.2 Numerical Lang-Firsov transformation

As derived before, the Lang-Firsov transformation removes the coupling term, but modifies the electronic creation and annihilation operators on the impurity like $\bar{c}_f = e^{\gamma(b^\dagger - b)} c_f$. The matrix elements of $e^{\gamma(b^\dagger - b)}$ can – in principle – be calculated analytically. However, when used in a basis with a cutoff for the bosonic occupation number, this operator with the elements $L^{\mathrm{an}}_{mn} = \langle m | e^{\gamma(b^\dagger - b)} | n \rangle_{\mathrm{b}}$ (where it is sufficient to consider the purely bosonic basis) is no longer unitary, which has some undesired consequences. Applying a transformed creation or annihilation operator to a state now effectively lowers its norm, which, in turn, leads to e. g. the spectral function no longer being normalized.

To avoid this, we can, instead of using $\underline{L}^{\mathrm{an}}$ in the trucated basis, construct an operator that is in fact unitary for any cutoff. First, we evaluate $B_{mn} = \langle m | \gamma(b^\dagger - b) | n \rangle_{\mathrm{b}}$, and only then numerically exponentiate this matrix to $\underline{L} \coloneqq \exp(\underline{B})$. This operation is computationally very cheap, as the bosonic cutoff is usually on the order of 10–100. Because $\underline{B}$ is anti-Hermitian even in the truncated basis, $\underline{L}$ is always unitary.

Consequently, the matrix for the transformed annihilation operator at the impurity becomes $\underline{\bar{c}}_f = \underline{c}_f \otimes \underline{L}$, where $\underline{c}_f$ is the matrix representation of the annihilation operator in the electronic basis.

3.3 Steady state calculation

To find the steady state vector $|\rho_{\mathrm{ss}}\rangle$, one could in principle diagonalize $\hat{\mathcal{L}}$ to find the eigenvector with eigenvalue 0. But, because the Fock space is very large, this method is not feasible in most cases. Instead, we can use the properties of the time evolution of a state in the auxiliary system.

The density vector at arbitrary times is given by

$$|\rho(t)\rangle = e^{\hat{\mathcal{L}} t} |\rho(0)\rangle \,. \tag{3.1}$$

As mentioned before, the Liouville operator preserves trace, hermiticity, and semi-positive definiteness by construction. Using the spectral theorem, the time evolution becomes

$$|\rho(t)\rangle = \sum_m e^{\eta_m t} |m_{\mathrm{r}}\rangle \langle m_{\mathrm{l}} | \rho(0)\rangle \,, \tag{3.2}$$

where $|m_{\mathrm{r}}\rangle$ are the right-sided, and $|m_{\mathrm{l}}\rangle$ are the left-sided eigenvectors of $\hat{\mathcal{L}}$ with eigenvalues η_m. One can see that all eigenvalues must have $\mathrm{Re}(\eta_m) \leq 0$, otherwise the properties of $|\rho(t)\rangle$ could not be conserved. Because we assume the physical system to have a unique steady state, all except one eigenvector have $\mathrm{Re}(\eta_m) < 0$

and are exponentially damped. Therefore, for large t, any density vector $|\rho(t)\rangle$ (except for cases where $\langle\rho(0)|\rho_{\mathrm{ss}}\rangle = 0$) approaches the steady state.

$$\lim_{t\to\infty} |\rho(t)\rangle = |\rho_{\mathrm{ss}}\rangle$$

Unfortunately, direct calculation of the time evolution would require the exponentiation of a matrix with dimensions as large as the Fock space, which cannot be done numerically. Instead, we need to rely on an approximative algorithm. From eq. 3.2 one can see that for a small time interval Δt the most important summands are the ones where the $|\eta_m|$ are large, because they either oscillate or decay the fastest. It is therefore advisable to use a method which approximates large-magnitude eigenvalues and their associated eigenvectors.

A very simple candidate would be the so-called von Mises iteration [56], which uses the following simple principle. If a diagonalizable matrix $\underline{A}$ is multiplied by a random normalized vector $\boldsymbol{x}$, and the result is then again normalized, the new vector has the form

$$\frac{\underline{A}\boldsymbol{x}}{\|\underline{A}\boldsymbol{x}\|} = \frac{1}{\|\underline{A}\boldsymbol{x}\|}\underline{S}\underline{D}\underline{S}^{-1}\boldsymbol{x} = \frac{1}{\|\underline{A}\boldsymbol{x}\|}\sum_k \boldsymbol{r}_k\,\eta_k\,(\boldsymbol{l}_k^\dagger\,\boldsymbol{x})$$

where $\underline{S}$ contains the right-sided eigenvectors $\boldsymbol{r}_k$ in its columns, $\underline{S}^{-1}$ has the left-sided eigenvectors $\boldsymbol{l}_k^\dagger$ in its rows and $\underline{D}$ is a diagonal matrix with the corresponding eigenvalues η_k. The result is a sum of right-sided eigenvectors, weighted by the overlap of the left-sided eigenvectors with the original vector, and, more importantly, the associated eigenvalues of the eigenvectors. So within $\boldsymbol{x}$ the proportion of the largest-eigenvalue eigenvector, with which $\boldsymbol{x}$ had finite overlap, has increased.

Thus, doing this process iteratively, with some start vector $\boldsymbol{x}^{(0)} \coloneqq \boldsymbol{x}$, the sequence

$$\boldsymbol{x}^{(n)} = \frac{\underline{A}\boldsymbol{x}^{(n-1)}}{\left\|\underline{A}\boldsymbol{x}^{(n-1)}\right\|} \tag{3.3}$$

will converge to the right-sided eigenvector associated with the largest eigenvalue, given that the overlap of $\boldsymbol{x}^{(0)}$ with this eigenvector is non-zero.

From this result, one might expect the N largest eigenvalues to be approximated in the projection of $\underline{A}$ onto the space spanned by the first N iterations of this process. The subspace $\mathcal{K}_N(\underline{A}, \boldsymbol{x}) \coloneqq \mathrm{span}\{\boldsymbol{x}, \underline{A}\boldsymbol{x}, \underline{A}^2\boldsymbol{x}, \ldots, \underline{A}^{N-1}\boldsymbol{x}\}$ is called the N-th order Krylov space of $\underline{A}$ with start vector $\boldsymbol{x}$ [57]. A method using such a Krylov space to approximate the eigenvalues and eigenvectors of a non-Hermitian matrix was first described by Arnoldi [29] and is therefore often called Arnoldi iteration.

Even though the Arnoldi iteration only approximates the right-sided eigenvectors of $\hat{\mathcal{L}}$, is a suitable method to find the steady state, because we only need those in order to evaluate 3.1.

Working in $\mathcal{K}_N(\underline{A}, \boldsymbol{x})$, is most convenient with an orthonormal basis, which generally does not directly originate from eq. 3.3. Therefore, the Arnoldi iteration usually uses a stabilized Gram-Schmidt orthogonalization to extract such a basis from $\{\boldsymbol{x}, \underline{A}\boldsymbol{x}, \underline{A}^2\boldsymbol{x}, \ldots, \underline{A}^{N-1}\boldsymbol{x}\}$.

It can also happen that depending on the starting vector, it might not be possible to produce N linearly independent vectors by repeatedly applying $\underline{A}$, in which case $\mathcal{K}$ is an invariant subspace and eq. 3.1 becomes exact in this basis. The total Arnoldi algorithm works as follows.

function ARNOLDI($\underline{A}$, $\boldsymbol{x}$, N)
  $\underline{V} \leftarrow \underline{0}, \quad k \leftarrow 1, \quad \boldsymbol{x}_0 \leftarrow \boldsymbol{x}/\|\boldsymbol{x}\|$
  while $k \leq N$ **do** ▷ Loop over all vectors to produce
    $\boldsymbol{x}_k \leftarrow \underline{A} \cdot \boldsymbol{x}_{k-1}$
    for $l = 0, (k-2)$ **do** ▷ Loop for Gram-Schmidt
      $V_{l,k-1} \leftarrow \boldsymbol{x}_l^\dagger \cdot \boldsymbol{x}_k$ ▷ Overlap with previous basis vector
      $\boldsymbol{x}_k \leftarrow \boldsymbol{x}_k - V_{l,k-1} \cdot \boldsymbol{x}_l$
    $V_{k,k-1} \leftarrow \|\boldsymbol{x}_k\|$
    if $V_{k,k-1} = 0$ **then** ▷ Have we found an invariant subspace?
      $N \leftarrow k$ ▷ We can produce only k vectors
    else
      $\boldsymbol{x}_k \leftarrow \boldsymbol{x}_k / V_{k,k-1}$
    $k \leftarrow k + 1$
  return $\underline{V}, N, \boldsymbol{x}_0, \ldots, \boldsymbol{x}_{N-1}$

Algorithm 1: The Arnoldi iteration.

Note that to produce $\boldsymbol{x}_k$ it is sufficient to apply $\underline{A}$ to $\boldsymbol{x}_{k-1}$, instead of $\underline{A}^{k-1}$ to $\boldsymbol{x}_0$, because $\mathrm{span}\{\boldsymbol{x}_0, \underline{A}\boldsymbol{x}_0, \underline{A}^2\boldsymbol{x}_0, \ldots\} = \mathrm{span}\{\boldsymbol{x}_0, a_0\boldsymbol{x}_0 + a_1\boldsymbol{x}_1, \underline{A}(a_0\boldsymbol{x}_0 + a_1\boldsymbol{x}_1), \ldots\} = \mathrm{span}\{\boldsymbol{x}_0, \boldsymbol{x}_1, \underline{A}\boldsymbol{x}_1, \ldots\}$.

It is convenient to define a matrix $\underline{P} \coloneqq (\boldsymbol{x}_0, \boldsymbol{x}_1, \ldots, \boldsymbol{x}_{N-1})$, which has the new basis vectors in its columns. The projector onto $\mathcal{K}_N$ is then $\underline{P}\underline{P}^\dagger$. The projection of $\underline{A}$ can therefore be written as $\underline{A}_\mathcal{K} = \underline{P}\underline{P}^\dagger\underline{A}\underline{P}\underline{P}^\dagger = \underline{P}\underline{V}\underline{P}^\dagger$ with $\underline{V} \coloneqq \underline{P}^\dagger\underline{A}\underline{P}$. The elements of the matrix $\underline{V}$ are easily calculated as

$$\begin{aligned} V_{lk} = \boldsymbol{x}_l^\dagger \underline{A}\boldsymbol{x}_k &= \boldsymbol{x}_l^\dagger \Big(\|\underline{A}\boldsymbol{x}_k\| \boldsymbol{x}_{k+1} + \sum_{m=0}^{k} (\boldsymbol{x}_m^\dagger \underline{A}\boldsymbol{x}_k)\boldsymbol{x}_m \Big) \\ &= \|\underline{A}\boldsymbol{x}_k\| \underbrace{\boldsymbol{x}_l^\dagger \boldsymbol{x}_{k+1}}_{\delta_{l,k+1}} + \sum_{m=0}^{k} (\boldsymbol{x}_m^\dagger \underline{A}\boldsymbol{x}_k) \underbrace{\boldsymbol{x}_l^\dagger \boldsymbol{x}_m}_{\delta_{l,m}}, \end{aligned} \tag{3.4}$$

which already come up during the construction of the basis. Because this expression is zero whenever $k + 1 < l$, $\underline{V}$ has upper Hessenberg form.

To evaluate eq. 3.1 using this algorithm, we choose $\underline{A} \equiv \underline{\mathcal{L}}$, the Liouville matrix in our established manybody basis, and $\boldsymbol{x} \equiv \boldsymbol{\rho}_0$, the density vector at $t = 0$. By construction, the density vector in the Krylov basis is $\underline{P}^\dagger \boldsymbol{\rho}_0 = (\|\boldsymbol{\rho}_0\|, 0, 0, \dots)^{\mathrm{T}}$. With this, and $\underline{P}^\dagger \underline{P} = \mathbb{1}$, eq. 3.1 becomes

$$\boldsymbol{\rho}(t) = e^{t\underline{\mathcal{L}}}\boldsymbol{\rho_0} \approx e^{t\underline{\mathcal{L}}_\mathcal{K}}\boldsymbol{\rho_0} = e^{t\underline{P}\underline{V}\underline{P}^\dagger}\boldsymbol{\rho}_0 = \underline{P}e^{t\underline{V}}\underline{P}^\dagger\boldsymbol{\rho}_0$$

where $\underline{V}$ is now only an $N \times N$ matrix, which we can choose to be small, so $e^{t\underline{V}}$ is a numerically tractable operation.

How large t can be chosen without too much deviation from the exact solution, depends on the number of Krylov vectors N. Or, equivalently, how many Krylov vectors are needed depends on how big the timestep t should be. In both cases, a good criterion to inspect is the coefficient vector of the result in the Krylov space $\boldsymbol{c} \coloneqq e^{t\underline{V}}\underline{P}^\dagger\boldsymbol{\rho}_0$. Naturally, from the construction of the Krylov space, the magnitude of the elements in $\boldsymbol{c} = (c_1, c_2, \dots, c_N)^{\mathrm{T}}$ will become negligibly small at some index k, such that $c_j \ll \|\boldsymbol{c}\|$ for $j \geq k$. In the ideal case, k is equal to N, which means all but one Krylov vectors contribute to the result, so no computational time was wasted creating too many vectors, and the result is still accurate.

To evaluate the steady state, we decided to fix the number of Krylov vectors at $N = 20$ and adjust the timestep accordingly, such that the relative weight of the last coefficient is negligible. We chose this limit to be

$$\frac{c_N}{\|\boldsymbol{c}\|} \overset{!}{<} \varepsilon_{\boldsymbol{c}}. \tag{3.5}$$

A reliable choice was $\varepsilon_c = 10^{-10}$. One needs to be careful, however, when checking for this condition. An almost-vanishing coefficient c_N does not necessarily mean convergence. Instead, the timestep might be too large and the N-th vector just happens to not contribute to the result. Therefore, we always start at some small initial time step ($t = 0.01$ proved to be stable in most cases), and then repediately increase t until eq. 3.5 is no longer fulfilled, which means the result from the last iteration is still acceptable. This method is computationally cost-effective, because exponentiating a 20×20 matrix is much cheaper than generating Krylov vectors.

Finally, we chose $\boldsymbol{I}$ as the initial vector $\boldsymbol{\rho}_0$ and applied the procedure described above, i. e. time-evolved as far as permitted by the condition 3.5 to get $\boldsymbol{\rho}_1$. From this point, we time-evolved again to $\boldsymbol{\rho}_2$ and so on, until convergence was reached. The break condition was that the relative change of $\boldsymbol{\rho}_n$ is small.

$$\Delta_{\boldsymbol{\rho}_n} \coloneqq \frac{\|\dot{\boldsymbol{\rho}}_n\|}{\|\boldsymbol{\rho}_n\|} = \frac{\|\underline{\mathcal{L}}\boldsymbol{\rho}_n\|}{\|\boldsymbol{\rho}_n\|} \overset{!}{<} \Delta_{\boldsymbol{\rho}}$$

In our calculations $\Delta_{\boldsymbol{\rho}} = 10^{-6}$ in inverse time units given by the parameters showed to be sufficient and was therefore used for all produced results.

3.4 Green functions

From the steady state, we are now interested in numerically calculating retarded and Keldysh Green functions $G^{\mathrm{R}}_{\sigma\sigma}(\omega)$ and $G^{\mathrm{K}}_{\sigma\sigma}(\omega)$.

3.4.1 Time evolution

Since we already implemented a time evolution algorithm, one obvious choice would be to calculate equations 2.19 directly in the time domain and then Fourier transform the results to get $G^{\mathrm{R}}_{\sigma\sigma}(\omega)$ and $G^{\mathrm{K}}_{\sigma\sigma}(\omega)$. One detail in contrast to the last chapter must be considered, which is that the size of the time steps has to be constant for every step. Therefore, the number of Krylov vectors must be adapted accordingly.

This method, however, turned out to be inefficient and suffer from numerical instabilities. All results given later were therefore achieved using the two-sided Lanczos method discussed below.

3.4.2 Two-sided Lanczos

One other option to calculate the Green functions is to calculate them directly in the frequency domain using the equations 2.20. Therefore, we need to numerically evaluate

$$\boldsymbol{I}^\dagger \underline{c}^\dagger_{f\sigma} \frac{1}{\omega + i\underline{\mathcal{L}}} \underline{c}_{f\sigma}\, \boldsymbol{\rho}_{\mathrm{ss}} \qquad \text{and} \qquad \boldsymbol{I}^\dagger \underline{c}_{f\sigma} \frac{1}{\omega - i\underline{\mathcal{L}}}\, \underline{c}^\dagger_{f\sigma} \boldsymbol{\rho}_{\mathrm{ss}}. \tag{3.6}$$

These expressions suggest that eigenvalues of $\hat{\mathcal{L}}$ whose imaginary part lies in the range of the ω-values we consider will have the largest contribution. However, the matrix is again far too large to invert numerically, which is why we approximate it by a Krylov space method.

One major drawback of the Arnoldi iteration is that the Gram-Schmidt orthogonalization becomes more and more expensive for each added vector, because it must be orthogonalized against the full already existing basis. Since for the time evolution we could simply choose a sufficiently small number of Krylov vectors, this did not pose a problem. For the Green functions, however, we can not make that choice. We need a subspace that approximates all important eigenvalues of $\hat{\mathcal{L}}$ at once, which might be significantly larger than is practical for the Arnoldi scheme.

An algorithm without this orthogonalization problem is the two-sided Lanczos method [30], sometimes also called unsymmetric Lanczos or Bilanczos. Instead of relying on only products of the start vector with the matrix from the left to form a basis – which approximates the right-sided eigenbasis – the two-sided Lanczos algorithm uses also an approximation to the left-sided eigenbasis.

Two pairwise orthogonal bases, $\boldsymbol{l}_j$ and $\boldsymbol{r}_j$, are constructed such that $\boldsymbol{l}_i^\dagger \boldsymbol{r}_j = \delta_{ij}$. The former is extracted from the already known right-sided Krylov vectors with some start vector $\boldsymbol{r}$, which are $\boldsymbol{k}_j^\mathrm{r} = \underline{A}^j \boldsymbol{r}$, $j \in \mathbb{N}_0$, and the latter comes from the Krylov vectors approximating the left eigenbasis with a possibly different start vector $\boldsymbol{l}$, which are $\boldsymbol{k}_j^\mathrm{l} = \boldsymbol{l}^\dagger \underline{A}^j$, $j \in \mathbb{N}_0$.

function Bilanczos($\underline{A}$, $\boldsymbol{l}$, $\boldsymbol{r}$, N)
- $\underline{V} \leftarrow \underline{0}, \quad k \leftarrow 1$
- $\boldsymbol{l}_0 \leftarrow \boldsymbol{l}/\sqrt{\boldsymbol{l}^\dagger \cdot \boldsymbol{r}}, \quad \boldsymbol{r}_0 \leftarrow \boldsymbol{r}/\sqrt{\boldsymbol{l}^\dagger \cdot \boldsymbol{r}}$
- $\boldsymbol{l}_1 \leftarrow \boldsymbol{0}, \quad \boldsymbol{r}_1 \leftarrow \boldsymbol{0}$
- $\boldsymbol{l}_2 \leftarrow \boldsymbol{0}, \quad \boldsymbol{r}_2 \leftarrow \boldsymbol{0}$
- $V_{0,0} \leftarrow \boldsymbol{l}_0^\dagger \cdot \underline{A} \cdot \boldsymbol{r}_0$
- **while** $k < N$ **do**
  - $\boldsymbol{l}_{k \bmod 3}^\dagger \leftarrow \boldsymbol{l}_{(k-1) \bmod 3}^\dagger \cdot \underline{A} - V_{k-1,k-1} \cdot \boldsymbol{l}_{(k-1) \bmod 3}^\dagger - V_{k-1,k-2} \cdot \boldsymbol{l}_{(k-2) \bmod 3}^\dagger$
  - $\boldsymbol{r}_{k \bmod 3} \leftarrow \underline{A} \cdot \boldsymbol{r}_{(k-1) \bmod 3} - V_{k-1,k-1} \cdot \boldsymbol{r}_{(k-1) \bmod 3} - V_{k-1,k-2} \cdot \boldsymbol{r}_{(k-2) \bmod 3}$
  - $V_{k,k-1} \leftarrow \sqrt{\boldsymbol{l}_{k \bmod 3}^\dagger \cdot \boldsymbol{r}_{k \bmod 3}}$
  - $V_{k-1,k} \leftarrow V_{k,k-1}$
  - **if** $V_{k,k-1} = 0$ **then**
    - **if** $\|\boldsymbol{l}_{k \bmod 3}\| = 0$ **or** $\|\boldsymbol{r}_{k \bmod 3}\| = 0$ **then** ▷ Invariant subspace?
      - $N \leftarrow k$ ▷ We can only produce k vectors
    - **else**
      - **error** Breakdown at iteration k
  - **else**
    - $\boldsymbol{l}_{k \bmod 3}^\dagger \leftarrow \boldsymbol{l}_{k \bmod 3}^\dagger / V_{k,k-1}, \quad \boldsymbol{r}_{k \bmod 3} \leftarrow \boldsymbol{r}_{k \bmod 3} / V_{k,k-1}$ ▷ Normalize
    - $V_{k,k} \leftarrow \boldsymbol{l}_{k \bmod 3}^\dagger \cdot \underline{A} \cdot \boldsymbol{r}_{k \bmod 3}$
  - $k \leftarrow k + 1$
- **return** $\underline{V}, N$

Algorithm 2: Algorithmic sketch of the two-sided Lanczos method. Corrections for finite-precision errors and numerical optimizations are omitted for readability.[1]

In our case, where we are only interested in the eigenvalues of $\underline{A}$, there are three possible end states. Normal termination occurs when either N Krylov vectors were produced, or invariant left- or right-sided subspaces were found. In the latter case, analogous to the Arnoldi iteration, at least one of the two last produced vectors had a norm of zero.

If, however, the overlap between two newly produced left- and right-sided vectors vanishes without one of them being zero, a so-called breakdown occurs, from which the algorithm can not recover. Even though there are methods to prevent this [58], we did not encounter such problems in the first place.

[1] In this symbolic sketch, Matrix elements of negative indices are defined to be 0.

In contrast to the Arnoldi scheme, the newly produced vectors only need to be orthogonalized against the last two. This can be seen by explicitly calculating the unnormalized vector $\boldsymbol{r}'_{k+1}$.

$$\boldsymbol{r}'_{k+1} = \underline{A}\boldsymbol{r}_k - \sum_{m=0}^{k} (\boldsymbol{l}_m^\dagger \underline{A}\boldsymbol{r}_k)\boldsymbol{r}_m = \underline{A}\boldsymbol{r}_k - \sum_{m=k-1}^{k} (\boldsymbol{l}_m^\dagger \underline{A}\boldsymbol{r}_k)\boldsymbol{r}_m$$

$$= \underline{A}\boldsymbol{r}_k - (\boldsymbol{l}_{k-1}^\dagger \underline{A}\boldsymbol{r}_k)\boldsymbol{r}_{k-1} - (\boldsymbol{l}_k^\dagger \underline{A}\boldsymbol{r}_k)\boldsymbol{r}_k$$

The second equality holds because $\boldsymbol{l}_m^\dagger \underline{A}$ is in $\operatorname{span}\{\boldsymbol{l}_0, \ldots, \boldsymbol{l}_{m+1}\}$, which is orthogonal to $\boldsymbol{r}_k$ if $m < k-1$. The results for $\boldsymbol{l}'_{k+1}$ are analogous. In addition to this saving computational time, this three-term recurrence has the benefit of saving memory, because at all times only six vectors (three for each basis) must be kept in memory.

Since all $\boldsymbol{r}_i$ can be multiplied by some factor α and $\boldsymbol{l}_i$ by α^{-1} without violating the orthonormality, there is an additional degree of freedom for the bases. We chose to split the normalization evenly between the left- and right-sided vectors, which makes the super- and subdiagonals equal.

$$\boldsymbol{r}_{k+1} = \boldsymbol{r}'_{k+1} \left(\boldsymbol{l}'^\dagger_{k+1} \boldsymbol{r}'_{k+1}\right)^{-\frac{1}{2}} \qquad \boldsymbol{l}^\dagger_{k+1} = \boldsymbol{l}'^\dagger_{k+1} \left(\boldsymbol{l}'^\dagger_{k+1} \boldsymbol{r}'_{k+1}\right)^{-\frac{1}{2}}$$

Analogous to the Arnoldi method, one can define matrices $\underline{P}_\mathrm{l} = (\boldsymbol{l}_0, \boldsymbol{l}_1, \ldots, \boldsymbol{l}_{N-1})$ and $\underline{P}_\mathrm{r} = (\boldsymbol{r}_0, \boldsymbol{r}_1, \ldots, \boldsymbol{r}_{N-1})$ with the new basis vectors in their columns. To get $\underline{A}$ in the subspace, an operation comparable to a similarity transformation with a cut-off basis is performed.

$$\underline{A} \approx \underline{P}_\mathrm{r} \underline{P}_\mathrm{l}^\dagger \underline{A} \underline{P}_\mathrm{r} \underline{P}_\mathrm{l}^\dagger = \underline{P}_\mathrm{r} \underline{V} \underline{P}_\mathrm{l}^\dagger$$

Here, $\underline{V} \coloneqq \underline{P}_\mathrm{l}^\dagger \underline{A} \underline{P}_\mathrm{r}$ is the representation of $\underline{A}$ in the subspace, and the eigenvalues of $\underline{V}$ approximate those of $\underline{A}$. The elements of $\underline{V}$ can be calculated analogous to equation 3.4, with $\underline{A}$ being the matrix to approximate. Unlike for the Arnoldi iteration, $\underline{A}$ can now also be applied to the left to give a different basis vector.

$$V_{jk} = \boldsymbol{l}_j^\dagger \underline{A}\boldsymbol{r}_k = \|\underline{A}\boldsymbol{r}_k\| \underbrace{\boldsymbol{l}_j^\dagger \boldsymbol{r}_{k+1}}_{\delta_{j,k+1}} + \sum_{m=0}^{k} (\boldsymbol{l}_m^\dagger \underline{A}\boldsymbol{r}_k) \underbrace{\boldsymbol{l}_j^\dagger \boldsymbol{r}_m}_{\delta_{j,m}}$$

$$= \|\boldsymbol{l}_j^\dagger \underline{A}\| \underbrace{\boldsymbol{l}_{j+1}^\dagger \boldsymbol{r}_k}_{\delta_{j+1,k}} + \sum_{m=0}^{j} (\boldsymbol{l}_j^\dagger \underline{A}\boldsymbol{r}_m) \underbrace{\boldsymbol{l}_m^\dagger \boldsymbol{r}_k}_{\delta_{m,k}}$$

This expression vanishes whenever $j > k+1$ (first line), or $k > j+1$ (second line). Thus, the representation $\underline{V}$ is tridiagonal, with $V_{kk} = \boldsymbol{l}_k^\dagger \underline{A}\boldsymbol{r}_k$ on its diagonal and $V_{j+1,k} = \|\boldsymbol{l}_j^\dagger \underline{A}\| = \|\underline{A}\boldsymbol{r}_k\| = V_{j,k+1}$ on its super- and subdiagonal. The center equality only holds with the our exact choice of basis normalization.

Because $\underline{P}_\mathrm{l}^\dagger \underline{P}_\mathrm{r} = \mathbb{1}$ by construction, the powers of $\underline{A}$ in the subspace are

$$(\underline{P}_\mathrm{r} \underline{V} \underline{P}_\mathrm{l}^\dagger)^n = \underline{P}_\mathrm{r} \underline{V}^n \underline{P}_\mathrm{l}^\dagger.$$

If we now start with

$$\boldsymbol{r} \equiv \underline{c}_{f\sigma}^{(\dagger)} \boldsymbol{\rho}_\mathrm{ss}, \quad \boldsymbol{l} \equiv \underline{c}_{f\sigma}^{(\dagger)} \boldsymbol{I}, \quad \text{and} \quad \underline{A} \equiv \underline{\mathcal{L}},$$

the representations in the subspaces are

$$\underline{P}_\mathrm{l}^\dagger \underline{c}_{f\sigma}^{(\dagger)} \boldsymbol{\rho}_\mathrm{ss} = \left(\left\| \underline{c}_{f\sigma}^{(\dagger)} \boldsymbol{\rho}_\mathrm{ss} \right\|, 0, 0, \ldots \right)^\mathrm{T}$$

$$\underline{c}_{f\sigma}^{(\dagger)} \boldsymbol{I}^\dagger \underline{P}_\mathrm{r} = \left(\left\| \underline{c}_{f\sigma}^{(\dagger)} \boldsymbol{I} \right\|, 0, 0, \ldots \right).$$

The eqs. 3.6 therefore turn into

$$\boldsymbol{I}^\dagger \underline{c}_{f\sigma}^{(\dagger)} \frac{1}{\omega \pm i\underline{\mathcal{L}}} \underline{c}_{f\sigma}^{(\dagger)} \boldsymbol{\rho}_\mathrm{ss} \approx \left(\frac{1}{\omega \pm i\underline{V}} \right)_{0,0}$$

which can be evaluated numerically, e. g. using left-division in MATLAB, because the dimension of $\underline{V}$ is typically smaller than 10 000.

To converge the Green functions $G_\sigma^\mathrm{R}(\omega)$ and $G_\sigma^\mathrm{K}(\omega)$ with this method, we first omit the spin index σ for a moment and denote the functions computed with N Krylov vectors as $G_N^\mathrm{R}(\omega)$ and $G_N^\mathrm{K}(\omega)$. We now produce Krylov vectors and calculate the Green functions when N is a multiple of some number n. During this iteration we check how much the functions changed within a given interval $[-\omega_\mathrm{max}, \omega_\mathrm{max}]$, which should include all sections of interest, by integrating the squared absolute difference between successive functions.

$$\Delta_{G_k} \coloneqq \frac{1}{2\omega_\mathrm{max}} \sum_{\alpha \in \{\mathrm{R,K}\}} \int_{-\omega_\mathrm{max}}^{\omega_\mathrm{max}} \left| G_{kn}^\alpha(\omega) - G_{kn+n}^\alpha(\omega) \right|^2 d\omega \overset{!}{<} \Delta_G$$

Convergence is reached when the change is smaller than some upper bound Δ_G. The choice $n = 10$ proved to be efficient in our calculations, while Δ_G must be adjusted depending on the model parameters. It is usually in the range 10^{-6}–10^{-8} in the inverse squared energy units the calculation was carried out in.

Chapter 4

Results

Here we will first show calculations to check the accuracy of the approach by comparing our results with previous work using different approximations [23, 27]. Then we present some further results on the Franck-Condon blockade and with on-site Coulomb repulsion.

4.1 General remarks

In the calculations carried out here, the hoppings and chemical potentials were always symmetrical, so

$$\mu_{\mathrm{R}} = -\mu_{\mathrm{L}} = \frac{\Phi}{2} \qquad \text{and} \qquad t_{\mathrm{L}} = t_{\mathrm{R}},$$

with Φ being the bias voltage. If not stated otherwise, the energy unit is always the negative height of the imaginary part of the retarded hybridization at $\omega = 0$, which is often referred to as the *hybridization strength* and denoted by $\Gamma \coloneqq -\operatorname{Im}[\Delta^{\mathrm{R}}_{\mathrm{phys}}(0)]$.

We worked with two different types of density of states in the leads. The first is a flat band with a finite bandwidth of $2\omega_{\mathrm{c}}$ and smoothed-out edges. Smooth edges are generated by fermi functions at a chosen inverse temperature β_{edge}. The spectral density is therefore

$$A_{\mathrm{lead}}(\omega) = \frac{1}{Z}\left[1 + e^{\beta_{\mathrm{edge}}(\omega-\omega_{\mathrm{c}})}\right]^{-1}\left[1 + e^{-\beta_{\mathrm{edge}}(\omega+\omega_{\mathrm{c}})}\right]^{-1},$$

where Z is the partition function. From eq. 2.12, the imaginary part of the retarded hybridization of lead α is directly given by $\operatorname{Im}[\Delta^{\mathrm{R}}_{\alpha}(\omega)] = -\pi t_{\alpha}^2 A_{\mathrm{lead}}(\omega)$. The real part is then fixed by the Kramers-Kronig relations [45, p. 147]

$$\operatorname{Re}[\Delta^{\mathrm{R}}_{\alpha}(\omega)] = -\frac{1}{\pi}\mathcal{P}\int_{-\infty}^{\infty}\frac{\operatorname{Im}[\Delta^{\mathrm{R}}_{\alpha}(\omega')]}{\omega-\omega'}d\omega',$$

where $\mathcal{P}$ means the Cauchy principal value, and the integration is carried out numerically to obtain the full retarded hybridization.

Because the band is flat, we do not shift the whole density of states by the chemical potential, but rather only the filling, i. e. the energy up to which the states are occupied. Consequently, the total retarded hybridization is

$$\mathrm{Im}[\Delta^{\mathrm{R}}(\omega)] = \sum_{\alpha} \mathrm{Im}[\Delta^{\mathrm{R}}_{\alpha}(\omega)] = \Gamma \left[1 + e^{\beta_{\mathrm{edge}}(\omega-\omega_{\mathrm{c}})}\right]^{-1} \left[1 + e^{-\beta_{\mathrm{edge}}(\omega+\omega_{\mathrm{c}})}\right]^{-1}$$

with its numerically determined real part. The Keldysh hybridization is purely imaginary (cf. eq. A.3), and because the disconnected leads are in equilibrium, it satisfies the fluctuation-dissipation theorem.

$$\Delta^{\mathrm{K}}(\omega) = \Delta^{\mathrm{K}}_{\mathrm{L}}(\omega) + \Delta^{\mathrm{K}}_{\mathrm{R}}(\omega) = 2i\,\mathrm{Im}[\Delta^{\mathrm{R}}(\omega)](1 - f(\omega; T, \mu_{\mathrm{L}}) - f(\omega; T, \mu_{\mathrm{R}}))$$

The second type of lead density of states we worked with was a single Lorentzian as in [27], which results in

$$\Delta^{\mathrm{R}}_{\alpha}(\omega) = \frac{\Gamma}{2} \frac{D}{(\omega - \mu_{\alpha}) + iD}$$

and

$$\Delta^{\mathrm{R}} = \Delta^{\mathrm{R}}_{\mathrm{R}} + \Delta^{\mathrm{R}}_{\mathrm{L}},$$

which can effectively be turned into a flat band again by choosing D very large. As above, the Keldysh part of the hybridization is determined by $\Delta^{\mathrm{R}}_{\alpha}$, T, and μ_{α}.

In the following, we will refer to the former density of states as flat band, and to the latter as Lorentzian. Additionally, whenever no U is mentioned in the parameters, the calculation was done without spin.

4.2 Lang-Firsov transformation

As a first integrity check, we performed calculations with identical parameters, with and without the Lang-Firsov transformation. Since for $N_{b,\max} \to \infty$ both the transformed and untransformed systems are equivalent, their characteristics – and with that their Green functions – must converge to the same results. However, for reasons discussed in sec. 2.8, we expect smaller deviations from the true result in the transformed system.

The check is done in the auxiliary system only, because then the accuracy of the convergence is more easily controllable. The results shown here were calculated with no potential difference between the leads and for a system without spin. The results with a bias voltage and the ones with spin show very similar behavior to the ones plotted.

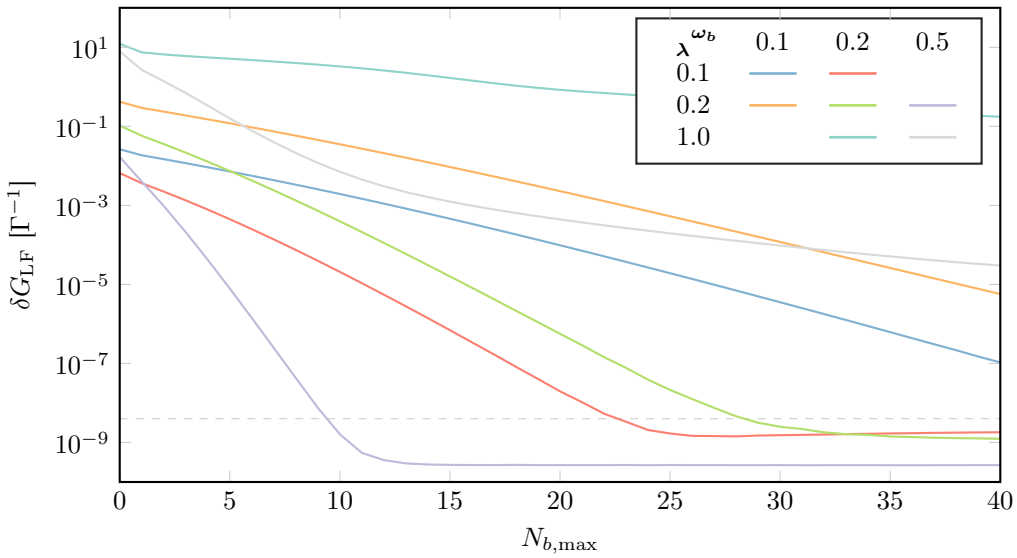

Figure 4.1: Sum of the integrated quadratic differences of the auxiliary Green functions with and without Lang-Firsov transformation δG_{LF} vs the maximum bosonic occupation numbers $N_{b,\max}$. The grey dashed line marks the maximum expected deviation of $\delta G_{\mathrm{LF}} = 4 \cdot 10^{-9}\,\Gamma^{-1}$.

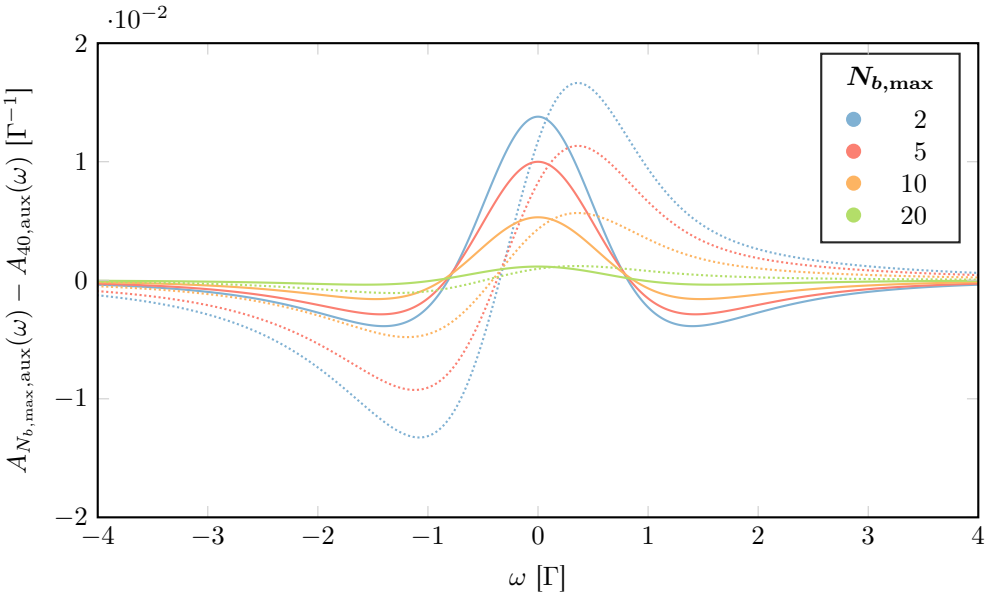

Figure 4.2: Exemplary convergence behavior of the spectral function $A(\omega)$ for both transformed (solid lines) and untransformed (dotted lines) systems with the parameters $\omega_b = 0.1\,\Gamma$, $\lambda = 0.1\,\Gamma$, $\varepsilon_f = 0.1\,\Gamma$. The plot shows the difference of the impurity spectral functions to the converged solution at $N_{b,\max} = 40$ for different cutoffs.

We used a flat band with the parameters

$$\omega_b \in \{0.1, 0.2, 0.5\}\,\Gamma \qquad \lambda \in \{0.1, 0.2, 0.5\}\,\Gamma \qquad \varepsilon_f = \lambda^2/\omega_b \qquad T = 0.05\,\Gamma$$
$$N = 3 \qquad \Phi = 0\,\Gamma \qquad \omega_c = 10\,\Gamma \qquad \beta_{\text{edge}} = 2\,\Gamma^{-1}.$$

Because this is only a consistency check within our approach, three sites were used for faster computational time. A plot of the physical and the auxiliary hybridizations is given in figure B.1. The chosen onsite energy ensures a symmetric spectral density.

To measure the deviation from the converged result we used the integrated quadratic absolute difference of the transformed and untransformed systems, summed over the Keldysh and retarded Green function.

$$\delta G_{\text{LF}} = \sum_{\alpha \in \{\text{R,K}\}} \int_{-\omega_{\max}}^{+\omega_{\max}} |G^{\alpha}_{\text{aux,LF}}(\omega) - G^{\alpha}_{\text{aux}}(\omega)|^2 \, d\omega$$

The convergence criterion for the individual results was chosen to be $\Delta_G = 10^{-9}\,\Gamma^{-1}$, which means we can expect δG_{LF} to drop to the order of $4 \cdot 10^{-9}\,\Gamma^{-1}$ for sufficiently large cutoff.

We see good convergence in fig. 4.1, which of course depends on the specific choice of parameters. Higher ratios of λ/ω_b tend to converge slower than lower ones. For equal ratios, higher bosonic energies also accelerate convergence. Furthermore, upon inspection of the spectral functions – like in the example in fig. 4.2 – we see that the transformed calculations converge quicker than their untransformed counterparts, in the sense that for equal cutoff they have a smaller total deviation from the converged result.

4.3 Limit of weak coupling to the leads

To ensure correct asymptotic behavior, we examined the case of diminishing electronic coupling to the leads, so $t_{\text{L,R}} \to 0$. In this case, the spectral density of the interacting system should approach that of the isolated impurity, which is easy to calculate by numerically evaluating the analytical formulas for the Green functions in sec. A.4. This is possible because the Fock space of the isolated impurity is reasonably small. As small imaginary unit we used $5i \cdot 10^{-4}$, and the density operator at the impurity was set to thermal equilibrium.

The fit was the same as for the Lang-Firsov transformation check (fig. B.1) and the parameters were

$$\omega_b = 0.5\,\Gamma \qquad \lambda = 0.5\,\Gamma \qquad \varepsilon_f = 0.5\,\Gamma \qquad T = 0.05\,\Gamma$$
$$N = 3 \qquad \Phi = 0\,\Gamma \qquad \omega_c = 10\,\Gamma \qquad \beta_{\text{edge}} = 2\,\Gamma^{-1}.$$

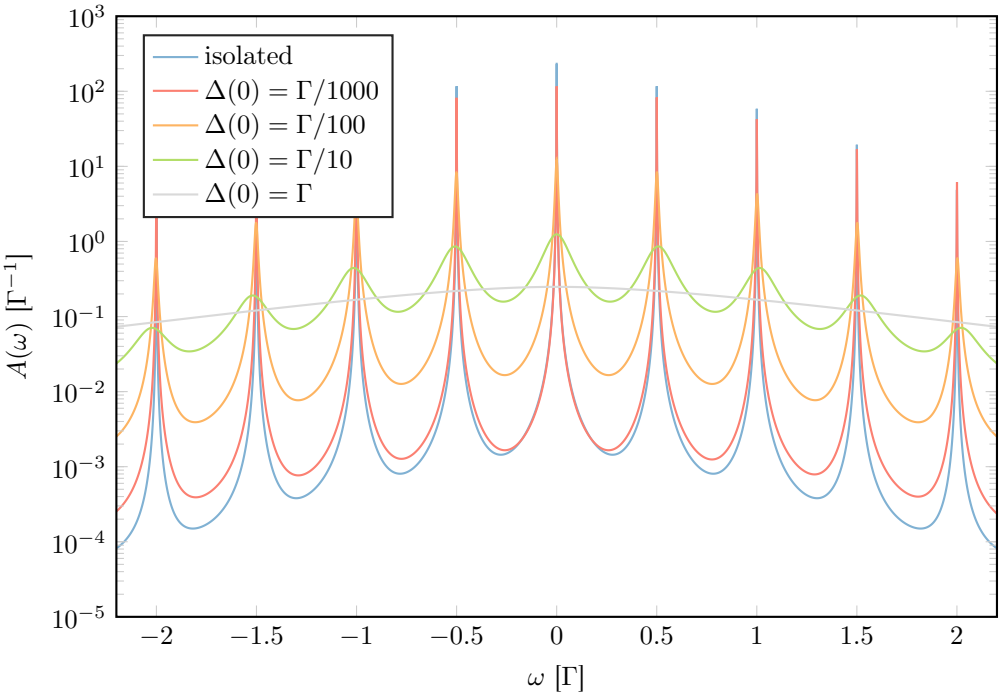

Figure 4.3: Impurity spectral functions in the limit of weak coupling to the leads.

We then repeated the calculation with smaller values of $t_{\mathrm{L/R}}$, such that the height of the hybridization was scaled down by powers of ten. In contrast to before, the results are those for the physical system with only the self energy estimated from the auxiliary one.

Figure 4.3 shows the results. We see very good agreement in the position of the peaks for the weak couplings. Upon close inspection, the peak heights of the manybody calculations do not perfectly match up with the ones of the isolated impurity. This could be attributed to the fact that the temperature is not accurately reproduced by the auxiliary system.

For weak electronic lead couplings, the two-sided Lanczos converges quite slowly, because the many narrow peaks necessitate a large number of Krylov vectors. Therefore, we did not repeat this calculation with more bath sites.

4.4 Comparison with other approximate methods

We now compare our results to two previous results, which treat the Anderson-Holstein model in the spinless case, but with different methods. These are the *real-time path integral approach* (RTPIA) by Mühlbacher and Rabani [23], and the *hierarchical quantum master equation approach* (HQME) by Schinabeck et al. [27].

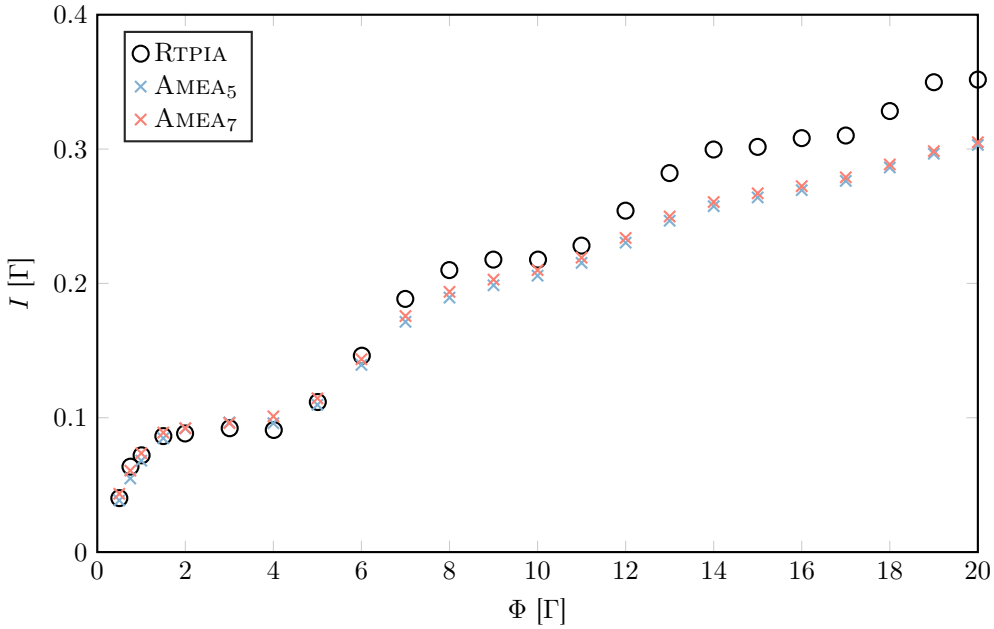

Figure 4.4: Comparison of current I vs bias voltage Φ with results obtained by the real-time path integral approach at $\omega_b = 3\,\Gamma$. The AMEA subscript stands for the number of sites used.

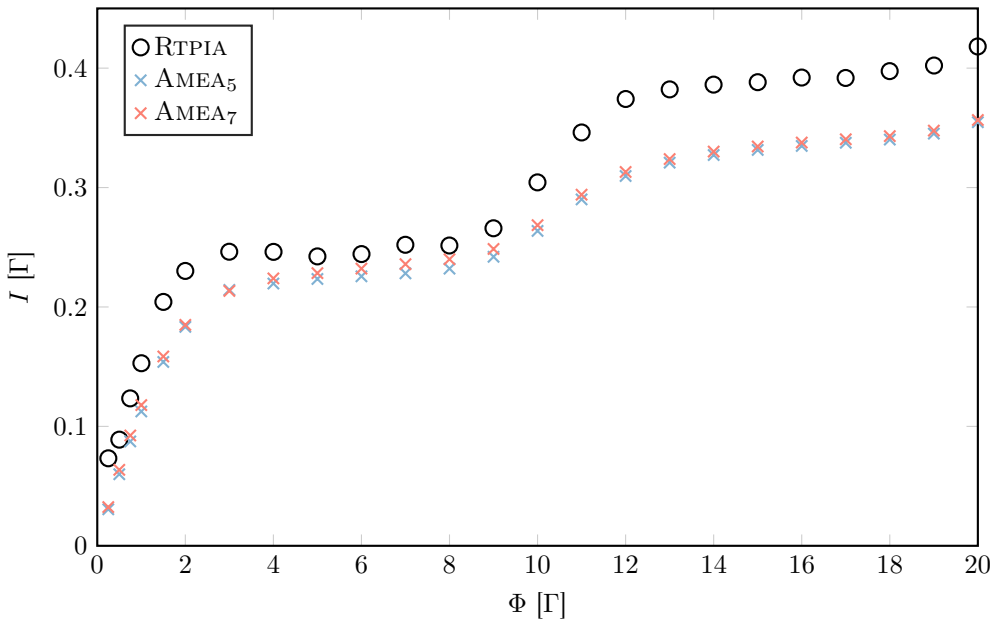

Figure 4.5: Comparison of current I vs bias voltage Φ with results obtained by the real-time path integral approach at $\omega_b = 5\,\Gamma$. The AMEA subscript stands for the number of sites used.

4.4.1 Real-time path integral approach

The real-time path integral approach is an approximative Monte Carlo method that uses time evolution to calculate the steady state current. The reference paper [23] starts from an initially empty impurity. Because the numerical time evolution becomes exponentially more expensive over time, convergence may not be obtainable for all sets of parameters. Our results even suggest that the published data for high bias voltages might not be completely converged.

In accordance with the parameters in the paper, we used a flat band density of states and performed calculations with the following parameters.

$$\begin{array}{llll} \omega_b \in \{3,5\}\,\Gamma & \lambda = 4\,\Gamma & \varepsilon_f = \lambda^2/\omega_b & T = 0.2\,\Gamma \\ N \in \{5,7\} & \Phi \in \{0.25 \ldots 20\}\,\Gamma & \omega_c = 20\,\Gamma & \beta_{\text{edge}} = 5\,\Gamma^{-1} \end{array}$$

Two example fits for $N = 5$ and $N = 7$ at $\Phi = 8\,\Gamma$ are depicted in the appendix (figures B.2 and B.3).

The results are shown in fig. 4.4 and 4.5. The step-like shape is typical for such a phononic system. With the chosen onsite energy, the density of states shows symmetric peaks around zero with the spacing of roughly the phonon energy (see fig. 4.6 and 4.7). Because the bias voltage is applied symmetrically, the steps in the current show a separation of twice the phonon energy.

In the case of $\omega_b = 3\,\Gamma$, we see very good agreement for low voltages up to about $\Phi = 6\,\Gamma$. For higher biases, our results consistently show a lower current, even though the positions of the steps still match.

Because of the finite number of bath sites, Amea sometimes tends to wash out results a bit, since sharp features in the hybridization cannot be resolved. This could also be the case here, as in our results the steps are not as pronounced as in the reference.

However, if we consider the fits for 4 and 6 bath sites, i. e. 5 and 7 total sites, they show a great improvement in accuracy. Still, the corrections to the current are minor. It is therefore justified to assume that the further corrections for even more bath sites will also be small. We are therefore confident that our results are very close to the exact manybody solution.

Similar arguments apply for the case of $\omega_b = 5\,\Gamma$. The qualitative agreement is good, while the heights of the steps are smaller in our calculation. However, the corrections for more bath sites remain small, which again suggests that the differences to the exact result are at most of the same order.

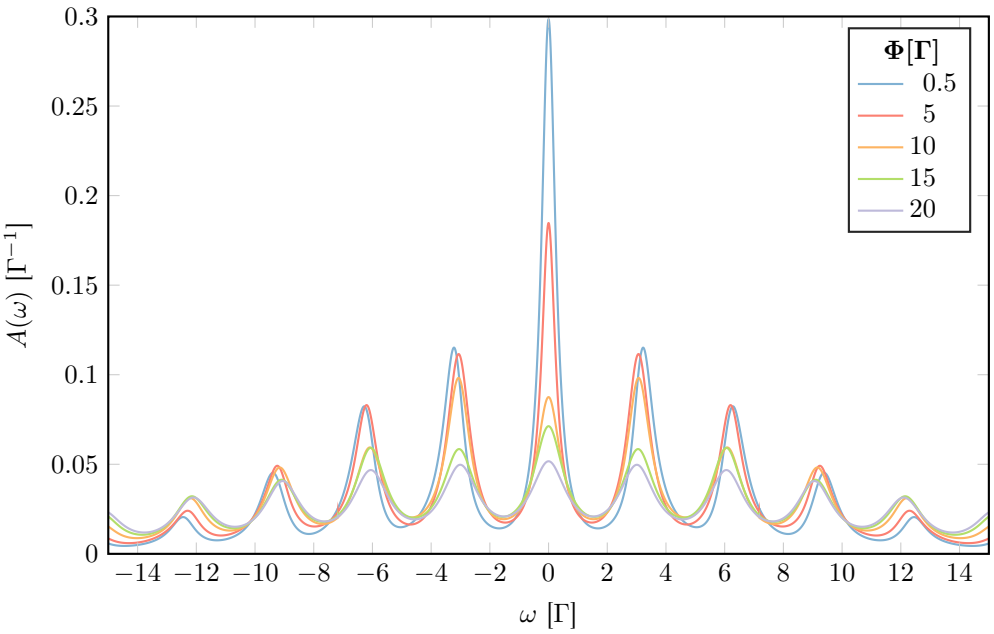

Figure 4.6: Impurity spectral functions of the calculations used for the comparison with Rtpia at $\omega_b = 3\,\Gamma$.

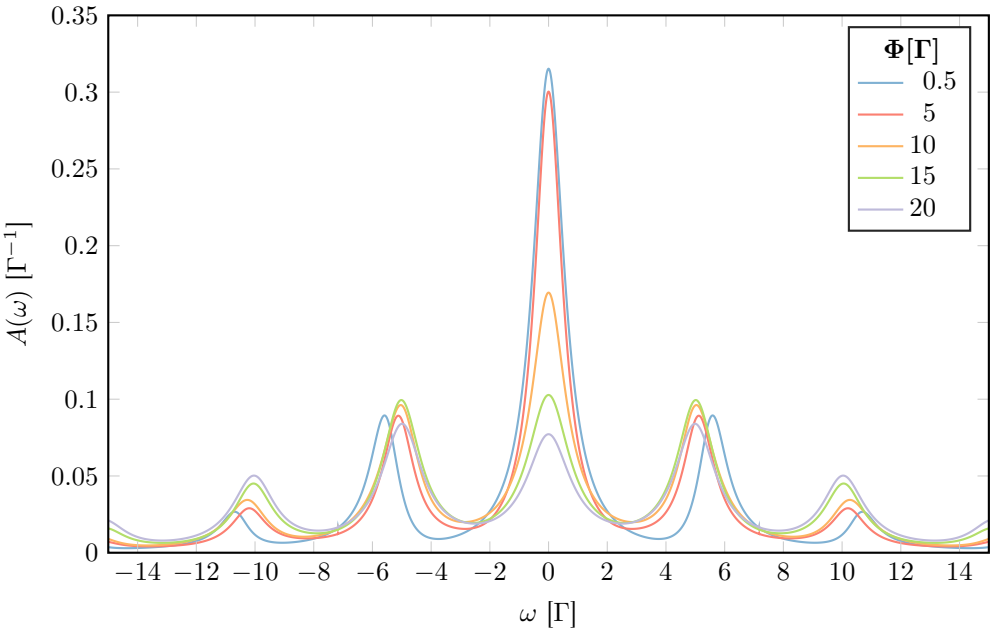

Figure 4.7: Impurity spectral functions of the calculations used for the comparison with Rtpia at $\omega_b = 5\,\Gamma$.

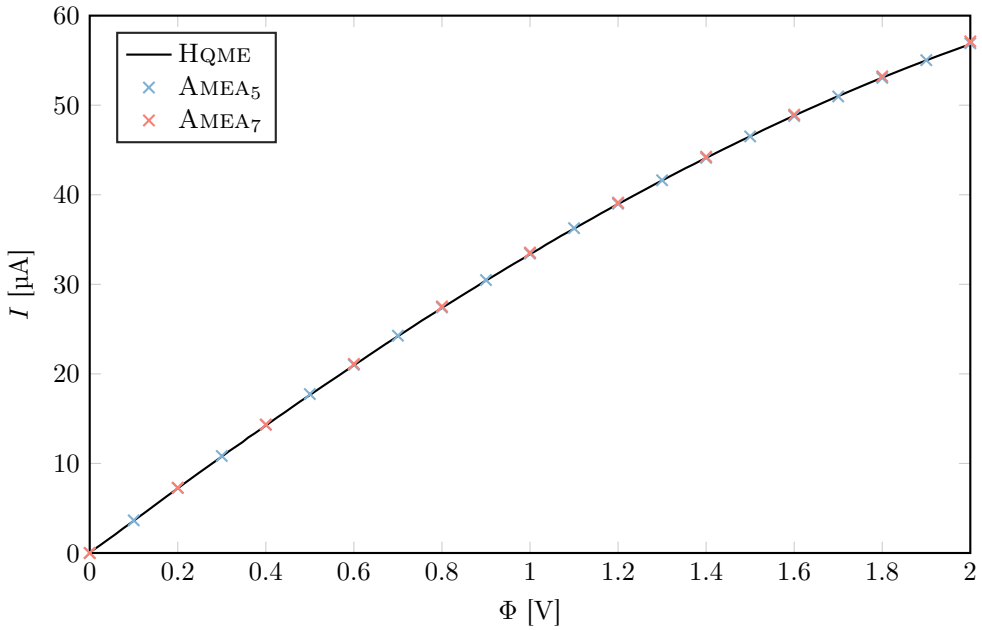

Figure 4.8: Comparison of current I vs bias voltage Φ with results obtained by the hierarchical quantum master equation approach at $\lambda = 0.12\,\mathrm{eV}$ and $\Gamma = 1\,\mathrm{eV}$. The AMEA subscript stands for the number of sites used.

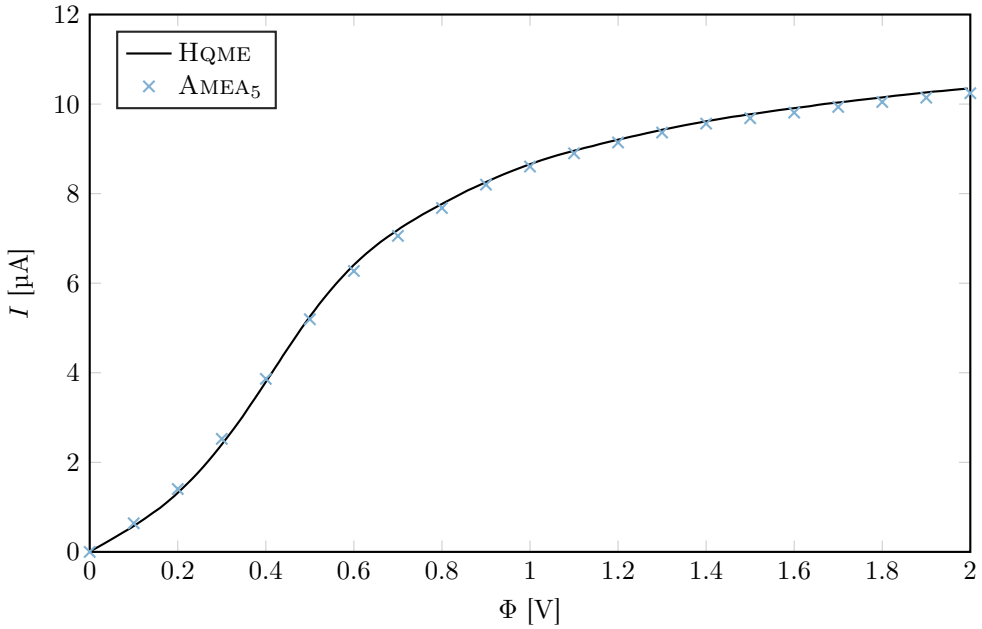

Figure 4.9: Comparison of current I vs bias voltage Φ with results obtained by the hierarchical quantum master equation approach at $\lambda = 0.12\,\mathrm{eV}$ and $\Gamma = 0.1\,\mathrm{eV}$. The AMEA subscript stands for the number of sites used.

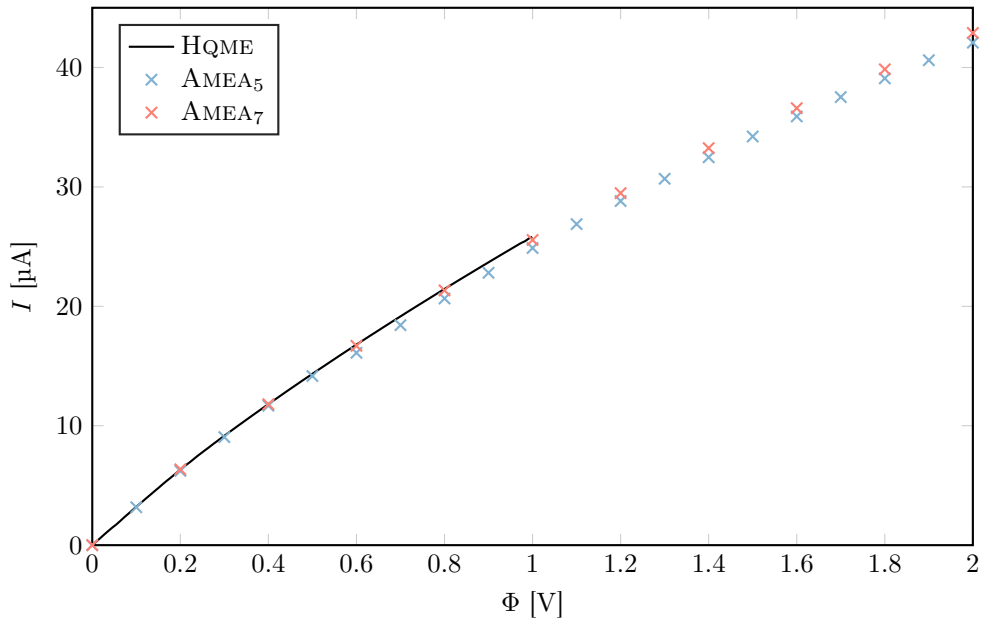

Figure 4.10: Comparison of current I vs bias voltage Φ with results obtained by the hierarchical quantum master equation approach with $\lambda = 0.4\,\mathrm{eV}$ and $\Gamma = 1\,\mathrm{eV}$. The AMEA subscript stands for the number of sites used.

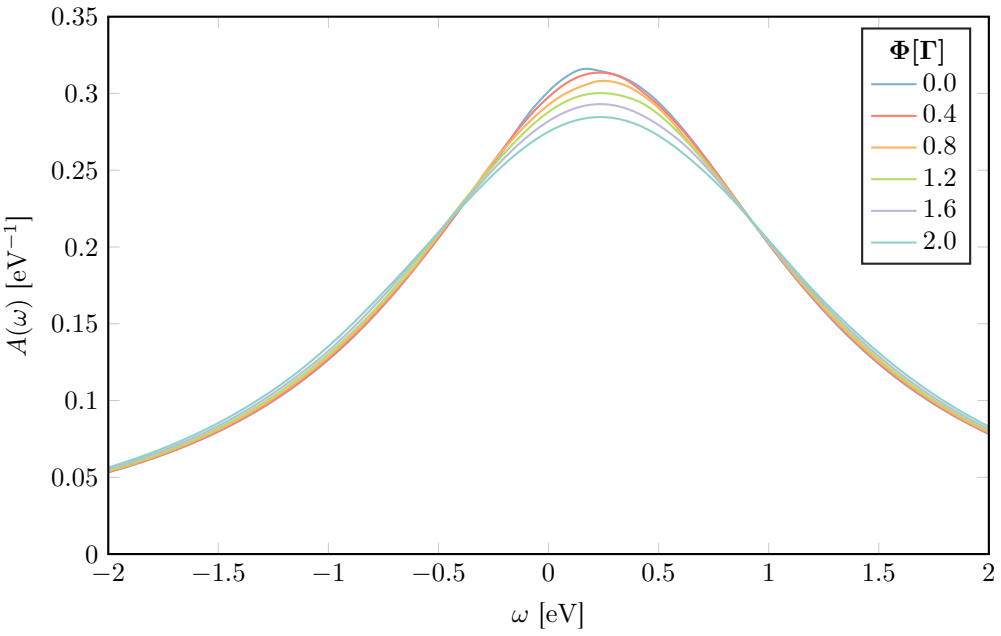

Figure 4.11: Impurity spectral functions of the calculations used for comparison with HQME at $\lambda = 0.12\,\mathrm{eV}$, $\Gamma = 1\,\mathrm{eV}$, and $N = 7$.

4.4.2 Hierarchical quantum master equation approach

The hierarchical quantum master equation approach is a perturbative method, i. e. its strengths are in the regime of small hybridizations Δ. Naturally, one would expect some drawbacks in systems with bigger hybridizations. Nevertheless, we were able to confirm the results for the largest hybridization published in the paper [27] with a high degree of accuracy.

The paper uses a Lorentzian density of states exactly as described in the general remarks with $D = 10^4\,\mathrm{eV}$. Even though with such a large width the Lorentzian essentially describes a flat band again, it influences the real part of the retarded hybridization. We therefore also used such a Lorentzian and performed the first calculation with the following parameters.

$$\begin{array}{llll} \omega_b = 0.2\,\mathrm{eV} & \lambda = 0.12\,\mathrm{eV} & \varepsilon_f = 0.3\,\mathrm{eV} & T = 0.026\,\mathrm{eV} \\ N \in \{5, 7\} & \Phi \in \{0 \ldots 2\}\,\mathrm{eV} & D = 10^4\,\mathrm{eV} & \Gamma \in \{1, 0.1\}\,\mathrm{eV} \end{array}$$

The second set of parameters was

$$\begin{array}{llll} \omega_b = 0.2\,\mathrm{eV} & \lambda = 0.4\,\mathrm{eV} & \varepsilon_f = 1.05\,\mathrm{eV} & T = 0.026\,\mathrm{eV} \\ N \in \{5, 7\} & \Phi \in \{0 \ldots 2\}\,\mathrm{eV} & D = 10^4\,\mathrm{eV} & \Gamma = 1\,\mathrm{eV}. \end{array}$$

Again, example fits at $\Phi = 1\,\mathrm{eV}$ for $N = 5$ and $N = 7$ are in the appendix (fig. B.4 and B.5).

The first thing to note is that the step-like structure from the last section is no longer present in these results. This is a consequence of the low phonon energy. The phononic peaks are so closely spaced that they merge together when broadened by the hybridization with the leads, as can be seen in figure 4.11. Also note that because the onsite energy is no longer λ^2/ω_b, the whole spectrum is shifted off to the right. Spectral densities for the other parameter sets can be found in the appendix. Figures 4.8 and 4.9 show results for the lower of the two electron-phonon couplings.

As mentioned before, the two-sided Lanczos has some convergence issues when there are too many narrow peaks in the spectral density, which is why we only used $N = 5$ for the lower electronic lead coupling of $\Gamma = 0.1\,\mathrm{eV}$. Still we see very good agreement even for $N = 5$. The case of $\Gamma = 1\,\mathrm{eV}$ shows excellent agreement with the reference, and the results for $N = 7$ even cover the $N = 5$ result markers, so we can assume that these are converged.

For stronger electron-phonon coupling (figure 4.10), we find good agreement for low voltages already at $N = 5$, but see slight deviations for $\Phi \gtrsim 0.6\,\mathrm{eV}$. However, with $N = 7$, these disagreements vanish and the data matches up very well.

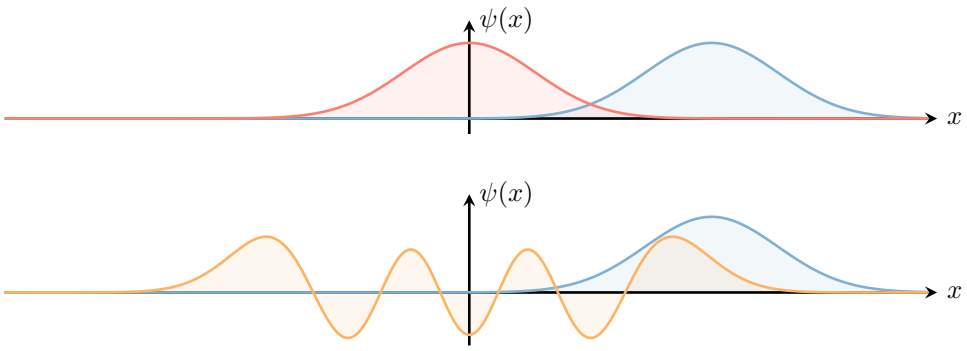

Figure 4.12: Wavefunctions of the harmonic oscillator to visualize the overlap between the unshifted (——) and shifted (——) ground state wavefunctions (top), and between the shifted ground state and the sixth excited state (——) wavefunctions (bottom).

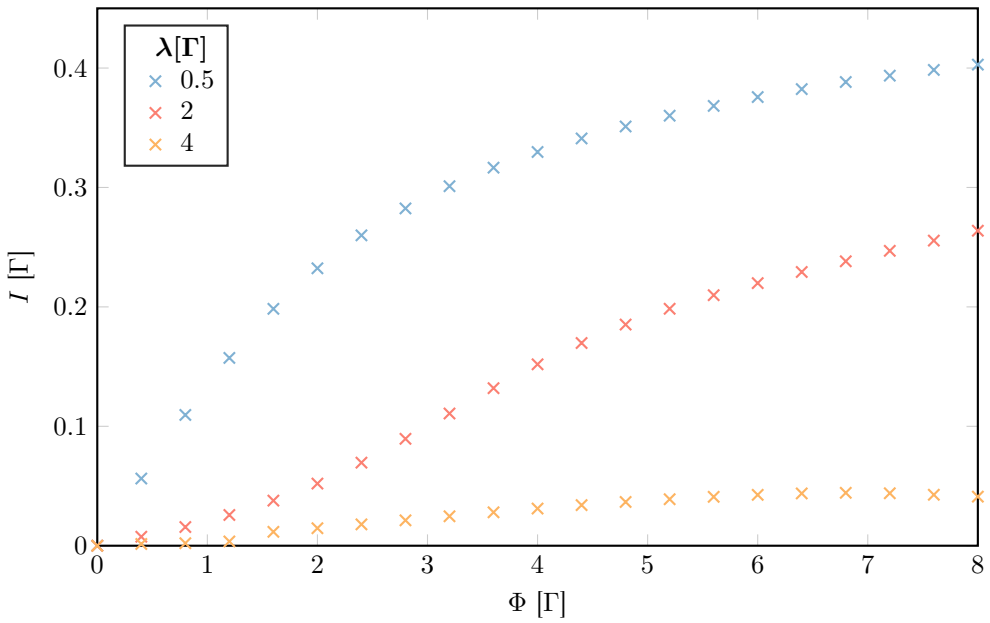

Figure 4.13: Current I versus bias voltage Φ reproducing the Franck-Condon blockade for different coupling strengths λ and $\omega_b = 2\,\Gamma$.

4.5 Franck-Condon blockade

One effect correctly reproduced by our calculations is the so-called Franck-Condon blockade. In a very simple sequential tunneling picture without spin at $T = 0$, the transport takes place as follows. The empty impurity is in its ground state, of which the harmonic oscillator wavefunction is a Gaussian centered at zero. To transfer an electron onto the impurity without expending extra energy to the oscillator, it must also be in the charged ground state, which is a shifted Gaussian (see fig. 4.12). The rate for this process is – by Fermi's golden rule – proportional to the overlap of the two wavefunctions, which decreases exponentially with the spatial shift of the charged oscillator. Therefore, the higher the electron-phonon coupling, the smaller the rate for this process will be.

Other processes, like transferring an electron onto the impurity and at the same time exciting the harmonic oscillator, have a higher rate due to the greater overlap of the wavefunctions (see again fig. 4.12), but require the additional phonon energy in order to take place. In this very simplified picture, we therefore expect the current to be suppressed for large electron-phonon couplings and low bias voltages.

To investigate this effect, we performed a calculation with a Lorentzian density of states (example fit in figure B.10) and the following parameters.

$\omega_b = 2\,\Gamma$	$\lambda \in \{0.5, 2, 4\}\,\Gamma$	$\varepsilon_f = 0\,\Gamma$	$T = 0.2\,\Gamma$
$N = 5$	$\Phi \in \{0 \dots 8\}\,\Gamma$	$D = 10^4\,\Gamma$	

The results in figure 4.13 confirm that this behavior is also present for the full interacting manybody system at finite temperature. Weak coupling ($\lambda = 0.5\,\Gamma$) leads to a fairly steep and linear increase in the current, while for moderate coupling ($\lambda = 2\,\Gamma$) the slope decreases significantly. Upon further increasing the coupling to $\lambda = 4\,\Gamma$, the current is almost completely suppressed for low biases.

4.6 On-site Coulomb repulsion

We also investigated the effect of on-site Coulomb repulsion on the current characteristics. To this end, we used the same fits as in section 4.5 and performed calculations with the following parameters.

$\omega_b = 2\,\Gamma$	$\lambda = 2\,\Gamma$	$\varepsilon_f = -U/2$	$T = 0.2\,\Gamma$
$N = 5$	$\Phi \in \{0 \dots 8\}\,\Gamma$	$D = 10^4\,\Gamma$	$U \in \{1, 2, 4\}\,\Gamma$

Figure 4.14 shows the results for the current, which for this choice of parameters increases for bigger U, but seems to keep its general shape. This is a consequence

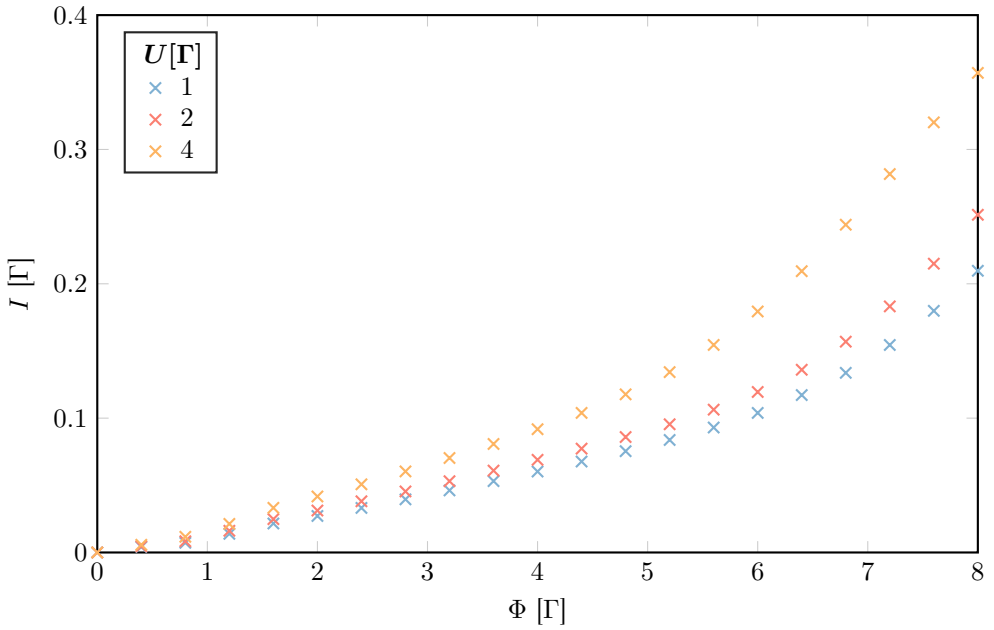

Figure 4.14: Current I versus bias voltage Φ of the model with finite Coulomb repulsion U.

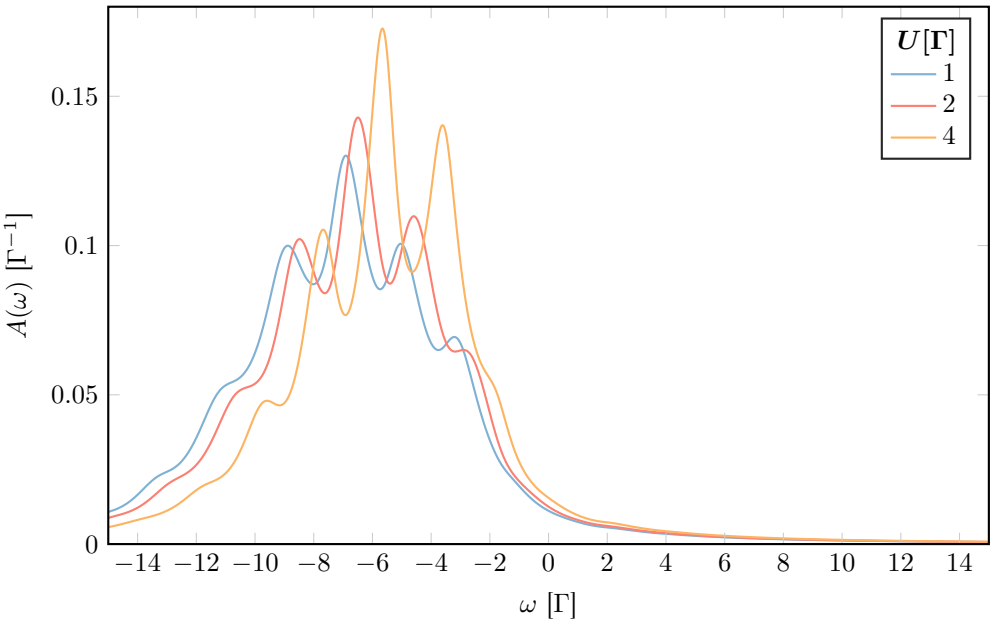

Figure 4.15: Spectral functions for the model with finite Coulomb repulsion U at bias voltage $\Phi = 0\,\Gamma$.

of the spectral functions depicted in figure 4.15, as well as figures B.14 and B.15 in the appendix.

We will try to motivate these changes by investigating the Lang-Firsov transformed Hamiltonian of the isolated impurity (eq. 2.24 without the leads).

$$\hat{H}_{\text{iso}} = \sum_{\sigma} \varepsilon_f c^\dagger_{f\sigma} c_{f\sigma} + U c^\dagger_{f\uparrow} c_{f\uparrow} c^\dagger_{f\downarrow} c_{f\downarrow} + \omega_b \, b^\dagger b - \frac{1}{\omega_b} \Big(\sum_{\sigma} \lambda c^\dagger_{f\sigma} c_{f\sigma} \Big)^2$$

For simplicity, we will leave out the factor of Γ in this discussion. The eigenstates and their energies of the purely electronic part of the impurity can immediately be identified as

$$\hat{H}_{\text{iso}} \, |0\rangle = 0 \, |0\rangle \qquad \hat{H}_{\text{iso}} \, |\uparrow\rangle = \left(-\frac{U}{2} - \frac{\lambda^2}{\omega_b} \right) |\uparrow\rangle$$

$$\hat{H}_{\text{iso}} \, |\downarrow\rangle = \left(-\frac{U}{2} - \frac{\lambda^2}{\omega_b} \right) |\downarrow\rangle \qquad \hat{H}_{\text{iso}} \, |\uparrow\downarrow\rangle = -\frac{4\lambda^2}{\omega_b} \, |\uparrow\downarrow\rangle$$

because $\varepsilon_f = -U/2$. This makes the doubly occupied state the ground state consistently over all chosen parameters, and we can assume that it will constitute the main contribution to the steady state. The electronic transition energies from the doubly to the singly occupied state are also easily calculated to be

$$\Delta E = -\frac{3\lambda^2}{\omega_b} + \frac{U}{2} = \begin{cases} -5.5 & U = 1 \\ -5 & U = 2 \\ -4 & U = 4 \end{cases}$$

Combined electron-phonon transitions will then have the energies $\Delta E \pm n\omega_b$ with $n \in \mathbb{N}_0$. Therefore we can expect the whole spectrum to be shifted to more positive energies with increasing U, as can be seen in figure 4.15. The exact positions of the peaks and their weights are subject to manybody interactions, but this can serve as a sketch of the general process going on.

The shift to more positive energies and the changing weights of the peaks give rise to a higher density of states around zero energy, which then in turn leads to a higher current (cf. eq. 2.14) observed in figure 4.14.

These results can of course not cover all aspects of different parameter regimes involving Coulomb repulsion. As of writing of this thesis, further calculations investigating this behavior are still underway, and the results presented here should serve more as a proof-of-concept rather than a full coverage of the topic.

Chapter 5

Conclusions

In this work we were able to successfully apply the auxiliary master equation approach (Amea) to the Anderson-Holstein model and reproduce results from other methods with varying degrees of agreement.

Amea has some distinct advantages over many other methods, of which the most noteworthy is the access to all local – and especially dynamical – quantities at the impurity, like spectral functions, even in nonequilibrium. This comes about from the fact that the intractable infinite environment is approximated by a finite, numerically treatable system, making it possible to estimate the Green functions of the impurity, and thereby all its local properties. Even though not implemented in the course of this work, it is in principle possible to also calculate the bosonic Green functions, giving more detailed insight into the dynamics of the harmonic oscillator. For other schemes – especially Monte Carlo methods – this is often not possible out of equilibrium.

Furthermore, it is a non-perturbative approach, meaning that it does not depend on any quantity being small and it is – in principle – possible to perform calculations in any parameter regime. With that in mind, it is worth mentioning – as can immediately be seen from the example fits in appendix B – that the approach performs better for higher temperatures, as the features in the hybridization are then smoother and easier to approximate using a small number of bath sites.

There are also some shortcomings of the numerical methods used for this work. First, depending on the parameters, the convergence of the time evolution to the steady state can be quite slow. This is an intrinsic property of some parameter sets and tends to happen whenever vastly different energy scales are present, i. e. when one or more parameters is significantly smaller or larger than the others. Since the task of finding the steady state essentially reduces to finding the eigenvector to the eigenvalue zero, it might be worth looking into alternative numerical methods

to obtain it. We should mention, however, that the method of time evolution is numerically extremely stable, as errors are by nature damped exponentially.

Secondly, the two-sided Lanczos scheme used for calculating the Green functions is very efficient for strong electronic couplings to the environment – i. e. high values of the hybridization – because then the peaks in the Green functions are significantly broadened and yield a smoother shape, for which a small number of Krylov vectors is sufficient. If, however, the hybridization is small, the peaks tend to be very slim and – even if the phonon energy is small – do not merge with each other. Such a finely peaked structure needs very many Krylov vectors, to the extent that in some rare cases accurate calculations become infeasable. This is mostly the case whenever the phonon energy and the hybridization are simultaneously much smaller than the bias voltage and electron-phonon coupling. However, as the reference calculations in [27] show, in these cases existing perturbative approaches like the Born-Markov master equation and the fourth order non-Markovian master equation work very well.

Another aspect to consider is the limited number of auxiliary bath sites that can be included, especially when dealing with a system with spin. In this case, the maximum treatable number of sites with our code on a node with e. g. 64 GB memory is $N = 5$. For the spinless case, $N = 7$ or 9 can be reached, depending on the cutoff for the bosonic occupation number. Fortunately, due to the fast convergence upon increasing the number of bath sites, even for $N = 5$ the results show remarkable accuracy.

The code written was shown to produce accurate results in the tested parameter regimes and can be used to study further properties of the model. We were able to demonstrate the suitability of Amea for this system and give some preliminary results for the model with on-site Coulomb repulsion. These are still being investigated and provide an interesting possibility for further research.

Appendix A

Mathematical Details

In this appendix, we collect longer derivations of mathematical results that would disrupt the main text. These results – with the exception of section A.6 and the bosonic part of section A.5 – are known from the literature (see for example references [35–39, 45]) but are still useful to be presented here for completeness and later reference.

A.1 Charged position shift

To show that an additional term $\lambda(b^\dagger + b)$ in the Hamiltonian of an harmonic oscillator is equivalent to a spatial shift and an energy correction, one can complete the square in $\hat{x}$.

$$\begin{aligned}
\omega_b b^\dagger b + \lambda(b^\dagger + b) &= \frac{\hat{p}^2}{2m} + \frac{m\omega_b^2 \hat{x}^2}{2} + \lambda\sqrt{\frac{2m\omega_b}{\hbar}}\,\hat{x} \\
&= \frac{\hat{p}^2}{2m} + \left(\sqrt{\frac{m\omega_b^2}{2}}\,\hat{x} + \lambda\sqrt{\frac{1}{\hbar\omega_b}}\right)^2 - \frac{\lambda^2}{\omega_b\hbar} \\
&= \frac{\hat{p}^2}{2m} + \frac{m\omega_b^2}{2}\left(\hat{x} + \underbrace{\lambda\sqrt{\frac{2}{m\hbar\omega_b^3}}}_{x_0}\right)^2 - \underbrace{\frac{\lambda^2}{\hbar\omega_b}}_{\Delta E} \\
&= \frac{\hat{p}^2}{2m} + \frac{m\omega_b^2}{2}(\hat{x} + x_0)^2 - \Delta E
\end{aligned}$$

In this form it is easy to see that the linear term shifts the equilibrium position by x_0 and corrects the energy by ΔE.

A.2 Partial trace

The fact that the partial trace leaves the expectation value of an operator acting only in the subspace s undisturbed can be seen as follows.

$$\begin{aligned}
\mathrm{tr}(\hat{\rho}\,\hat{O}) &= \sum_{i,j} \langle s_i| \otimes \langle e_j|\, \hat{\rho}(\hat{O}_s \otimes \mathbb{1})\, |s_i\rangle \otimes |e_j\rangle \\
&= \sum_{i,j,k,l} \langle s_i| \otimes \langle e_j|\, \hat{\rho}\, \underbrace{|s_k\rangle \otimes |e_l\rangle \langle s_k| \otimes \langle e_l|}_{\mathbb{1}} (\hat{O}_s \otimes \mathbb{1})\, |s_i\rangle \otimes |e_j\rangle \\
&= \sum_{i,j,k,l} \langle s_i| \otimes \langle e_j|\, \hat{\rho}\, |s_k\rangle \otimes |e_l\rangle\ \langle s_k|\hat{O}_s|s_i\rangle\, \underbrace{\langle e_l|e_j\rangle}_{\delta_{l,j}} \\
&= \sum_{i,j,k} \langle s_i|\, \underbrace{|s_i\rangle \langle s_i| \otimes \langle e_j|\, \hat{\rho}\, |s_k\rangle \otimes |e_j\rangle \langle s_k|}_{\mathrm{tr}_e(\hat{\rho})}\, |s_k\rangle\ \langle s_k|\hat{O}_s|s_i\rangle \\
&= \sum_{i,k} \langle s_i|\hat{\rho}_s|s_k\rangle\ \langle s_k|\hat{O}_s|s_i\rangle = \sum_i \langle s_i|\hat{\rho}_s\hat{O}_s|s_i\rangle = \mathrm{tr}(\hat{\rho}_s\hat{O}_s) \qquad \square
\end{aligned}$$

A.3 Reduced density matrix of an entangled state

The fact that an entangled state of the universe does not yield a pure reduced density matrix can be seen by straightforwardly calculating the example of

$$|\Psi\rangle = \frac{1}{\sqrt{2}}(|{\downarrow\uparrow}\rangle + |{\uparrow\downarrow}\rangle),$$

where the first spin belongs to the environment, and the second one to the system. The density operator is then

$$\hat{\rho} = |\Psi\rangle\langle\Psi| = \frac{1}{2}(|{\downarrow\uparrow}\rangle\langle{\downarrow\uparrow}| + |{\downarrow\uparrow}\rangle\langle{\uparrow\downarrow}| + |{\uparrow\downarrow}\rangle\langle{\downarrow\uparrow}| + |{\uparrow\downarrow}\rangle\langle{\uparrow\downarrow}|).$$

In the $|s_1 s_2\rangle$ basis this becomes

$$\rho = \frac{1}{2}\begin{pmatrix} 0 & 0 & 0 & 0 \\ 0 & 1 & 1 & 0 \\ 0 & 1 & 1 & 0 \\ 0 & 0 & 0 & 0 \end{pmatrix}.$$

With the definition of the partial trace as given in sec. 2.2, the reduced density matrix is

$$\hat{\rho}_s = \sum_{m,n,k} |m\rangle\ \langle k, m|\hat{\rho}|k, n\rangle\, \langle n| = \frac{1}{2}(|{\uparrow}\rangle\langle{\uparrow}| + |{\downarrow}\rangle\langle{\downarrow}|)$$

which in the $|s_2\rangle$ basis becomes

$$\rho_s = \frac{1}{2}\begin{pmatrix} 1 & 0 \\ 0 & 1 \end{pmatrix}.$$

This density matrix is no longer pure, because $\rho_s^2 \neq \rho_s$.

A.4 Green functions in the frequency domain

To Fourier transform the retarded Green function to the frequency domain, it is best to split it in two parts in the time domain and transform individually.

$$\begin{aligned} G^{\mathrm{R}}(r) &= -i\Theta(t)(\,\langle c(t)c^\dagger\rangle + \,\langle c^\dagger c(t)\rangle) \\ &= -i(\underbrace{\Theta(t)\,\langle c(t)c^\dagger\rangle}_{G_1^{\mathrm{R}}(t)} + \underbrace{\Theta(t)\,\langle c^\dagger c(t)\rangle}_{G_2^{\mathrm{R}}(t)}) \end{aligned}$$

$$\begin{aligned} G_1^{\mathrm{R}}(\omega) &= \int_{-\infty}^{\infty} \Theta(t)\,\mathrm{tr}(\hat{\rho}c(t)c^\dagger)e^{i(\omega+i0^+)t}dt \\ &= \int_0^{\infty} \sum_k p_k\,\langle\psi_k|e^{i\hat{H}t}ce^{-i\hat{H}t}c^\dagger|\psi_k\rangle\,e^{i(\omega+i0^+)t}dt \\ &= \int_0^{\infty} \sum_{k,l,m} p_k\,\langle\psi_k|l\rangle\,\langle l|e^{iE_lt}ce^{-iE_mt}|m\rangle\,\langle m|c^\dagger|\psi_k\rangle\,e^{i(\omega+i0^+)t}dt \\ &= \int_0^{\infty} \sum_{k,l,m} p_k\,\langle\psi_k|l\rangle\,\langle l|c|m\rangle\,\langle m|c^\dagger|\psi_k\rangle\,e^{i(E_l-E_m+\omega+i0^+)t}dt \\ &= \sum_{k,l,m} p_k\,\langle\psi_k|l\rangle\,\langle l|c|m\rangle\,\langle m|c^\dagger|\psi_k\rangle\,\frac{e^{i(E_l-E_m+\omega+i0^+)t}}{i(E_l-E_m+\omega+i0^+)}\Bigg|_{t=0}^{\infty} \\ &= i\sum_{k,l,m} p_k\frac{\langle\psi_k|l\rangle\,\langle l|c|m\rangle\,\langle m|c^\dagger|\psi_k\rangle}{E_l-E_m+\omega+i0^+} \end{aligned}$$

$$\begin{aligned} G_2^{\mathrm{R}}(\omega) &= \int_{-\infty}^{\infty} \Theta(t)\,\mathrm{tr}(\hat{\rho}c^\dagger c(t))e^{i(\omega+i0^+)t}dt \\ &= \int_0^{\infty} \sum_k p_k\,\langle\psi_k|c^\dagger e^{i\hat{H}t}ce^{-i\hat{H}t}|\psi_k\rangle\,e^{i(\omega+i0^+)t}dt \\ &= \int_0^{\infty} \sum_{k,l,m} p_k\,\langle\psi_k|c^\dagger|l\rangle\,\langle l|e^{iE_lt}ce^{-iE_mt}|m\rangle\,\langle m|\psi_k\rangle\,e^{i(\omega+i0^+)t}dt \\ &= \int_0^{\infty} \sum_{k,l,m} p_k\,\langle\psi_k|c^\dagger|l\rangle\,\langle l|c|m\rangle\,\langle m|\psi_k\rangle\,e^{i(E_l-E_m+\omega+i0^+)t}dt \end{aligned}$$

$$= \sum_{k,l,m} p_k \ \langle\psi_k|c^\dagger|l\rangle \ \langle l|c|m\rangle \langle m|\psi_k\rangle \ \frac{e^{i(E_l - E_m + \omega + i0^+)t}}{i(E_l - E_m + \omega + i0^+)}\Bigg|_{t=0}^{\infty}$$
$$= i \sum_{k,l,m} p_k \frac{\langle\psi_k|c^\dagger|l\rangle \ \langle l|c|m\rangle \langle m|\psi_k\rangle}{E_l - E_m + \omega + i0^+}$$

Here, l and k label the eigenstates of the Hamiltonian, $E_{l,k}$ are the corresponding energies, and $i0^+$ means an infinitesimal positive imaginary quantitiy with the formal definition

$$i0^+ := \lim_{\varepsilon \searrow 0} i\varepsilon.$$

where of course the limit of the whole expression containing $i0^+$ must be taken, and the order of operations is usually important.

The total retarded Green function is then given by

$$\begin{aligned} G^{\mathrm{R}}(\omega) &= -i(G_1^{\mathrm{R}}(\omega) + G_2^{\mathrm{R}}(\omega)) \\ &= \sum_{k,l,m} p_k \frac{\langle\psi_k|l\rangle \ \langle l|c|m\rangle \ \langle m|c^\dagger|\psi_k\rangle + \ \langle\psi_k|c^\dagger|l\rangle \ \langle l|c|m\rangle \langle m|\psi_k\rangle}{E_l - E_m + \omega + i0^+}. \end{aligned} \tag{A.1}$$

The calculation for G^{A} is very similar and straightforward, which is why we only state the result here. The only difference is an overall sign and that instead of $\Theta(t)$ it contains a $\Theta(-t)$, which necessitates a $(-i0^+)$ in the exponent in order for the integral to converge. The sign exactly cancels with the fact that 0 is now the upper bound of the integral.

$$G^{\mathrm{A}}(\omega) = \sum_{k,l,m} p_k \frac{\langle\psi_k|l\rangle \ \langle l|c|m\rangle \ \langle m|c^\dagger|\psi_k\rangle + \ \langle\psi_k|c^\dagger|l\rangle \ \langle l|c|m\rangle \langle m|\psi_k\rangle}{E_l - E_m + \omega - i0^+} \tag{A.2}$$

It is easy to see that $G^{\mathrm{A}}(\omega) = G^{\mathrm{R}\dagger}(\omega)$.

For the Keldysh Green function, the greater and lesser must first be evaluated separately.

$$\begin{aligned} G^{>}(\omega) &= \int_{-\infty}^{\infty} -i \langle c(t)c^\dagger\rangle \, e^{i\omega t} dt = -i \int_{-\infty}^{\infty} \mathrm{tr}(\hat{\rho} e^{i\hat{H}t} c e^{-i\hat{H}t} c^\dagger) e^{i\omega t} dt \\ &= -i \int_{-\infty}^{\infty} \sum_k \langle\psi_k|e^{i\hat{H}t} c e^{-i\hat{H}t} c^\dagger|\psi_k\rangle \, e^{i\omega t} dt \\ &= -i \int_{-\infty}^{\infty} \sum_{k,l,m} \langle\psi_k|l\rangle \ \langle l|e^{iE_l t} c e^{-iE_m t}|m\rangle \ \langle m|c^\dagger|\psi_k\rangle \, e^{i\omega t} dt \\ &= -i \sum_{k,l,m} \langle\psi_k|l\rangle \ \langle l|c|m\rangle \ \langle m|c^\dagger|\psi_k\rangle \int_{-\infty}^{\infty} e^{i(E_l - E_m + \omega)t} dt \end{aligned}$$

With the inverse transfromation of a δ-distribution being

$$\mathcal{F}^{-1}[\delta(\omega-a)] = \frac{1}{2\pi}\int_{-\infty}^{\infty}\delta(\omega-a)e^{-i\omega t}d\omega = \frac{1}{2\pi}e^{-iat},$$

the integral in the last line is proportional to $\delta(\omega+E_l-E_m)$ and the Green function becomes

$$G^{>}(\omega) = -2\pi i\sum_{k,l,m}\langle\psi_k|l\rangle\ \langle l|c|m\rangle\ \langle m|c^\dagger|\psi_k\rangle\,\delta(\omega+E_l-E_m).$$

The lesser Green function is again very similar.

$$\begin{aligned}
G^{<}(\omega) &= \int_{-\infty}^{\infty} i\,\langle c^\dagger c(t)\rangle\, e^{i\omega t}dt \\
&= i\int_{-\infty}^{\infty}\mathrm{tr}(\hat{\rho}c^\dagger e^{i\hat{H}t}ce^{-i\hat{H}t})e^{i\omega t}dt \\
&= i\int_{-\infty}^{\infty}\sum_k\langle\psi_k|c^\dagger e^{i\hat{H}t}ce^{-i\hat{H}t}|\psi_k\rangle\, e^{i\omega t}dt \\
&= i\int_{-\infty}^{\infty}\sum_{k,l,m}\langle\psi_k|c^\dagger|l\rangle\ \langle l|e^{iE_lt}ce^{-iE_mt}|m\rangle\,\langle m|\psi_k\rangle\, e^{i\omega t}dt \\
&= i\sum_{k,l,m}\langle\psi_k|c^\dagger|l\rangle\ \langle l|c|m\rangle\,\langle m|\psi_k\rangle\int_{-\infty}^{\infty}e^{i(E_l-E_m+\omega)t}dt \\
&= 2\pi i\sum_{k,l,m}\langle\psi_k|c^\dagger|l\rangle\ \langle l|c|m\rangle\,\langle m|\psi_k\rangle\,\delta(\omega+E_l-E_m)
\end{aligned}$$

Therefore, the Keldysh Green function $G^{\mathrm{K}} = G^{<} + G^{>}$ in the frequency domain is is

$$\begin{aligned}
G^{\mathrm{K}}(\omega) = 2\pi i\sum_{k,l,m}\delta(\omega+E_l-E_m)\Big[&\langle\psi_k|c^\dagger|l\rangle\ \langle l|c|m\rangle\,\langle m|\psi_k\rangle \\
&-\langle\psi_k|l\rangle\ \langle l|c|m\rangle\ \langle m|c^\dagger|\psi_k\rangle\Big]. \quad \text{(A.3)}
\end{aligned}$$

A.5 Tilde conjugation rules

Proving eqs. 2.7 is straightforward.

$$\begin{aligned}
c_k\,|I\rangle &= c_k\sum_{\boldsymbol{m}}(-i)^{\sum_p m_p}\,|\boldsymbol{m},\widetilde{\boldsymbol{m}}\rangle = c_k\sum_{\boldsymbol{m}}(-i)^{\sum_p m_p}\prod_p(c_p^\dagger\tilde{c}_p^\dagger)^{m_p}\,|0\rangle \\
&= c_k\sum_{\boldsymbol{m}}(-i)^{\sum_p m_p}\ldots(c_{k-1}^\dagger\tilde{c}_{k-1}^\dagger)^{m_{k-1}}(c_k^\dagger\tilde{c}_k^\dagger)^{m_k}(c_{k+1}^\dagger\tilde{c}_{k+1}^\dagger)^{m_{k+1}}\ldots|0\rangle
\end{aligned}$$

$$= \sum_{\boldsymbol{m}} (-i)^{\sum_p m_p} \dots (c_{k-1}^\dagger \tilde{c}_{k-1}^\dagger)^{m_{k-1}} \, \delta_{1,m_k} c_k c_k^\dagger \tilde{c}_k^\dagger \, (c_{k+1}^\dagger \tilde{c}_{k+1}^\dagger)^{m_{k+1}} \dots |0\rangle$$

$$= \sum_{\substack{\boldsymbol{m} \\ m_k=1}} (-i)^{\sum_p m_p} \dots (c_{k-1}^\dagger \tilde{c}_{k-1}^\dagger)^{m_{k-1}} \, \tilde{c}_k^\dagger (1 - c_k^\dagger \underbrace{c_k}_{0}) \, (c_{k+1}^\dagger \tilde{c}_{k+1}^\dagger)^{m_{k+1}} \dots |0\rangle$$

$$= (-i) \, \tilde{c}_k^\dagger \sum_{\substack{\boldsymbol{m} \\ m_k=1}} (-i)^{\sum_{p \neq k} m_p} (c_{k-1}^\dagger \tilde{c}_{k-1}^\dagger)^{m_{k-1}} (c_{k+1}^\dagger \tilde{c}_{k+1}^\dagger)^{m_{k+1}} \dots |0\rangle$$

$$= (-i) \, \tilde{c}_k^\dagger \sum_{\substack{\boldsymbol{m} \\ m_k=0}} (-i)^{\sum_p m_p} \prod_p (c_p^\dagger \tilde{c}_p^\dagger)^{m_p} |0\rangle = -i \tilde{c}_k^\dagger |I\rangle \qquad \square$$

The summation switches from $m_k = 1$ to $m_k = 0$ because summing over all states where the k-th single-particle state would be occupied, but removing the creation operator at index k, is equal to summing over all states where the single-particle state k is empty. The last equality holds true, because application of $\tilde{c}_k^\dagger$ to $|I\rangle$ will yield a δ_{0,m_k}, since $(\tilde{c}_k^\dagger)^2 = 0$. Also, note that no fermi signs appear when swapping the operators to their final positions, because they are only interchanged with pairs of operators. The calculation for $c_k^\dagger |I\rangle$ is similar to the one for $c_k |I\rangle$.

$$c_k^\dagger |I\rangle = c_k^\dagger \sum_{\boldsymbol{m}} (-i)^{\sum_p m_p} |\boldsymbol{m}, \widetilde{\boldsymbol{m}}\rangle = c_k^\dagger \sum_{\boldsymbol{m}} (-i)^{\sum_p m_p} \prod_p (c_p^\dagger \tilde{c}_p^\dagger)^{m_p} |0\rangle$$

$$= c_k^\dagger \sum_{\boldsymbol{m}} (-i)^{\sum_p m_p} \dots (c_{k-1}^\dagger \tilde{c}_{k-1}^\dagger)^{m_{k-1}} (c_k^\dagger \tilde{c}_k^\dagger)^{m_k} (c_{k+1}^\dagger \tilde{c}_{k+1}^\dagger)^{m_{k+1}} \dots |0\rangle$$

$$= \sum_{\boldsymbol{m}} (-i)^{\sum_p m_p} \dots (c_{k-1}^\dagger \tilde{c}_{k-1}^\dagger)^{m_{k-1}} \, \delta_{0,m_k} c_k^\dagger \, (c_{k+1}^\dagger \tilde{c}_{k+1}^\dagger)^{m_{k+1}} \dots |0\rangle$$

$$= \sum_{\substack{\boldsymbol{m} \\ m_k=0}} (-i)^{\sum_p m_p} \dots (c_{k-1}^\dagger \tilde{c}_{k-1}^\dagger)^{m_{k-1}} \, c_k^\dagger \underbrace{\tilde{c}_k \tilde{c}_k^\dagger}_{1} (c_{k+1}^\dagger \tilde{c}_{k+1}^\dagger)^{m_{k+1}} \dots |0\rangle$$

$$= -\tilde{c}_k \sum_{\substack{\boldsymbol{m} \\ m_k=0}} (-i)^{\sum_{p \neq k} m_p} \dots (c_{k-1}^\dagger \tilde{c}_{k-1}^\dagger)^{m_{k-1}} \, c_k^\dagger \tilde{c}_k^\dagger \, (c_{k+1}^\dagger \tilde{c}_{k+1}^\dagger)^{m_{k+1}} \dots |0\rangle$$

$$= -\tilde{c}_k \sum_{\substack{\boldsymbol{m} \\ m_k=1}} \frac{(-i)^{\sum_p m_p}}{-i} \prod_p (c_p^\dagger \tilde{c}_p^\dagger)^{m_p} |0\rangle = -i \tilde{c}_k |I\rangle \qquad \square$$

When swapping $\tilde{c}_k$ to the beginning of the expression, there is a fermi sign from exchanging it with $c_k^\dagger$. All other operators are in pairs. Moreover, the sum changes from $m_k = 0$ to $m_k = 1$, because summing over all states with the k-th single-particle state being empty and inserting creators with index k is the same as summing over all states where the single-particle state k is occupied. However, the sum in the exponent then gets an extra 1, which leads to a factor of $-i$ that needs to be divided out. The last equality holds true, because applying $\tilde{c}_k$ to $|I\rangle$ yields a $\delta_{1,k}$.

Eq. 2.9 for the annihilation operator can be proven as follows.

$$
\begin{aligned}
b\,|I\rangle &= b \sum_{\boldsymbol{m}} \sum_{q=0}^{\infty} (-i)^{\sum_k m_k} \,|\boldsymbol{m}, \widetilde{\boldsymbol{m}}, q, \widetilde{q}\rangle \\
&= \sum_{\boldsymbol{m}} \sum_{q=0}^{\infty} \sqrt{q}\,(-i)^{\sum_k m_k} \,|\boldsymbol{m}, \widetilde{\boldsymbol{m}}, q-1, \widetilde{q}\rangle \\
&= \sum_{\boldsymbol{m}} \sum_{q=1}^{\infty} \sqrt{q}\,(-i)^{\sum_k m_k} \,|\boldsymbol{m}, \widetilde{\boldsymbol{m}}, q-1, \widetilde{q}\rangle \\
&= \sum_{\boldsymbol{m}} \sum_{q=0}^{\infty} \sqrt{q+1}\,(-i)^{\sum_k m_k} \,|\boldsymbol{m}, \widetilde{\boldsymbol{m}}, q, \widetilde{q+1}\rangle \\
&= \sum_{\boldsymbol{m}} \sum_{q=0}^{\infty} \sqrt{q+1}\,(-i)^{\sum_k m_k} \frac{\tilde{b}^\dagger}{\sqrt{q+1}} \,|\boldsymbol{m}, \widetilde{\boldsymbol{m}}, q, \widetilde{q}\rangle \\
&= \tilde{b}^\dagger \sum_{\boldsymbol{m}} \sum_{q=0}^{\infty} (-i)^{\sum_k m_k} \,|\boldsymbol{m}, \widetilde{\boldsymbol{m}}, q, \widetilde{q}\rangle = \tilde{b}^\dagger\,|I\rangle
\end{aligned}
$$

□

The creation operator is analogous.

$$
\begin{aligned}
b^\dagger\,|I\rangle &= b^\dagger \sum_{\boldsymbol{m}} \sum_{q=0}^{\infty} (-i)^{\sum_k m_k} \,|\boldsymbol{m}, \widetilde{\boldsymbol{m}}, q, \widetilde{q}\rangle \\
&= \sum_{\boldsymbol{m}} \sum_{q=0}^{\infty} \sqrt{q+1}\,(-i)^{\sum_k m_k} \,|\boldsymbol{m}, \widetilde{\boldsymbol{m}}, q+1, \widetilde{q}\rangle \\
&= \sum_{\boldsymbol{m}} \sum_{q=1}^{\infty} \sqrt{q}\,(-i)^{\sum_k m_k} \,|\boldsymbol{m}, \widetilde{\boldsymbol{m}}, q, \widetilde{q-1}\rangle \\
&= \sum_{\boldsymbol{m}} \sum_{q=0}^{\infty} \sqrt{q}\,(-i)^{\sum_k m_k} \,|\boldsymbol{m}, \widetilde{\boldsymbol{m}}, q, \widetilde{q-1}\rangle \\
&= \sum_{\boldsymbol{m}} \sum_{q=0}^{\infty} \sqrt{q}\,(-i)^{\sum_k m_k} \frac{\tilde{b}}{\sqrt{m}} \,|\boldsymbol{m}, \widetilde{\boldsymbol{m}}, q, \widetilde{q}\rangle \\
&= \tilde{b} \sum_{\boldsymbol{m}} \sum_{q=0}^{\infty} (-i)^{\sum_k m_k} \,|\boldsymbol{m}, \widetilde{\boldsymbol{m}}, q, \widetilde{q}\rangle = \tilde{b}\,|I\rangle
\end{aligned}
$$

□

A.6 Basis reordering sign

For the order of fermionic operators used in this thesis, the number of permutations to sort all tilde operators to the left of non-tilde operators can be counted as follows.

The first tilde operator, if present, changes place with only the first non-tilde operator, also if present.

$$N^{\text{basis}}_{\boldsymbol{m},\boldsymbol{n},1} = n_1 m_1$$

The second tilde operator then changes places with all present non-tilde operators with index 1 and 2.

$$N^{\text{basis}}_{\boldsymbol{m},\boldsymbol{n},2} = n_2(m_1 + m_2)$$

Applying this procedure to all tilde operators, for the k-th tilde operator we find

$$N^{\text{basis}}_{\boldsymbol{m},\boldsymbol{n},k} = n_k \sum_{l=1}^{k} m_l.$$

The total number of permutations is then the sum over all k.

$$N^{\text{basis}}_{\boldsymbol{m},\boldsymbol{n}} = \sum_{k=1}^{N} \left(n_k \sum_{l=1}^{k} m_l \right)$$

A.7 Liouville operator in superfermion formalism

For the Hermitian part of the Liouville superoperator we find

$$\begin{aligned}
i\hat{\hat{\mathcal{L}}}_{\text{H}} \hat{\rho} \, |I\rangle &= [\hat{H}_{\text{aux}}, \hat{\rho}] \, |I\rangle \\
&= \hat{H}_{\text{aux}} \, \hat{\rho} \, |I\rangle - \hat{\rho} \, \hat{H}_{\text{aux}} \, |I\rangle \\
&= \hat{H}_{\text{aux}} \, |\rho\rangle - \hat{\rho} \left[\sum_{k,l} \sum_{\sigma} E_{kl} \, c^{\dagger}_{k\sigma} c_{l\sigma} + \sum_{\sigma} \lambda (b^{\dagger} + b) \, c^{\dagger}_{f\sigma} c_{f\sigma} \right. \\
&\qquad \left. + U c^{\dagger}_{f\uparrow} c_{f\uparrow} c^{\dagger}_{f\downarrow} c_{f\downarrow} + \omega_b \, b^{\dagger} b \right] |I\rangle \\
&= \hat{H}_{\text{aux}} \, |\rho\rangle - \hat{\rho} \left[\sum_{k,l} \sum_{\sigma} E_{kl} \, \tilde{c}^{\dagger}_{l\sigma} \tilde{c}_{k\sigma} + \sum_{\sigma} \lambda (\tilde{b} + \tilde{b}^{\dagger}) \, \tilde{c}^{\dagger}_{f\sigma} \tilde{c}_{f\sigma} \right. \\
&\qquad \left. + U \tilde{c}^{\dagger}_{f\downarrow} \tilde{c}_{f\downarrow} \tilde{c}^{\dagger}_{f\uparrow} \tilde{c}_{f\uparrow} + \omega_b \, \tilde{b}^{\dagger} \tilde{b} \right] |I\rangle
\end{aligned}$$

$$= \hat{H}_{\text{aux}} |\rho\rangle - \hat{\rho}\, \hat{\tilde{H}}_{\text{aux}} |I\rangle = \hat{H}_{\text{aux}} |\rho\rangle - \hat{\tilde{H}}_{\text{aux}}\, \hat{\rho}\, |I\rangle$$

$$= \hat{H}_{\text{aux}} |\rho\rangle - \hat{\tilde{H}}_{\text{aux}} |\rho\rangle = (\hat{H}_{\text{aux}} - \hat{\tilde{H}}_{\text{aux}}) |\rho\rangle\,. \qquad \square$$

$\hat{\rho}$ only contains bilinear fermi operators and therefore commutes with any tilde fermi operator. Additionally, bosonic operators in original space commute with all bosonic operators in tilde space. So since $\widetilde{\hat{H}}_{\text{aux}}$ does not contain non-tilde operators, it can simply be swapped with $\hat{\rho}$.

A similar calculation can be done for the dissipative part, where the same properties as above are used.

$$\begin{aligned}
\hat{\tilde{\mathcal{L}}}_{\text{D}} \hat{\rho}\, |I\rangle &= \sum_{k,l} \sum_{\sigma} \Big[\Gamma^{(1)}_{lk} \left(2\, c_{k\sigma}\, \hat{\rho}\, c^{\dagger}_{l\sigma} - \{ \hat{\rho}, c^{\dagger}_{l\sigma} c_{k\sigma} \} \right) \\
&\qquad + \Gamma^{(2)}_{lk} \left(2\, c^{\dagger}_{l\sigma}\, \hat{\rho}\, c_{k\sigma} - \{ \hat{\rho}, c_{k\sigma} c^{\dagger}_{l\sigma} \} \right) \Big] |I\rangle \\
&= \sum_{k,l} \sum_{\sigma} \Big[\Gamma^{(1)}_{lk} \left(-2i\, c_{k\sigma}\, \hat{\rho}\, \tilde{c}_{l\sigma} - \hat{\rho}\, \tilde{c}^{\dagger}_{k\sigma} \tilde{c}_{l\sigma} - c^{\dagger}_{l\sigma} c_{k\sigma}\, \hat{\rho} \right) \\
&\qquad + \Gamma^{(2)}_{lk} \left(-2i\, c^{\dagger}_{l\sigma}\, \hat{\rho}\, \tilde{c}^{\dagger}_{k\sigma} - \hat{\rho}\, c_{k\sigma} c^{\dagger}_{l\sigma} - \tilde{c}_{l\sigma} \tilde{c}^{\dagger}_{k\sigma}\, \hat{\rho} \right) \Big] |I\rangle \\
&= \sum_{k,l} \sum_{\sigma} \Big[\Gamma^{(1)}_{lk} \left(-2i\, c_{k\sigma} \tilde{c}_{l\sigma} - \tilde{c}^{\dagger}_{k\sigma} \tilde{c}_{l\sigma} - c^{\dagger}_{l\sigma} c_{k\sigma} \right) \\
&\qquad + \Gamma^{(2)}_{lk} \left(-2i\, c^{\dagger}_{l\sigma} \tilde{c}^{\dagger}_{k\sigma} - c_{k\sigma} c^{\dagger}_{l\sigma} - \tilde{c}_{l\sigma} \tilde{c}^{\dagger}_{k\sigma} \right) \Big] \hat{\rho}\, |I\rangle \\
&= \sum_{k,l} \sum_{\sigma} \Big[\Gamma^{(1)}_{lk} \left(-2i\, c_{k\sigma} \tilde{c}_{l\sigma} - \tilde{c}^{\dagger}_{k\sigma} \tilde{c}_{l\sigma} - c^{\dagger}_{l\sigma} c_{k\sigma} \right) \\
&\qquad + \Gamma^{(2)}_{lk} \left(-2i\, c^{\dagger}_{l\sigma} \tilde{c}^{\dagger}_{k\sigma} - c_{k\sigma} c^{\dagger}_{l\sigma} - \tilde{c}_{l\sigma} \tilde{c}^{\dagger}_{k\sigma} \right) \Big] |\rho\rangle \qquad \square
\end{aligned}$$

A.8 Green functions of the auxiliary system

The Green functions of the auxiliary system in the frequency domain are again obtained by a Fourier transformation.

$$\begin{aligned}
G^{>}(\omega) &= \int_{-\infty}^{\infty} -i\Theta(t) \langle c(t) c^{\dagger} \rangle\, e^{i\omega t} - \Theta(-t)(-i \langle c(-t) c^{\dagger} \rangle)^{\dagger} e^{i\omega t} dt \\
&= \int_{0}^{\infty} -i \langle c e^{\hat{\mathcal{L}} t} c^{\dagger} \rangle\, e^{i\omega t} dt - i \int_{-\infty}^{0} \langle c e^{-\hat{\mathcal{L}} t} c^{\dagger} \rangle^{\dagger}\, e^{i\omega t} dt \\
&= -i \left\langle c \frac{e^{(\hat{\mathcal{L}} + i\omega) t}}{\hat{\mathcal{L}} + i\omega} c^{\dagger} \right\rangle \Bigg|_{t=0}^{\infty} - i \left\langle c \frac{e^{(-\hat{\mathcal{L}} - i\omega) t}}{-\hat{\mathcal{L}} - i\omega} c^{\dagger} \right\rangle^{\dagger} \Bigg|_{-\infty}^{0}
\end{aligned}$$

$$= i\left\langle c\frac{1}{\hat{\mathcal{L}}+i\omega}c^\dagger\right\rangle + i\left\langle c\frac{1}{\hat{\mathcal{L}}+i\omega}c^\dagger\right\rangle^\dagger$$
$$= \left\langle c(\omega - i\hat{\mathcal{L}})^{-1}c^\dagger\right\rangle - \left\langle c(\omega - i\hat{\mathcal{L}})^{-1}c^\dagger\right\rangle^\dagger$$

The calculation for the lesser Green function is very similar.

$$\begin{aligned} G^<(\omega) &= \int_{-\infty}^{\infty} \Theta(-t) i \langle c^\dagger(-t)c\rangle\, e^{i\omega t} - \Theta(t)(i\langle c^\dagger(t)c\rangle)^\dagger e^{i\omega t} dt \\ &= \int_{-\infty}^{0} i\langle c^\dagger e^{-\hat{\mathcal{L}}t}c\rangle\, e^{i\omega t}dt + i\int_0^\infty \langle c^\dagger e^{\hat{\mathcal{L}}t}c\rangle^\dagger\, e^{i\omega t}dt \\ &= i\left\langle c^\dagger\frac{1}{i\omega-\hat{\mathcal{L}}}c\right\rangle - i\left\langle c^\dagger\frac{1}{\hat{\mathcal{L}}-i\omega}c\right\rangle^\dagger \\ &= \left\langle c(\omega+i\hat{\mathcal{L}})^{-1}c^\dagger\right\rangle - \left\langle c(\omega+i\hat{\mathcal{L}})^{-1}c^\dagger\right\rangle^\dagger \end{aligned}$$

In the superfermion formalism all these expectation values become expressions in the form of $\langle I|\cdots|\rho_{\mathrm{ss}}\rangle$. $G^{\mathrm{R}}(\omega)$ and $G^{\mathrm{A}}(\omega)$ can be deduced by simply taking only the relevant integral of the derivation above.

A.9 Lang-Firsov transformation of the auxiliary Hamiltonian

To make it more readable, the unitary transformation matrix is renamed to $\hat{L} \coloneqq e^{\hat{S}}$, with $\hat{S}$ as in eq. 2.22. Because a unit-operator in the form of $\mathbb{1} = \hat{L}\hat{L}^\dagger$ can be inserted between any two operators, it is sufficient to transform all the operators appearing in $\hat{H}_{\mathrm{aux}}$ separately.

$$\begin{aligned} \hat{L}^\dagger\hat{H}_{\mathrm{aux}}\hat{L} &= \sum_{k,l}\sum_\sigma E_{kl}\,\hat{L}^\dagger c_{k\sigma}^\dagger\hat{L}\hat{L}^\dagger c_{l\sigma}\hat{L} + \sum_\sigma \lambda(\hat{L}^\dagger b^\dagger\hat{L} + \hat{L}^\dagger b\hat{L})\,\hat{L}^\dagger c_{f\sigma}^\dagger\hat{L}\hat{L}^\dagger c_{f\sigma}\hat{L} \\ &\quad + U\hat{L}^\dagger c_{f\uparrow}^\dagger\hat{L}\hat{L}^\dagger c_{f\uparrow}\hat{L}\hat{L}^\dagger c_{f\downarrow}^\dagger\hat{L}\hat{L}^\dagger c_{f\downarrow}\hat{L}^\dagger + \omega_b\,\hat{L}^\dagger b^\dagger\hat{L}\hat{L}^\dagger b\hat{L} \\ &= \sum_{k,l}\sum_\sigma E_{kl}\,\bar{c}_{k\sigma}^\dagger\bar{c}_{l\sigma} + \sum_\sigma\lambda(\bar{b}^\dagger+\bar{b})\,\bar{c}_{f\sigma}^\dagger\bar{c}_{f\sigma} + U\bar{c}_{f\uparrow}^\dagger\bar{c}_{f\uparrow}\bar{c}_{f\downarrow}^\dagger\bar{c}_{f\downarrow} + \omega_b\,\bar{b}^\dagger\bar{b} \\ &=: \hat{\bar{H}}_{\mathrm{aux}} \end{aligned} \tag{A.4}$$

The number operator $\hat{n}_{f\sigma} \coloneqq c_{f\sigma}c_{f\sigma}^\dagger$ commutes with all creation and annihilation operators with an index different from f. Therefore, the transformed electronic

creators and annihilators for indices except f simplify to

$$\bar{c}_{k\sigma} = e^{-\sum_{\sigma'} \gamma \hat{n}_{f\sigma'}(b^\dagger - b)}\, c_{k\sigma}\, e^{\sum_{\sigma'} \gamma \hat{n}_{f\sigma'}(b^\dagger - b)} = c_{k\sigma}$$

and $\bar{c}^\dagger_{k\sigma} = c^\dagger_{k\sigma}$.

For $c_{f\sigma}$, first the commutator with the number operator must be evaluated.

$$\hat{n}_{f\sigma} c_{f\sigma} = c^\dagger_{f\sigma} \underbrace{c_{f\sigma} c_{f\sigma}}_{0} = 0$$

$$c_{f\sigma} \hat{n}_{f\sigma} = c_{f\sigma} \underbrace{c^\dagger_{f\sigma} c_{f\sigma}}_{1 - c_{f\sigma} c^\dagger_{f\sigma}} = c_{f\sigma} - \underbrace{c_{f\sigma} c_{f\sigma}}_{0} c^\dagger_{f\sigma} = c_{f\sigma}$$

From this, it is obvious that also

$$\hat{n}^k_{f\sigma} c_{f\sigma} = 0 \qquad \text{and} \qquad c_{f\sigma} \hat{n}^k_{f\sigma} = c_{f\sigma}$$

hold. Taking the Hermitian conjugate of the above equations and using that $\hat{n}$ is self-adjoint, the equations for the creators read as

$$c^\dagger_{f\sigma} \hat{n}^k_{f\sigma} = 0 \qquad \text{and} \qquad \hat{n}^k_{f\sigma} c^\dagger_{f\sigma} = c^\dagger_{f\sigma}.$$

Also note that the above relations are only valid if the spin component also matches. If it does not, the operators commute. With these results, the transformed electronic operators are

$$\begin{aligned}
\bar{c}_{f\sigma} &= e^{-\sum_{\sigma'} \gamma \hat{n}_{f\sigma'}(b^\dagger - b)}\, c_{f\sigma}\, e^{\sum_{\sigma'} \gamma \hat{n}_{f\sigma'}(b^\dagger - b)} = e^{-\gamma \hat{n}_{f\sigma}(b^\dagger - b)}\, c_{f\sigma}\, e^{\gamma \hat{n}_{f\sigma}(b^\dagger - b)} \\
&= \sum_{k=0}^{\infty} \frac{\left[-\gamma \hat{n}_{f\sigma}(b^\dagger - b)\right]^k}{k!}\, c_{f\sigma} \sum_{k=0}^{\infty} \frac{\left[\gamma \hat{n}_{f\sigma}(b^\dagger - b)\right]^k}{k!} \\
&= c_{f\sigma} \sum_{k=0}^{\infty} \frac{\left[\gamma (b^\dagger - b)\right]^k}{k!} = c_{f\sigma}\, e^{\gamma(b^\dagger - b)}
\end{aligned}$$

and

$$\begin{aligned}
\bar{c}^\dagger_{f\sigma} &= e^{-\sum_{\sigma'} \gamma \hat{n}_{f\sigma'}(b^\dagger - b)}\, c^\dagger_{f\sigma}\, e^{\sum_{\sigma'} \gamma \hat{n}_{f\sigma'}(b^\dagger - b)} = e^{-\gamma \hat{n}_{f\sigma}(b^\dagger - b)}\, c^\dagger_{f\sigma}\, e^{\gamma \hat{n}_{f\sigma}(b^\dagger - b)} \\
&= \sum_{k=0}^{\infty} \frac{\left[-\gamma \hat{n}_{f\sigma}(b^\dagger - b)\right]^k}{k!}\, c^\dagger_{f\sigma} \sum_{k=0}^{\infty} \frac{\left[\gamma \hat{n}_{f\sigma}(b^\dagger - b)\right]^k}{k!} \\
&= \sum_{k=0}^{\infty} \frac{\left[-\gamma (b^\dagger - b)\right]^k}{k!}\, c^\dagger_{f\sigma} = e^{-\gamma(b^\dagger - b)}\, c^\dagger_{f\sigma}.
\end{aligned}$$

The needed basic commutators to calculate the transformed bosonic ladder operators are

$$\begin{aligned}[b,(b^\dagger-b)^k] &= \sum_{j=0}^{k-1}(b^\dagger-b)^{k-1-j}\underbrace{[b,b^\dagger-b]}_{1}(b^\dagger-b)^j \\ &= \sum_{j=0}^{k-1}(b^\dagger-b)^{k-1} = k(b^\dagger-b)^{k-1}\end{aligned}$$

and

$$\begin{aligned}[b^\dagger,(b^\dagger-b)^k] &= \sum_{j=0}^{k-1}(b^\dagger-b)^{k-1-j}\underbrace{[b^\dagger,b^\dagger-b]}_{1}(b^\dagger-b)^j \\ &= \sum_{j=0}^{k-1}(b^\dagger-b)^{k-1} = k(b^\dagger-b)^{k-1}.\end{aligned}$$

With these, the transformed bosonic operators become

$$\begin{aligned}\bar{b} &= e^{-\sum_\sigma \gamma\hat{n}_{f\sigma}}\, b\, e^{\sum_\sigma \gamma\hat{n}_{f\sigma}} \\ &= e^{-\sum_\sigma \gamma\hat{n}_{f\sigma}}\, b \sum_{k=0}^{\infty}\frac{\left[\sum_\sigma \gamma\hat{n}_\sigma(b^\dagger-b)\right]^k}{k!} \\ &= \underbrace{e^{-\sum_\sigma \gamma\hat{n}_{f\sigma}}\, e^{\sum_\sigma \gamma\hat{n}_{f\sigma}}}_{1} b + e^{-\sum_\sigma \gamma\hat{n}_{f\sigma}}\sum_{k=0}^{\infty}\frac{k\left[\sum_\sigma \gamma\hat{n}_{f\sigma}\right]\left[\sum_\sigma \gamma\hat{n}_{f\sigma}(b^\dagger-b)\right]^{k-1}}{k!} \\ &= b + e^{-\sum_\sigma \gamma\hat{n}_{f\sigma}}\sum_{k=1}^{\infty}\frac{\left[\sum_\sigma \gamma\hat{n}_{f\sigma}\right]\left[\sum_\sigma \gamma\hat{n}_{f\sigma}(b^\dagger-b)\right]^{k-1}}{(k-1)!} \\ &= b + e^{-\sum_\sigma \gamma\hat{n}_{f\sigma}}\Big[\sum_\sigma \gamma\hat{n}_{f\sigma}\Big]\sum_{k=0}^{\infty}\frac{\left[\sum_\sigma \gamma\hat{n}_{f\sigma}(b^\dagger-b)\right]^k}{k!} \\ &= b + e^{-\sum_\sigma \gamma\hat{n}_{f\sigma}}\Big[\sum_\sigma \gamma\hat{n}_{f\sigma}\Big]e^{\sum_\sigma \gamma\hat{n}_{f\sigma}} \\ &= b + \sum_\sigma \gamma\hat{n}_{f\sigma}\end{aligned}$$

and, because the commutator of $(b^\dagger - b)$ with $b^\dagger$ is the same as with b,

$$\bar{b}^\dagger = b^\dagger + \sum_\sigma \gamma\hat{n}_{f\sigma}.$$

So in eq. A.4, the hopping term becomes

$$\sum_{k,l,\sigma} E_{kl}\bar{c}^\dagger_{k\sigma}\bar{c}_{l\sigma} = \sum_{\substack{k\neq f\\ l\neq f}}\sum_{\sigma} E_{kl}c^\dagger_{k\sigma}c_{l\sigma} + \sum_{k\sigma}\left(E_{kf}c^\dagger_{k\sigma}c_{f\sigma}e^{-\frac{\lambda}{\omega_b}(b^\dagger-b)} + E_{fk}c^\dagger_{f\sigma}e^{\frac{\lambda}{\omega_b}(b^\dagger-b)}c_{k\sigma}\right),$$

the electron-phonon coupling is

$$\begin{aligned}\sum_{\sigma}\lambda(\bar{b}^\dagger+\bar{b})\,\bar{c}^\dagger_{f\sigma}\bar{c}_{f\sigma} &= \sum_{\sigma}\lambda\Big(b^\dagger+\sum_{\sigma'}\gamma\hat{n}_{f\sigma'}+b+\sum_{\sigma'}\gamma\hat{n}_{f\sigma'}\Big)\,\hat{n}_{f\sigma}\\ &= \sum_{\sigma}\lambda(b^\dagger+b)\,\hat{n}_{f\sigma}+2\lambda\sum_{\sigma,\sigma'}\gamma\hat{n}_{f\sigma'}\hat{n}_{f\sigma}\\ &= \sum_{\sigma}\lambda(b^\dagger+b)\,\hat{n}_{f\sigma}-\frac{2}{\omega_b}\Big(\sum_{\sigma}\lambda\hat{n}_{f\sigma}\Big)^2,\end{aligned}$$

the Coulomb repulsion remains unchanged

$$U\bar{c}^\dagger_{f\uparrow}\bar{c}_{f\uparrow}\bar{c}^\dagger_{f\downarrow}\bar{c}_{f\downarrow} = Uc^\dagger_{f\uparrow}c_{f\uparrow}c^\dagger_{f\downarrow}c_{f\downarrow},$$

and the energy of the phonons transforms to

$$\begin{aligned}\omega_b\,\bar{b}^\dagger\bar{b} &= \omega_b\left(b^\dagger+\sum_{\sigma}\gamma\hat{n}_{f\sigma}\right)\left(b+\sum_{\sigma}\gamma\hat{n}_{f\sigma}\right)\\ &= \omega_b\,b^\dagger b+\omega_b\,b\sum_{\sigma}\gamma\hat{n}_{f\sigma}+\omega_b\,b^\dagger\sum_{\sigma}\gamma\hat{n}_{f\sigma}+\omega_b\Big(\sum_{\sigma}\gamma\hat{n}_{f\sigma}\Big)^2\\ &= \omega_b\,b^\dagger b+\omega_b\gamma(b^\dagger+b)\Big(\sum_{\sigma}\hat{n}_{f\sigma}\Big)+\omega_b\Big(\sum_{\sigma}\gamma\hat{n}_{f\sigma}\Big)^2\\ &= \omega_b\,b^\dagger b-\sum_{\sigma}\lambda(b^\dagger+b)\hat{n}_{f\sigma}+\frac{1}{\omega_b}\Big(\sum_{\sigma}\lambda\hat{n}_{f\sigma}\Big)^2.\end{aligned}$$

When added together, these terms combine to the final result

$$\hat{\bar{H}}_{\text{aux}} = \sum_{\substack{k\neq f\\ l\neq f}}\sum_{\sigma}E_{kl}\,c^\dagger_{k\sigma}c_{l\sigma}+Uc^\dagger_{f\uparrow}c_{f\uparrow}c^\dagger_{f\downarrow}c_{f\downarrow}+\omega_b\,b^\dagger b-\frac{1}{\omega_b}\Big(\sum_{\sigma}\lambda c^\dagger_{f\sigma}c_{f\sigma}\Big)^2 + \sum_{k\sigma}\left(E_{kf}c^\dagger_{k\sigma}c_{f\sigma}e^{-\frac{\lambda}{\omega_b}(b^\dagger-b)}+E_{fk}c^\dagger_{f\sigma}e^{\frac{\lambda}{\omega_b}(b^\dagger-b)}c_{k\sigma}\right). \qquad \square$$

A.10 Left- and right-sided eigenvalues

A right eigenvector $\boldsymbol{x}_\mathrm{R}$ to the eigenvalue λ_R of a matrix $\underline{M}$ satisfies the equation

$$(\underline{M} - \lambda_\mathrm{R}\mathbb{1})\boldsymbol{x}_\mathrm{R} = 0.$$

For solutions except the trivial $\boldsymbol{x}_\mathrm{R} = \mathbf{0}$, the determinant of the coefficient matrix must vanish.

$$\det(\underline{M} - \lambda_\mathrm{R}\mathbb{1}) = 0$$

The determinant is invariant with respect to transposing its argument, so also

$$\det\left(\underline{M}^\mathrm{T} - \lambda_\mathrm{R}\mathbb{1}\right) = 0$$

must hold. But this equation implies that

$$(\underline{M}^\mathrm{T} - \lambda_\mathrm{R}\mathbb{1})\boldsymbol{x}_\mathrm{L}^\mathrm{T} = 0 \tag{A.5}$$

has non-tivial solutions for the row vector $\boldsymbol{x}_\mathrm{L}$. Transposing the whole equation gives

$$\boldsymbol{x}_\mathrm{L}(\underline{M} - \lambda_\mathrm{R}\mathbb{1}) = 0 \tag{A.6}$$

which is the definition of a left eigenvector of $\underline{M}$ with eigenvalue λ_R. Therefore, λ_R is also a left-sided eigenvalue of $\underline{M}$, which is better called $\lambda \coloneqq \lambda_\mathrm{R}$.

Appendix B

Additional Plots

In this appendix we collect plots which are not absolutely necessary for the main text but could be useful as a later reference.

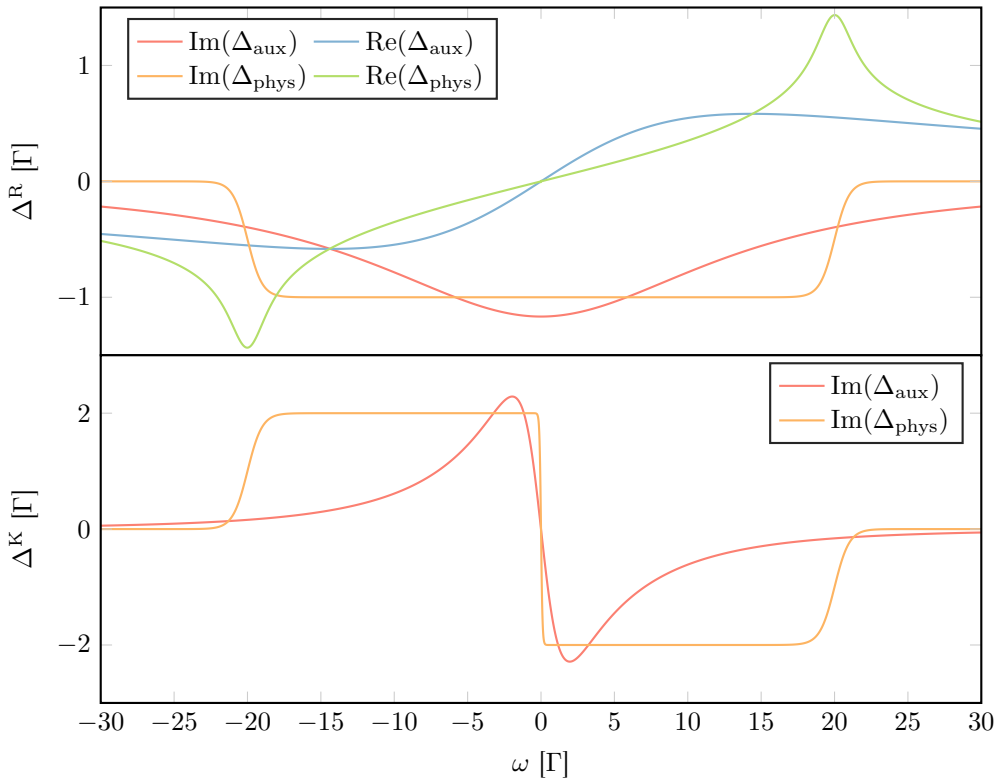

Figure B.1: Fits used for the calculation of the convergence behavior of the Lang-Firsov transformation, with the parameters as given in section 4.2.

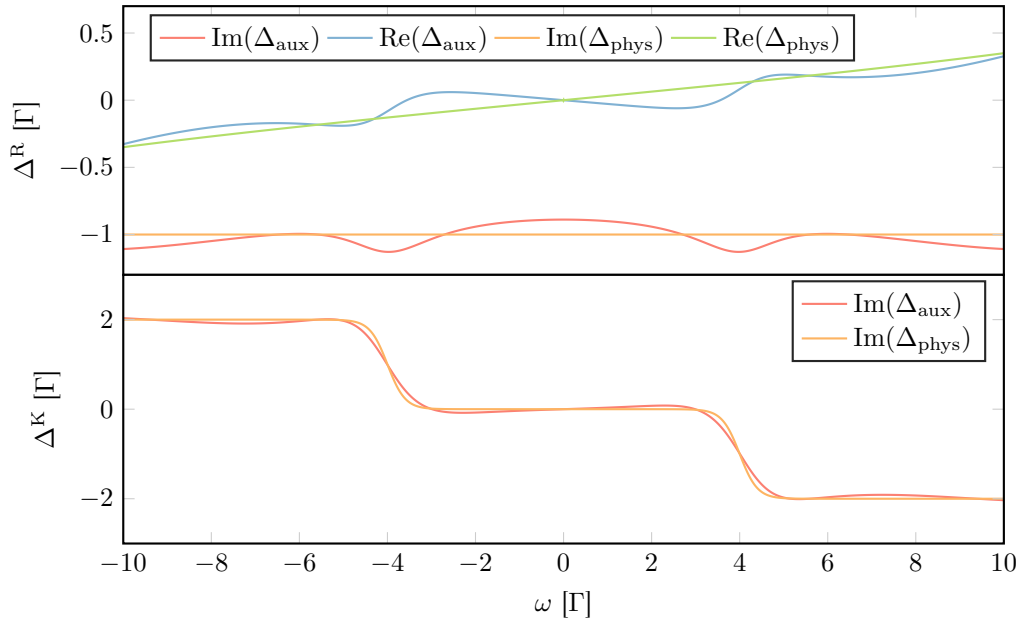

Figure B.2: Example fit for the RTPIA calculations with $N = 5$, $\Phi = 8\,\Gamma$, and all other parameters as given in section 4.4.1.

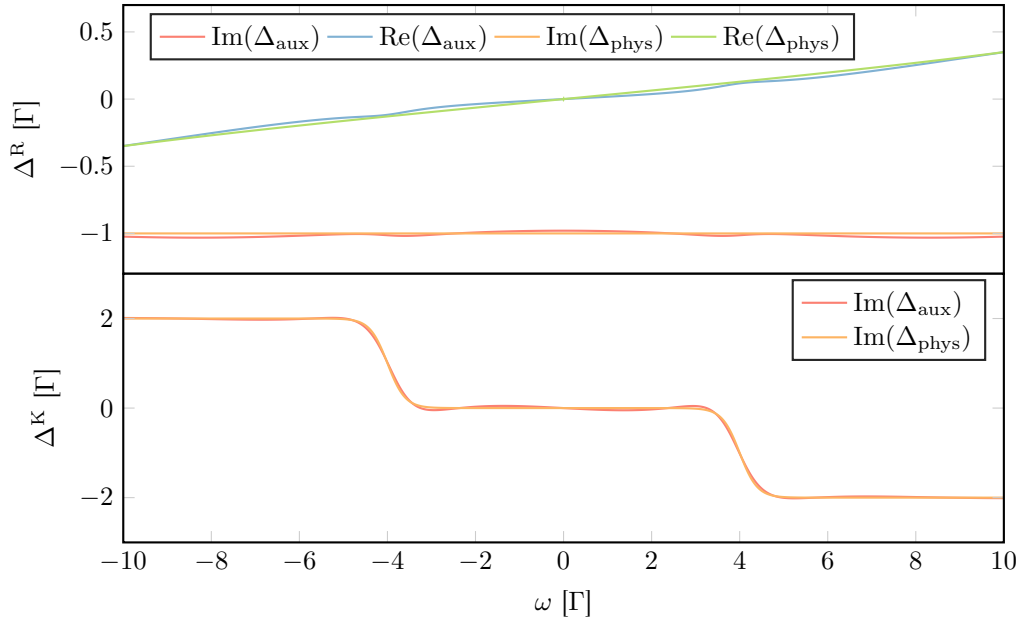

Figure B.3: Example fit for the RTPIA calculations with $N = 5$, $\Phi = 8\,\Gamma$, and all other parameters as given in section 4.4.1.

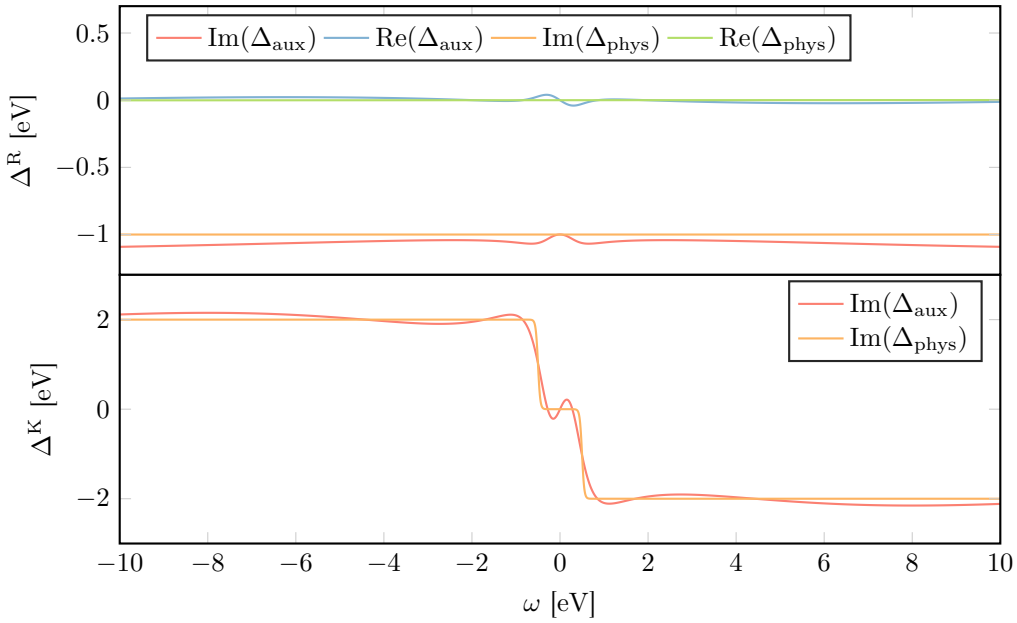

Figure B.4: Example fit for the HQME calculations with $N = 5$, $\Phi = 1\,\mathrm{eV}$, and all other parameters as given in section 4.4.2.

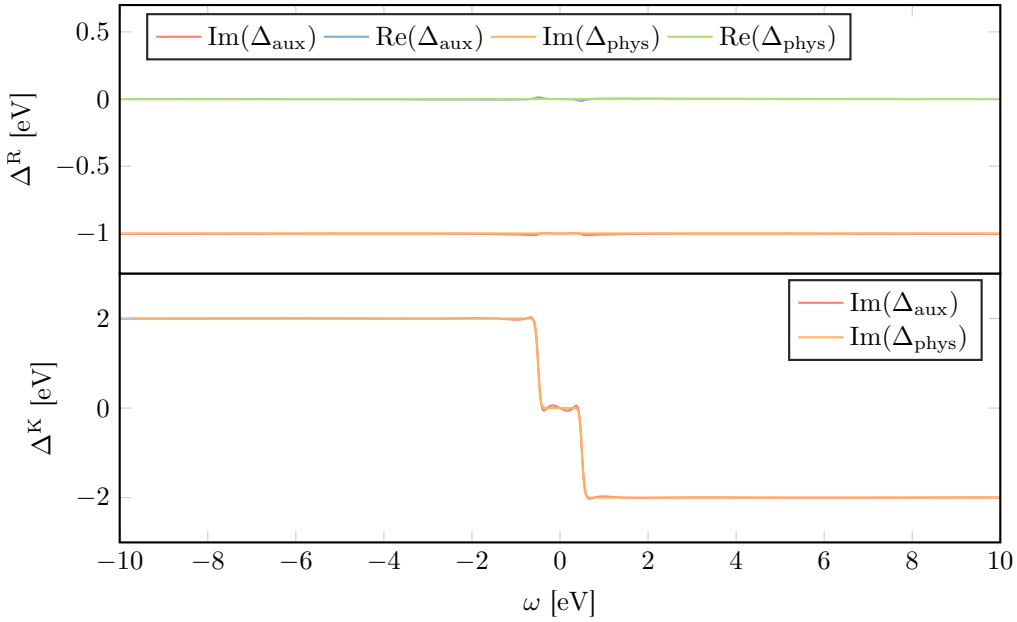

Figure B.5: Example fit for the HQME calculations with $N = 7$, $\Phi = 1\,\mathrm{eV}$, and all other parameters as given in section 4.4.2.

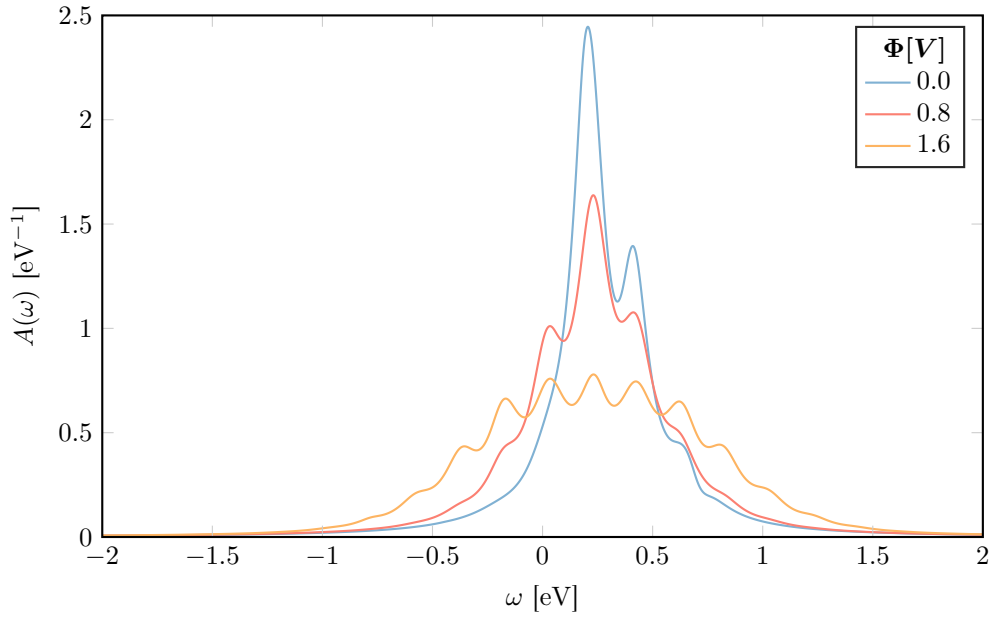

Figure B.6: Impurity spectral functions of the calculations used for comparison with HQME at $\lambda = 0.12\,\text{eV}$, $\Gamma = 0.1\,\text{eV}$, $N = 5$, and all other parameters as given in section 4.4.2.

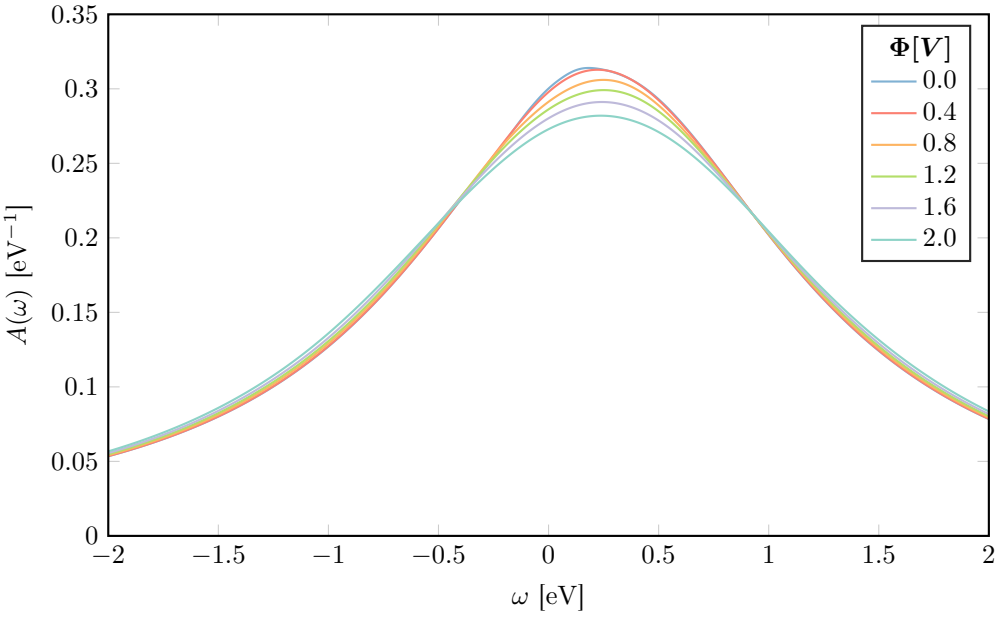

Figure B.7: Impurity spectral functions of the calculations used for comparison with HQME at $\lambda = 0.12\,\text{eV}$, $\Gamma = 1\,\text{eV}$, $N = 5$, and all other parameters as given in section 4.4.2.

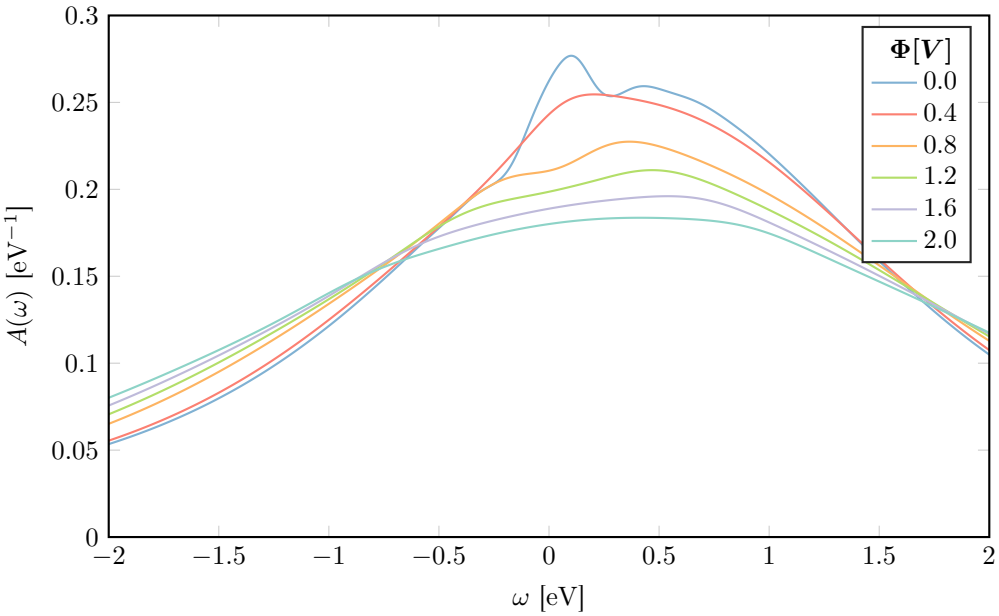

Figure B.8: Impurity spectral functions of the calculations used for comparison with HQME at $\lambda = 0.4\,\mathrm{eV}$, $\Gamma = 1\,\mathrm{eV}$, $N = 5$, and all other parameters as given in section 4.4.2.

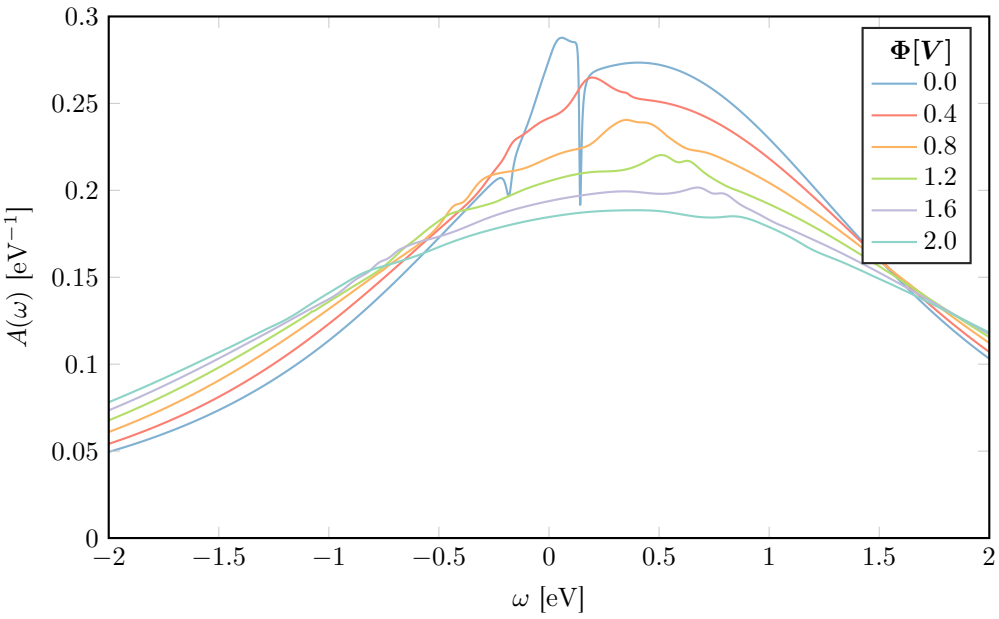

Figure B.9: Impurity spectral functions of the calculations used for comparison with HQME at $\lambda = 0.4\,\mathrm{eV}$, $\Gamma = 1\,\mathrm{eV}$, $N = 7$, and all other parameters as given in section 4.4.2. The dip at $\Phi = 0$ looks like numerical instabilities, but the results for $N = 5$ show a similar feature, albeit washed out. We therefore assume its origin is physical, not numerical.

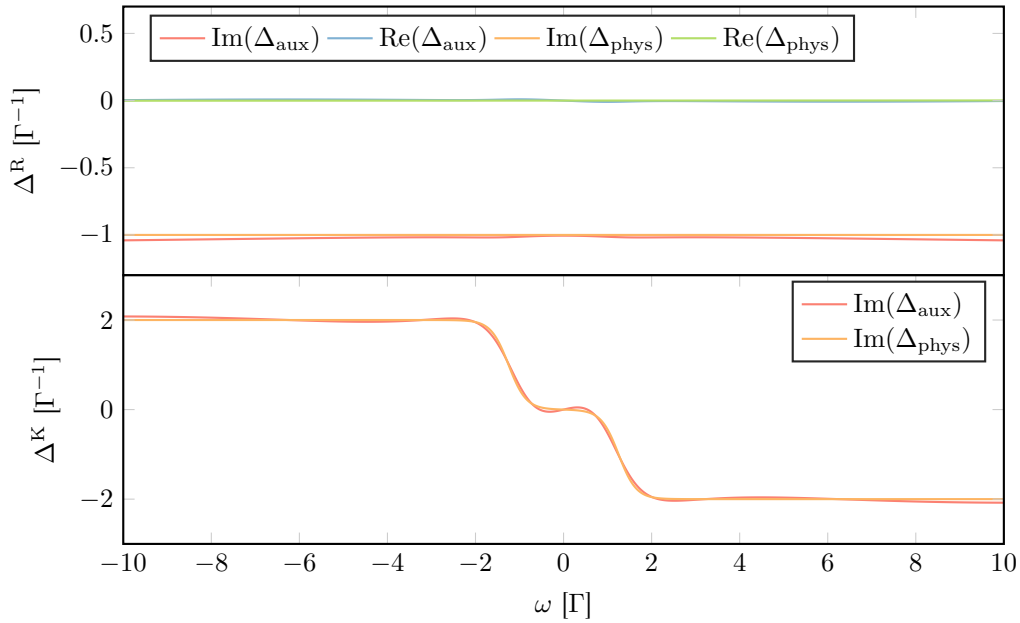

Figure B.10: Example fit for the calculations reproducing the Franck-Condon blockade with $N = 5$, $\Phi = 2.5\,\Gamma$, and all other parameters as given in section 4.5.

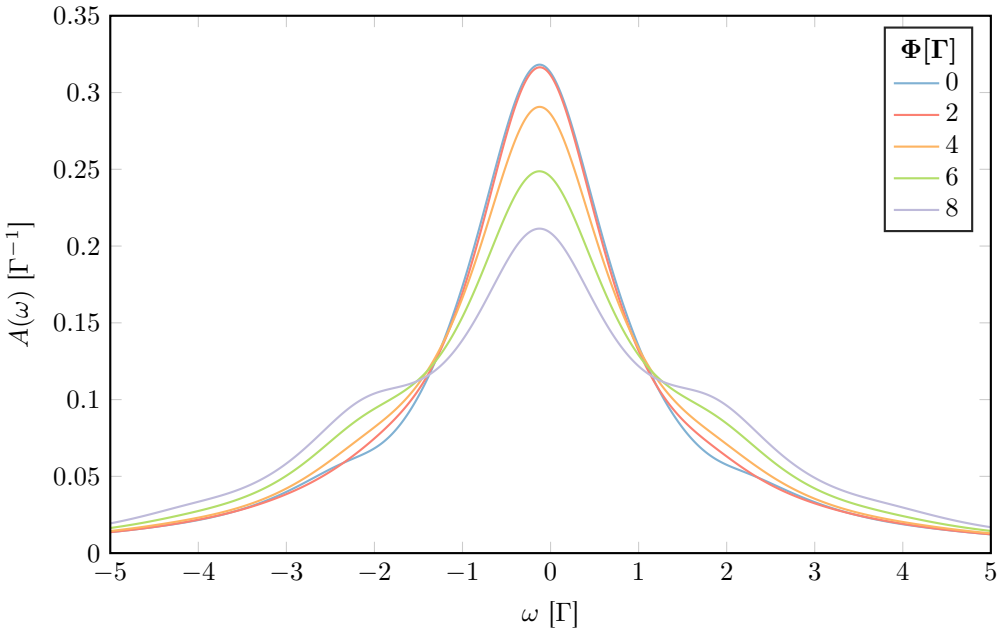

Figure B.11: Impurity spectral functions of the calculations reproducing the Franck-Condon blockade at $\lambda = 0.5\,\Gamma$, and all other parameters as given in section 4.5.

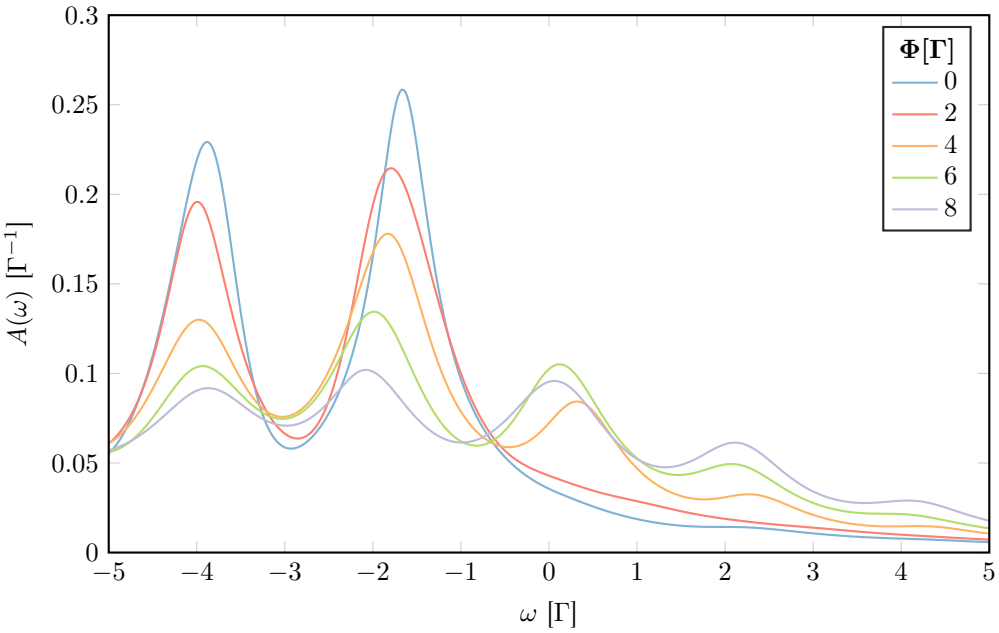

Figure B.12: Impurity spectral functions of the calculations reproducing the Franck-Condon blockade at $\lambda = 2\,\Gamma$, and all other parameters as given in section 4.5.

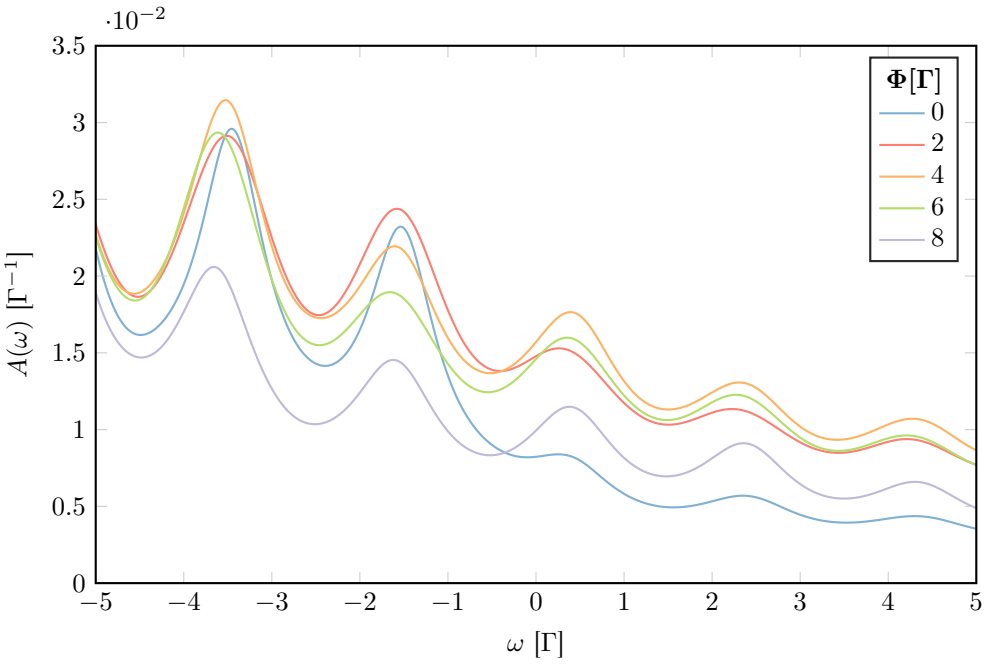

Figure B.13: Impurity spectral functions of the calculations reproducing the Franck-Condon blockade at $\lambda = 4\,\Gamma$, and all other parameters as given in section 4.5.

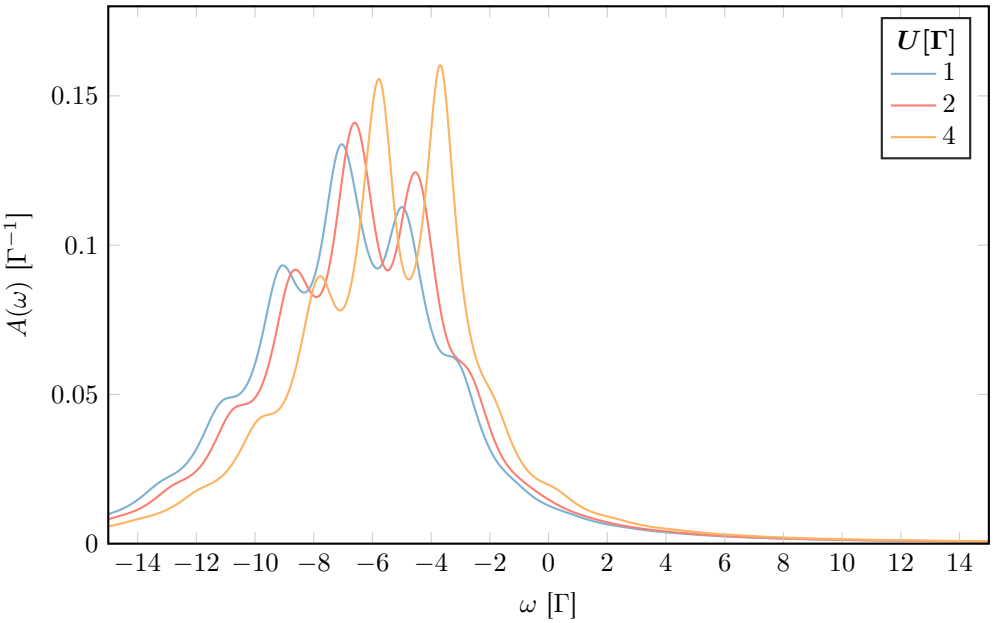

Figure B.14: Impurity spectral functions for the model with finite Coulomb repulsion at $\Phi = 4\,\Gamma$, and all other parameters as given in section 4.6.

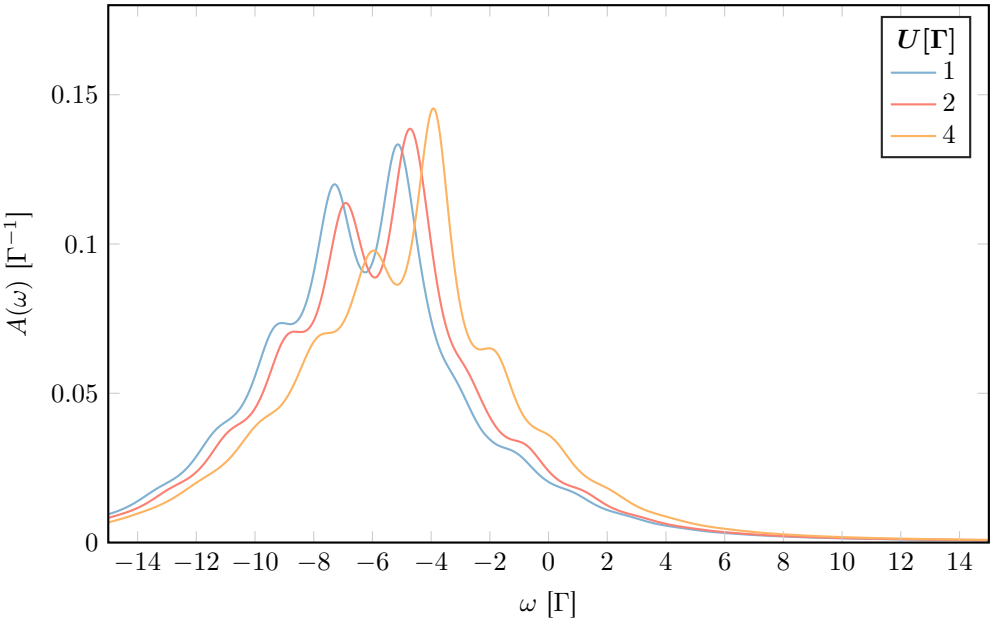

Figure B.15: Impurity spectral functions for the model with finite Coulomb repulsion at $\Phi = 8\,\Gamma$, and all other parameters as given in section 4.6.

Bibliography

[1] B. Becker and P. Molitor. *Technische Informatik: Eine einführende Darstellung*, page 13. Oldenbourg Verlag, 2008. ISBN: 978 3 486 58650 3.

[2] H. Wong and H. Iwai. The road to miniaturization. *Physics World*, 18(9):40, 2005. DOI: 10.1088/2058-7058/18/9/31.

[3] C. A. Mack. Seeing double. *IEEE Spectrum*, 45(11), 2008. DOI: 10/fdg6md.

[4] Y. Laplanche. Implementation of ARM® Cores in FinFET technolgies. In *45th European Solid State Device Research Conference*, pages 80–83. IEEE, 2015. DOI: 10.1109/ESSDERC.2015.7324718.

[5] A. Aviram and M. A. Ratner. Molecular rectifiers. *Chemical Physics Letters*, 29(2):277–283, 1974. DOI: 10.1016/0009-2614(74)85031-1.

[6] D. P. E. Smith. Quantum Point Contact Switches. *Science*, 269(5222):371, 1995. DOI: 10.1126/science.269.5222.371.

[7] Y. Cui and C. M. Lieber. Functional Nanoscale Electronic Devices Assembled Using Silicon Nanowire Building Blocks. *Science*, 291(5505):851–853, 2001. DOI: 10.1126/science.291.5505.851.

[8] F. Q. Xie, L. Nittler, C. Obermair, and T. Schimmel. Gate-Controlled Atomic Quantum Switch. *Physical Review Letters*, 93(12):128303, 2004. DOI: 10.1103/PhysRevLett.93.128303.

[9] K. Terabe, T. Hasegawa, T. Nakayama, and M. Aono. Quantized conductance atomic switch. *Nature*, 433(7021):47–50, 2005. DOI: 10.1038/nature03190.

[10] N. B. Zhitenev, H. Meng, and Z. Bao. Conductance of Small Molecular Junctions. *Physical Review Letters*, 88(22):226801, 2002. DOI: 10.1103/PhysRevLett.88.226801.

[11] J. J. Parks, A. R. Champagne, G. R. Hutchison, S. Flores-Torres, H. D. Abruna, and D. C. Ralph. Tuning the Kondo Effect with a Mechanically Controllable Break Junction. *Physical Review Letters*, 99(2):026601, 2007. DOI: 10.1103/PhysRevLett.99.026601.

[12] M. Kiguchi, O. Tal, S. Wohlthat, F. Pauly, M. Krieger, D. Djukic, J. C. Cuevas, and J. M. van Ruitenbeek. Highly Conductive Molecular Junctions Based on Direct Binding of Benzene to Platinum Electrodes. *Physical Review Letters*, 101(4):046801, 2008. DOI: 10.1103/PhysRevLett.101.046801.

[13] J. M. Beebe, B. Kim, C. D. Frisbie, and J. G. Kushmerick. Measuring Relative Barrier Heights in Molecular Electronic Junctions with Transition Voltage Spectroscopy. *ACS Nano*, 2(5):827–832, 2008. DOI: 10.1021/nn700424u.

[14] H. Song, Y. Kim, Y. H. Jang, H. Jeong, M. A. Reed, and T. Lee. Observation of molecular orbital gating. *Nature*, 462(7276):1039–1043, 2009. DOI: 10.1038/nature08639.

[15] S. Y. Quek, M. Kamenetska, M. L. Steigerwald, H. J. Choi, S. G. Louie, M. S. Hybertsen, J. B. Neaton, and L. Venkataraman. Mechanically controlled binary conductance switching of a single-molecule junction. *Nature Nanotechnology*, 4 (4):230–234, 2009. DOI: 10.1038/nnano.2009.10.

[16] M. Kiguchi. Electrical conductance of single C_{60} and benzene molecules bridging between Pt electrode. *Applied Physics Letters*, 95(7):213, 2009. DOI: 10.1063/1.3204466.

[17] S. Kaneko, T. Nakazumi, and M. Kiguchi. Fabrication of a Well-Defined Single Benzene Molecule Junction Using Ag Electrodes. *The Journal of Physical Chemistry Letters*, 1(24):3520–3523, 2010. DOI: 10.1021/jz101506u.

[18] H. Park, J. Park, A. K. L. Lim, E. H. Anderson, et al. Nanomechanical oscillations in a single-C_{60} transistor. *Nature*, 407(6800):57–60, 2000. DOI: 10.1038/35024031.

[19] W. G. van der Wiel, S. De Franceschi, J. M. Elzerman, T. Fujisawa, S. Tarucha, and L. P. Kouwenhoven. Electron transport through double quantum dots. *Reviews of Modern Physics*, 75(1):1, 2002. DOI: 10.1103/RevModPhys.75.1.

[20] A. N. Pasupathy, J. Park, C. Chang, A. V. Soldatov, S. Lebedkin, R. C. Bialczak, J. E. Grose, L. A. K. Donev, J. P. Sethna, D. C. Ralph, et al. Vibration-Assisted Electron Tunneling in C_{140} Transistors. *Nano Letters*, 5(2):203–207, 2005. DOI: 10.1021/nl048619c.

[21] J. Hihath, C. R. Arroyo, G. Rubio-Bollinger, N. Tao, and N. Agraït. Study of Electron-Phonon Interactions in a Single Molecule Covalently Connected to two Electrodes. *Nano Letters*, 8(6):1673–1678, 2008. DOI: 10.1021/nl080580e.

[22] O. Tal, M. Krieger, B. Leerink, and J. M. Van Ruitenbeek. Electron-Vibration Interaction in Single-Molecule Junctions: From Contact to Tunneling Regimes. *Physical Review Letters*, 100(19):196804, 2008. DOI: 10.1103/PhysRevLett.100.196804.

[23] L. Mühlbacher and E. Rabani. Real-Time Path Integral Approach to Nonequilibrium Many-Body Quantum Systems. *Physical Review Letters*, 100(17): 176403, 2008. DOI: 10.1103/PhysRevLett.100.176403.

[24] J. Mravlje and A. Ramšak. Electron Transport Through Molecules in the Kondo Regime: The Role of Molecular Vibrations. In *Physical Properties of Nanosystems*, pages 45–60. Springer, 2010. DOI: 10.1007/978-94-007-0044-4_4.

[25] S. Maier, T. L. Schmidt, and A. Komnik. Charge transfer statistics of a molecular quantum dot with strong electron-phonon interaction. *Physical Review B*, 83(8):085401, 2011. DOI: 10.1103/PhysRevB.83.085401.

[26] R. Hützen, S. Weiss, M. Thorwart, and R. Egger. Iterative summation of path integrals for nonequilibrium molecular quantum transport. *Physical Review B*, 85(12):121408, 2012. DOI: 10.1103/PhysRevB.85.121408.

[27] C. Schinabeck, A. Erpenbeck, R. Härtle, and M. Thoss. Hierarchical quantum master equation approach to electronic-vibrational coupling in nonequilibrium transport through nanosystems. *Physical Review B*, 94(20):201407, 2016. DOI: 10.1103/PhysRevB.94.201407.

[28] E. Arrigoni, M. Knap, and W. von der Linden. Nonequilibrium Dynamical Mean-Field Theory: An Auxiliary Quantum Master Equation Approach. *Physical review letters*, 110(8):086403, 2013. DOI: 10.1103/PhysRevLett.110.086403.

[29] W. E. Arnoldi. The principle of minimized iterations in the solution of the matrix eigenvalue problem. *Quarterly of Applied Mathematics*, 9(1):17–29, 1951. DOI: 10.1090/qam/42792.

[30] C. Lanczos. An Iteration Method for the Solution of the Eigenvalue Problem of Linear Differential and Integral Operators. *Journal of Research of the National Bureau of Standards*, 45(4):255–282, 1950. DOI: 10.6028/jres.045.026.

[31] P. W. Anderson. Localized Magnetic States in Metals. *Physical Review*, 124 (1):41, 1961. DOI: 10.1103/PhysRev.124.41.

[32] T. Holstein. Studies of Polaron Motion – Part I. The Molecular-Crystal Model. *Annals of Physics*, 8(3):325–342, 1959. DOI: 10.1016/0003-4916(59)90002-8.

[33] T. Holstein. Studies of Polaron Motion – Part II. The "Small" Polaron. *Annals of Physics*, 8(3):343–389, 1959. DOI: 10.1006/aphy.2000.6021.

[34] A. Dorda, M. Nuss, W. von der Linden, and E. Arrigoni. Auxiliary master equation approach to nonequilibrium correlated impurities. *Physical Review B*, 89(16):165105, 2014. DOI: 10.1103/PhysRevB.89.165105.

[35] H. P. Breuer and F. Petruccione. *The Theory of Open Quantum Systems*, chapter 3.3. Oxford University Press, 2002. ISBN: 978 0 19 852063 4.

[36] G. Schaller. *Open Quantum Systems Far from Equilibrium*, volume 881. Springer, 2014. ISBN: 978 3 319 03876 6.

[37] A. A. Dzhioev and D. S. Kosov. Super-fermion representation of quantum kinetic equations for the electron transport problem. *The Journal of Chemical Physics*, 134(4):044121, 2011. DOI: 10.1063/1.3548065.

[38] H. Haug and A. P. Jauho. *Quantum Kinetics in Transport and Optics of Semiconductors*. Springer, 2008. ISBN: 978 3 540 73561 8.

[39] I. G. Lang and Y. A. Firsov. Kinetic Theory of Semiconductors with Low Mobility. *Journal of Experimental and Theoretical Physics*, 16(5):1301, 1963. URL: jetp.ac.ru/cgi-bin/dn/e_016_05_1301.pdf.

[40] J. R. Norris. *Markov Chains*, chapter Introduction. Cambridge University Press, 1998. ISBN: 978 0 521 48181 6.

[41] A. Kossakowski. On quantum statistical mechanics of non-Hamiltonian systems. *Reports on Mathematical Physics*, 3(4):247–274, 1972. DOI: 10.1016/0034-4877(72)90010-9.

[42] G. Lindblad. On the Generators of Quantum Dynamical Semigroups. *Communications in Mathematical Physics*, 48(2):119–130, 1976. DOI: 10.1007/BF01608499.

[43] V. Gorini, A. Kossakowski, and E. C. G. Sudarshan. Completely positive dynamical semigroups of N-level systems. *Journal of Mathematical Physics*, 17(5):821–825, 1976. DOI: 10.1063/1.522979.

[44] L. P. Kadanoff and G. A. Baym. *Quantum Statistical Mechanics: Green's Function Methods in Equilibrium and Nonequilibirum Problems*. Benjamin, 1962. ISBN: 978 0 201 41046 4.

[45] W. Nolting. *Grundkurs Theoretische Physik 7 – Viel-Teilchen-Theorie*. Springer, eighth edition, 2015. ISBN: 978 3 642 25807 7.

[46] G. Tatara, H. Kohno, and J. Shibata. Microscopic approach to current-driven domain wall dynamics. *Physics Reports*, 468(6):213–301, 2008. DOI: 10.1016/j.physrep.2008.07.003.

[47] M. Gell-Mann and F. Low. Bound States in Quantum Field Theory. *Physical Review*, 84(2):350, 1951. DOI: 10.1103/PhysRev.84.350.

[48] F. J. Dyson. The S Matrix in Quantum Electrodynamics. *Physical Review*, 75 (11):1736, 1949. DOI: doi.org/10.1103/PhysRev.75.1736.

[49] L. V. Keldysh et al. Diagram Technique for Nonequilibrium Processes. *Journal of Experimental and Theoretical Physics*, 20(4):1018–1026, 1965. URL: jetp.ac.ru/cgi-bin/dn/e_020_04_1018.pdf.

[50] D. C. Langreth and J. W. Wilkins. Theory of Spin Resonance in Dilute Magnetic Alloys. *Physical Review B*, 6(9):3189, 1972. DOI: 10.1103/PhysRevB.6.3189.

[51] Y. Meir and N. S. Wingreen. Landauer formula for the current through an interacting electron region. *Physical Review Letters*, 68(16):2512, 1992. DOI: 10.1103/PhysRevLett.68.2512.

[52] A. Dorda, M. Sorantin, W. von der Linden, and E. Arrigoni. Optimized auxiliary representation of non-Markovian impurity problems by a Lindblad equation. *New Journal of Physics*, 19:063005, 2017. DOI: 10.1088/1367-2630/aa6ccc.

[53] M. Lax. Formal Theory of Quantum Fluctuations from a Driven State. *Physical Review*, 129(5):2342, 1963. DOI: 10.1103/PhysRev.129.2342.

[54] F. Schwarz, M. Goldstein, A. Dorda, E. Arrigoni, A. Weichselbaum, and J. von Delft. Lindblad-driven discretized leads for nonequilibrium steady-state transport in quantum impurity models: Recovering the continuum limit. *Physical Review B*, 94(15):155142, 2016. DOI: 10.1103/PhysRevB.94.155142.

[55] D. J. Earl and M. W. Deem. Parallel tempering: Theory, applications, and new perspectives. *Physical Chemistry Chemical Physics*, 7(23):3910–3916, 2005. DOI: 10.1039/B509983H.

[56] R. von Mises and H. Pollaczek-Geiringer. Praktische Verfahren der Gleichungsauflösung. *Zeitschrift für Angewandte Mathematik und Mechanik*, 9(1): 58–77, 1929. DOI: 10.1002/zamm.19290090206.

[57] A. N. Krylov. On the numerical solution of the equation by which, in technical questions, frequencies of small oscillations of material systems are determined. *Izvestija AN SSSR, Otdel. mat. i estest. nauk*, 7(4):491–539, 1931.

[58] B. N. Parlett, D. R. Taylor, and Z. A. Liu. A Look-Ahead Lanczos Algorithm for Unsymmetric Matrices. *Mathematics of Computation*, 44(169):105–124, 1985. DOI: 10.1090/S0025-5718-1985-0771034-2.